2012

Thin layer sonoelectrochemistry

Chester George Duda
University of Iowa

THIN LAYER SONOELECTROCHEMISTRY

by

Chester George Duda

An Abstract

Of a thesis submitted in partial fulfillment
of the requirements for the Doctor of
Philosophy degree in Chemistry
in the Graduate College of
The University of Iowa

May 2012

Thesis Supervisor: Associate Professor Johna Leddy

ABSTRACT

This research exploits mild sonication in a thin layer electrochemical cell to enhance rates of reaction in systems under voltammetric perturbation. Sound waves propagate through a thin layer of condensed fluid to provide energy to the electrode solution interface in the form of pressure and temperature. The sonic energy provided in three dimensions can be exploited to enhance rates of heterogeneous electron transfer as the energy is harnessed at the two dimensional electrode interface. Enhanced rates of heterogeneous electron transfer are of interest both for fundamental reasons and for exploitation in electrochemical energy systems.

The initial pilot studies were directed at demonstrating the impact of acoustic energy on heterogenous electron transfer. Redox couples with different electron transfer rates were evaluated. Whereas compounds with reversible electron transfer kinetics demonstrated little improvement, redox couples such as ferric ion (Fe^{3+}) with slow electron transfer kinetics exhibited an increase in the standard heterogeneous electron transfer rate constant, k^0 with an increase in acoustic energy.

The reduction of oxygen is a complex four proton, four electron process that is of technological importance. Slow kinetics of the oxygen reduction is a primary loss of efficiency in electrochemical power sources. Much like the ferric ion, oxygen kinetic rats improve. Preliminary studies in the oxidation of methanol demonstrated a sonocatalyic effect in methanol electrolysis that is of particular interest for the development of liquid based fuel cells.

Sonication can both clean and destroy surface materials. The cleaning power inherent in sonication improves electrocatalysis and removes deposits and oxides

from the electrode surface.

Abstract Approved: _____
Thesis Supervisor

_____
Title and Department

_____
Date

THIN LAYER SONOELECTROCHEMISTRY

by

Chester George Duda

A thesis submitted in partial fulfillment
of the requirements for the Doctor of
Philosophy degree in Chemistry
in the Graduate College of
The University of Iowa

May 2012

Thesis Supervisor: Associate Professor Johna Leddy

Graduate College
The University of Iowa
Iowa City, Iowa

CERTIFICATE OF APPROVAL

PH.D. THESIS

This is to certify that the Ph.D. thesis of

Chester George Duda

has been approved by the Examining Committee for the thesis requirement for the Doctor of Philosophy degree in Chemistry at the May 2012 graduation.

Thesis Committee:

Johna Leddy, Thesis Supervisor

Lei Geng

Mark A. Arnold

Norbert J. Pienta

Robert L. Merlino

To Brenda

ACKNOWLEDGMENTS

My most sincerest thanks goes to my advisor, Professor Johna Leddy for her acceptance, support and willingness to tolerate my bizarre ideas. Furthermore my thanks goes out to present and past members of the Leddy lab, particularly Luke Haverhals, Murat Ünlü, Stephanie Schmidt, Heung Chan Lee, Tim Paschkewitz, Perry Motsegood, Garrett Lee, Jessica Jewett, Krysti Knoche, Kevser Sahin Tiras and Sarah Cyrus for all their support. Special thanks also goes to the undergraduate research assistants Lan Doan, Andrew Wilson, Tracy Nguyen and Huy Nguyen for their time and effort. Financial assistance from the National Science Foundation is also appreciated.

TABLE OF CONTENTS

LIST OF TABLES

Table

LIST OF FIGURES

Figure

LIST OF SYMBOLS

Symbol	
α	1.) Transfer coefficient
	2.) Attenuation coefficient
γ	Ratio of the heat capacity at constant pressure to constant volume
η	Viscosity of the medium
κ	Thermal conductivity of the medium
ρ	Density of medium
a	Radius of circular plane source (length of line source)
A	1) Frequency factor
	2) Surface area through which the wave propagates, distance dependent
$C_O(0,t)$	Concentration of O at the electrode at time t
$C_R(0,t)$	Concentration of R at the electrode at time t
C_p	Molar heat capacity at constant pressure
C_v	Molar heat capacity at constant volume
c	Speed of sound in a given medium
E_A	Activation energy
$\Delta E^{\ddagger}$	Standard internal energy of activation
$E^{0\prime}$	Reference potential
f	Frequency of the sound wave
$\Delta G^{\ddagger}$	Standard free energy of activation
$\Delta H^{\ddagger}$	Standard enthalpy of activation

I	Sound Intensity, average acoustic intensity
$\overrightarrow{I}$	Acoustic intensity
I_s	Intensity at the source
I_θ	Intensity at angle from source
I_u	Intensity if the total power from the source were radiated uniformly in all directions
I_0	Reference intensity level, 1×10^{-12} W/m^2
i	Current
k	Rate constant
k_{red}	Rate constant of reduction
k_{ox}	Rate constant of oxidation
k^0	Standard rate constant
P	Sound power (frequency dependent)
P_0	Reference power level, 1×10^{-12} W
$\Delta(PV)^\ddagger$	Pressure and volume of activation
p	Sound pressure at the receiver (frequency dependent)
$\widetilde{p}$	r.m.s. value of the sound pressure
p_0	Reference pressure level, 20 μPa(rms)
Q	Geometric directivity factor
R	1.) Gas constant
	2.) Distance between the source and the receiver
$\Delta S^\ddagger$	Standard entropy of activation
SIL	Sound intensity level

SPL	Sound Pressure Level (frequency dependent)
SWL	Sound Power Level (frequency dependent)
T	Temperature
V_{rms}	Root mean square voltage
V_p	Peak voltage
v	Instantaneous particle velocity
$\overrightarrow{v}$	Particle velocity
w	Work
z	Characteristic acoustic impedance (of a medium)

CHAPTER 1

INTRODUCTION

This research exploits mild sonication to enhance rates of reaction in systems under voltammetric perturbation. Sound waves propagate through a condensed fluid to provide energy to the electrode solution interface. The sonic energy provided in three dimensions can be exploited to enhance rates of heterogeneous electron transfer as the energy is harnessed at the two dimensional electrode interface. Enhanced rates of heterogeneous electron transfer are of interest both for fundamental reasons and for exploitation in electrochemical energy systems.

1.1 Principles of Sonication

Sonication is application of sound (usually ultrasound) to a system such that energy is transferred to matter. Traditionally, ultrasonic sonication is implemented with either an ultrasonic bath or probe (horn). Sonication has practical application in numerous applications that include homogenization of biological cell samples, cleaning, and papermaking.

1.1.1 General

Sound is a mechanical wave that is an oscillation of pressure transmitted through matter. Sound waves are typically characterized by frequency (Hz) and intensity (W/cm^2). In preceptive terms, frequency corresponds to pitch (e.g., middle C is 261.63 Hz and the A above it is 440 Hz - same as an American dial tone); intensity corresponds to loudness or volume. Wavelength is seldom used to characterize

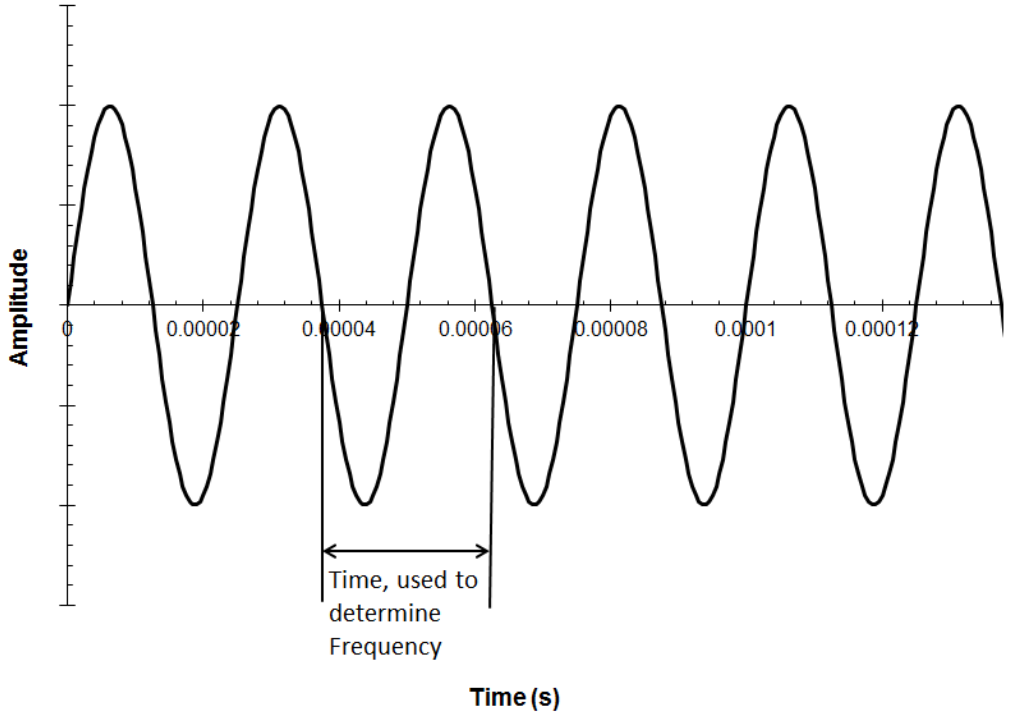

Figure 1. Image of a sinusoidal sound wave with amplitude and time used to determine frequency. Frequency: 40,000 Hz.

sound as the speed of sound differs dramatically from medium to medium.

When a sound wave is produced, matter (i.e., atoms and molecules) is compressed and rarefacted. In condensed fluids, compression densifies the particles of matter; rarefaction is expansion of the fluid such that interparticle interactions are lessened. Individual particles oscillate about their point of origin. The number of peak compressions (or rarefactions) every second correspond to frequency. The displacement of the particles from their point of origin corresponds to the intensity. The changes in pressure (density) generated by the displacement created by the

sound waves are the basis for the expected enhancements in kinetics.

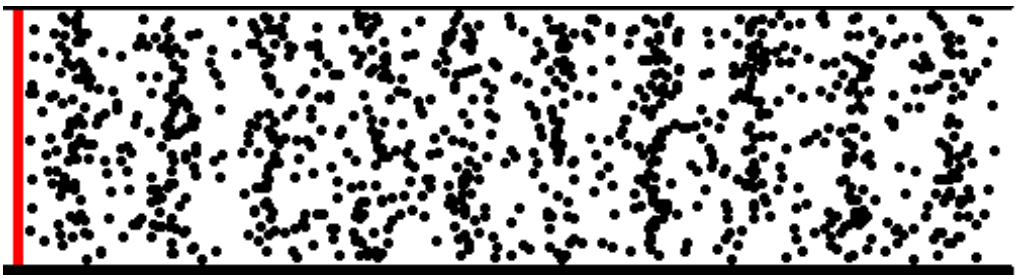

Figure 2. Propagation of a sound wave through matter. The zones of high density correspond to the peak amplitude of the sound wave. While the high density zones move would migrate across the image, each individual particle oscillates around a fixed point. The length of particle oscillation is proportional to acoustic wavelength. (Image courtesy of Dr. Dan Russell, Kettering University)

Ultrasonic waves have frequency above 20,000 Hz and are above the normal range of human hearing. Ultrasound provides compression on a timescale useful in electrochemistry and kinetics. Attenuation of ultrasonic waves is minimized in comparison to higher frequency sound wave because attenuation is proportional to the square of the frequency. See Section 2.4.3, attenuation.

1.1.2 Cavitation

Transducers are used to generate sound waves. The transducers are constructed of asymmetric crystals such as quartz, sodium potassium tartrate, and other modern ceramics that compress and rarefact when subjected to either electrical potential or current. Such sources are usually rated by either the maximum sustainable power (W) (e.g., a point source) or the maximum sustainable intensity (W/cm^2) of the system.

Because condensed fluids do not flow as fast as the transducers oscillate, rarefaction in the fluid produces small vacuum cavities. When the medium is again compressed, the cavities rapidly implode. This process in known as cavitation. It can occur within a single frequency cycle or over several cycles depending on the intensity of the transducer. Cavitation occurs at lower power when the medium contains intercalants such as dissolved gas or particulate. The level of temperature and pressure generated along the surface of the cavity and at the corresponding implosion is impressive. For a 10 W/cm^2 system, temperature exceeded 5000 K (approximately, the temperature on the surface of the sun) and 1000 atm (approximately, the pressure at the bottom of the ocean) [3]. These temperatures and pressures happen on sufficiently short physical scale (angstrom diameter bubbles) that the process has a relatively nominal effect on the bulk temperature and pressure of the medium.

For the surface tension of water, σ, 0.076 N/m and the radius of a bubble, R, as 4 Å, the pressure in the bubble, P_b, would be 3800 atm, based on [3]

$$P_b = \frac{2\sigma}{R} \tag{1}$$

The relationship between sonic intensity and pressure is defined as [3]

$$I = \frac{P_b^2}{2\rho c} \tag{2}$$

where I is sonic intensity, ρ is the density of the medium and c is the velocity of sound in the medium. Theoretically, for pure water this would require a sonic intensity of 5 MW/cm^2 to generate a 4 Å bubble. Despite this large theoretical

intensity requirement, most commercial sonic baths only generate around 0.3 W/cm^2 still generate cavitation bubbles. This is because the medium is not pure, but contains particulate and trapped gas vapor. This lowers the tensile strength of the liquid and allows easier cavitation.

Cavitation can easily pit surfaces. Anodized coating are often removed over time by cavitation. This is the basis for ultrasonic cleaning baths. The potential pitting and destruction of structural material and electrodes favors the use of low intensity sources for systems that are expected to last over time.

1.1.3 Prior Attempts at Sonoelectrochemistry

Over the last few decades, sonochemistry has been the subject of investigation by many research groups. In these studies, solutions are irradiated with high intensity sound waves. Devices such as sonic horns generate significant energy and turbulence throughout the bulk solution. The sound waves are of sufficient intensity to cause cavitation and the associated bubble formation. Suslick and his group have undertaken many fundamental studies into the physical phenomena attendant on high intensity sonochemistry [4–10]. Among these studies are various measurements of the temperature generated under sonication. Sonication of suspensions of small metal particles can generate sufficient heat that the particles fuse together. Metals with moderate melting points, such as nickel, can be fused under high intensity sonication whereas high melting metals such as platinum are not fused under sonication [10]. This allows an estimate of the thermal energy effect of sonication which creates localized effective temperatures between 2,600 °C and 3,400 °C at the

point of particle impact, sufficient to meld metal particles. Mason and coworkers have worked on fundamentals as well as sonochemical synthesis [3, 11–15]. Thorough reviews of sonochemistry in bulk phases at high and low intensity are found in references [3, 7, 11–22].

Estimates of the energy include extreme temperatures and pressures of 5000 Kelvin and 1000 atmospheres at the interface between the void and the solution as the bubble collapses [3]. Two sonochemical domains are recognized. In the high intensity domain, bubbles formed on rarefaction and collapse in a single cycle. This yields very small bubbles and the highest energy sonochemical events and requires acoustic intensities above 10 W/cm^2. In the low intensity domain, bubbles build on several cycles of rarefaction and collapse. This yields larger bubbles that on collapse yield lower energies than the high intensity cases, but the energies are still substantial [3].

Investigation of sonochemical events and electrochemical systems were first been undertaken by Coury and his group [23–27]. These are high intensity studies undertaken with an electrode placed in a solution where cavitation is generated with a high intensity device, a sonic horn. In these turbulent systems, increases in mass transport are observed. Voltammetric signals are rendered noisy by the turbulence and bubble activity. The signals are sufficiently distorted that evidence of impacts on heterogeneous electron transfer are literally lost in the noise. Coury's analysis and interpretation of the results were both careful and conservative.

Compton and several colleagues have undertaken more recent studies of sonoelectrochemistry [28–30]. Many of these studies are described as studies at

sonotrodes. The studies were also undertaken under conditions of high turbulence and high intensity sonication. Again, impacts were observed on mass transport but no evidence of impacts on electron transfer could be distinguished from the noisy signals.

Common across studies in the literature to date is the use of high power sonic horns and baths to generate acoustic power in the system. Cyclic voltammetric morphology tends from avian morphologies in unsonicated systems to nosier, sinusoidal morphologies under sonication [31, 32]. See Figures 3 and 4. The change in cyclic voltammetric morphology coupled with the level of noise associated with high power sonication make the extraction of kinetic data problematic.

In the studies reported here, a more delicate approach to harvest sonic energy at the electrode is implemented. A lower intensity crystal oscillator is used to input acoustic energy into the thin layer of solution. The intensity is low enough that there is no visible bubble formation and cavitation. The thin layer, unique in sonoelectrochemical studies, provides an opportunity to bounce sound waves back into the thin solvent layer at the solvent solution interface. Under these mild conditions, turbulence is eliminated and the voltammetric signals are clean. There are minor impacts on mass transport but the most evident effect are substantial increases in heterogeneous electron transfers. When redox probes that exhibit quasireversible or irreversible electron transfer rates in quiescent solutions are evaluated under thin layer sonoelectrochemical conditions, the rates of heterogeneous electron transfer are increased and the increases are substantial, greater than an order of magnitude.

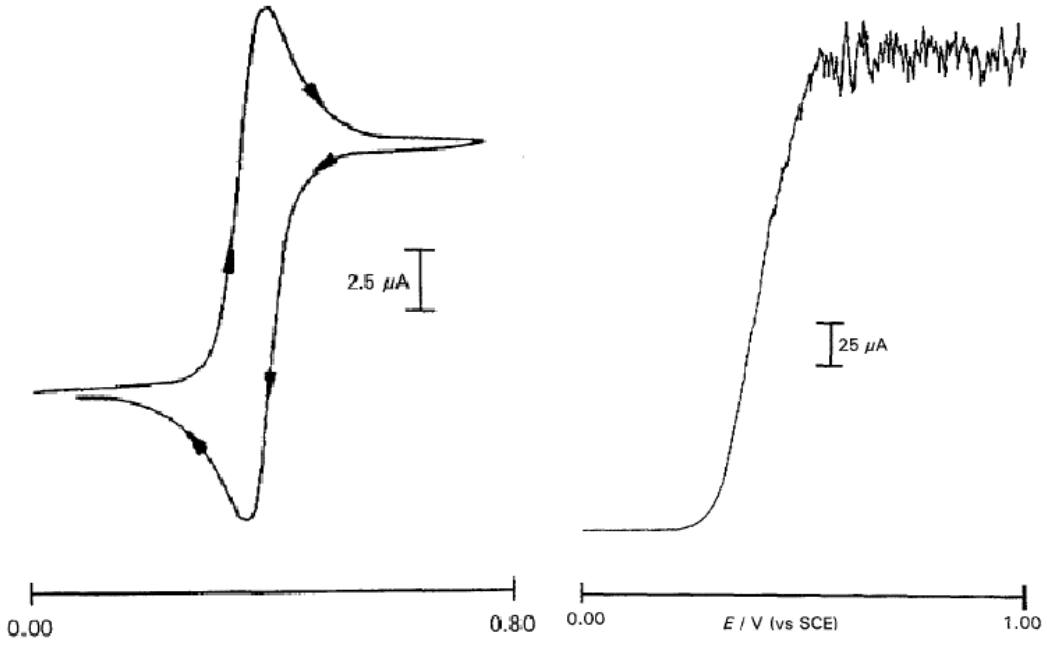

Figure 3. This figure is from reference [31] by Walton, et al. Voltammograms recorded with and without sonication for the oxidation of ferrocene (Cp_2Fe) (2.0 mM) in acetonitrile with 0.1 M TBAP (tetrabutyl ammonium perchlorate) electrolyte. Scan rate of 20 mV/s. Working electrode of 0.1 cm radius platinum. Sonication provided by 24 W/cm^2 sonic bath.

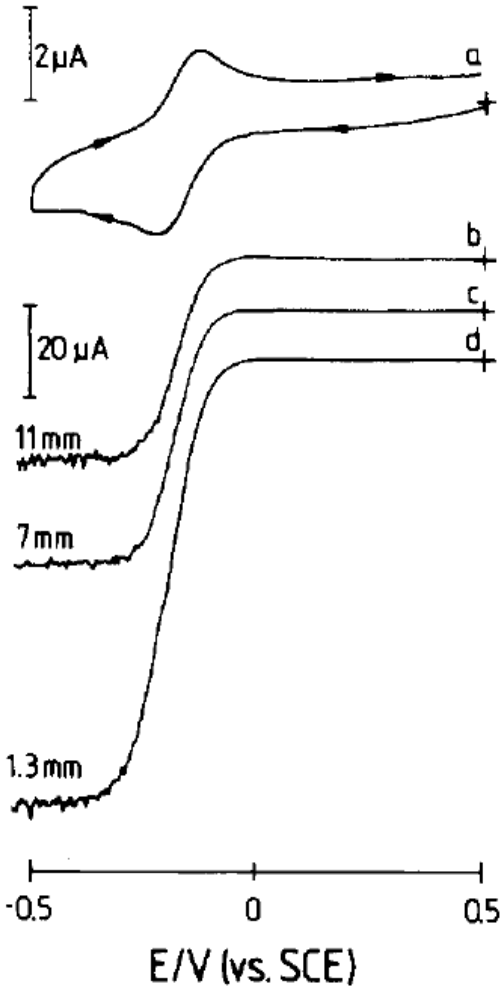

Figure 4. This figure is from reference [32] by Marken, et al. Voltammograms for the reduction of 0.23 mM $Ru(NH_3)_6^{3+}$ in aqueous 0.1 M KCl obtained at 22°C with a 2 mm diameter platinum wire electrode under (a) silent condition (scan rate 50 mV/s), and in the presence of ultrasound (scan rate 20 mV/s, 30 W/cm^2 ultrasonic power); (b) 11 mm, (c) 7 mm, (d) 1.3 mm electrode-horn separation.

Thin layer sonoelectrochemistry provides clean voltammetric signals and substantial effects on electron transfer rates. The transducers are highly efficient and operate with very low power consumption. Acoustic energy deployed in the thin but three dimensional solvent layer is harvested at the two dimensional electrode solution interface with strong effects. The enhanced rates are equivalent to significantly higher temperature and pressure. Because the solution is a thin layer, losses due to attenuation are reduced.

1.1.4 Thin Layer Sonoelectrochemistry

Prior attempts at sonoelectrochemistry have all involved the use of high power sonic baths and horns. The experiments conducted for this thesis attempt to minimize the acoustic power necessary to impact reactions by restriction of the solution to a thin layer.

This configuration increases the ratio of the path length of the sound wave to the solvent depth. Effectively, due to reflection at the solvent interfaces, the sound wave repeatedly passes though the solvent layer before it attenuates. This allows for the use of a low power transducer.

1.2 Expected Impact of Sonication on Electrochemical Reactions

In summary, sonication is expected to enhance standard heterogeneous electron transfer rates such that $\ln k^0 \propto \Delta\left(PV\right)$. Other impacts, such as on the transfer coefficient, α, may also occur. Mild sonication will not induce net solvent transport

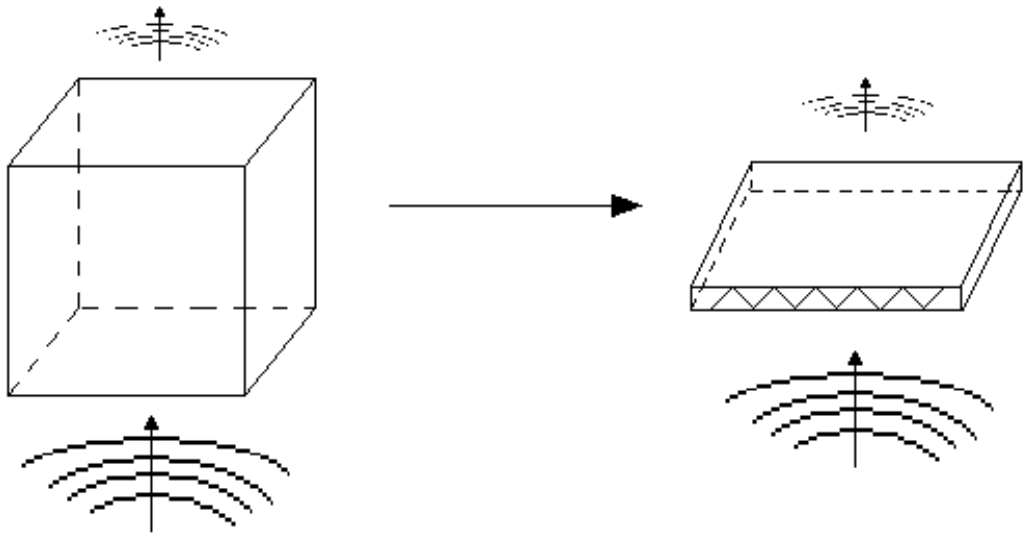

Figure 5. Acoustic wave are applied to a bulk phase (left) and a thin layer phase (right). The sound waves dissipate in the bulk phase. In the thin layer phase, sound waves are reflected off the liquid air interface back into the liquid.

and thus not induce large increases in mass transport and thereby current. Mild sonication may linearized the concentration profile locally as the fluid oscillates in response to the oscillator frequency. Linearization would tend to shift the voltammetric response from avian to sigmoidal.

CHAPTER 2

CONSTRUCTION AND GENERAL OPERATION OF THE THIN LAYER SONOELECTROCHEMICAL CELL

The sonoelectrochemical cells are based on an ultrasonic transducer that serves as the bottom face of a thin electrolyte volume in which three electrodes are deployed. The transducer and the electrochemical cell are on separate circuits. The electrodes are not in electrical contact with the transducer.

2.1 General Overview of System Components

Construction of the sonoelectrochemical cell system is a fusion of two independent systems: an acoustic energy generator and a standard electrochemical cell built around the transducer. Figure 6 is a schematic of the system.

2.2 Generation of Ultrasonic Waves

The central component of acoustic energy generation is the transducer, which acts as a speaker to produce mechanical vibrations of sound. The transducer is driven by a frequency generator, the signal of which is monitored with a digital oscilloscope.

2.2.1 Transducer

Ultrasonic sound waves are generated with a transducer. Commercial availability of low power, small scale transducers is limited. A commercially available Air Ultrasonic Ceramic Transducer (Prowave, T400ET/R180) was used. Figures 7 and

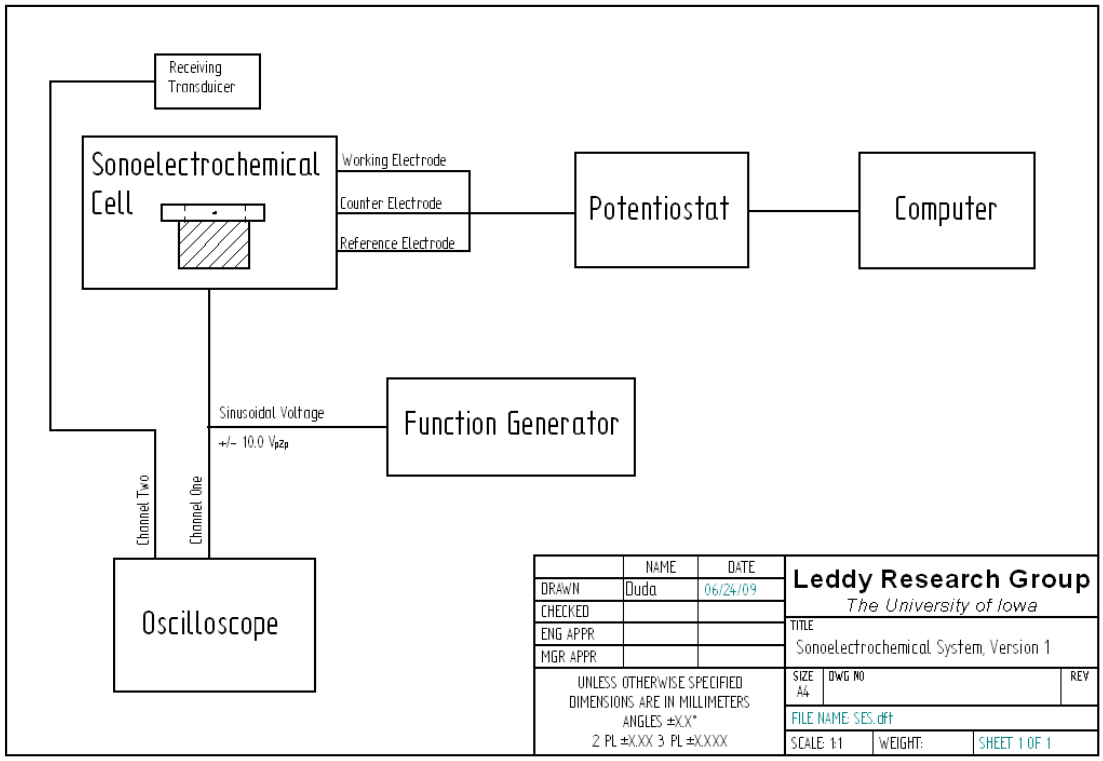

Figure 6. Schematic of the sonoelectrochemical system

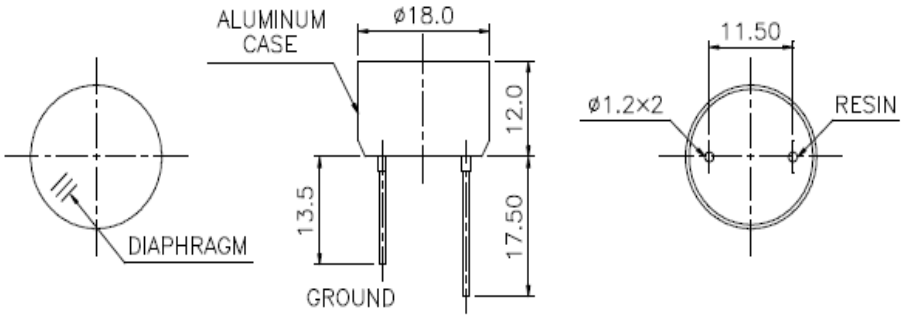

Figure 7. Manufacturer's diagram of transducer [1]

8. Aluminum encases a piece of piezoelectric material. The piezoelectric material expands and contracts in response to the oscillating potential. When the potential is modulated, sound waves at the frequency of modulation are produced. Intensity of the sound wave increases with increased potential.

2.2.2 Function Generator

The transducer is driven with a frequency generator that produces a sinusoidally modulated potential between -10 V and +10 V at a frequency of 41 kHz. The system utilizes a BK Precision 4011A 5 MHz Function Generator.

2.2.3 Signal Monitoring

Because the amplitude (intensity) of the modulated potential is not displayed by the function generator, the potential is monitored independently with a High Techniques IQ-300 Data Acquisition System (DAS) that serves as a dual channel oscilloscope.

Figure 8. Photograph of transducer components (Air Ultrasonic Ceramic Transducer, Prowave, T400ET/R180).

2.2.3.1 Direct Input Monitoring

The DAS was directly attached to the leads that connect the function generator to the transducer to monitor directly the driving potential applied to the transducer.

2.2.3.2 Indirect Output Monitoring

Because a transducer can perform as both transmitter and receiver (speaker and microphone), a second transducer was attached to a second channel on the DAS to confirm the generation of ultrasonic sound waves. The face of one transducer is placed directly in front of the face of the other transducer to make the measurement. This was primarily used to confirm that the transmitting transducer was functioning and was not included in other experimentation due to limited sensitivity.

2.3 Cell Configuration

The electrochemical cell is constructed above the face of the transducer. See Figure 9. The transducer forms the bottom of the well were the wall of the well is a hollow cylinder. The electrolyte solution rests in the well above the face of the transducer. The sides of the well support electrodes just above and parallel to the transducer face. The three electrodes are wires positioned radially between the inner cylinder wall and near the centerpoint of the circular cross section. See Figure 10, rightmost illustration for a topdown view.

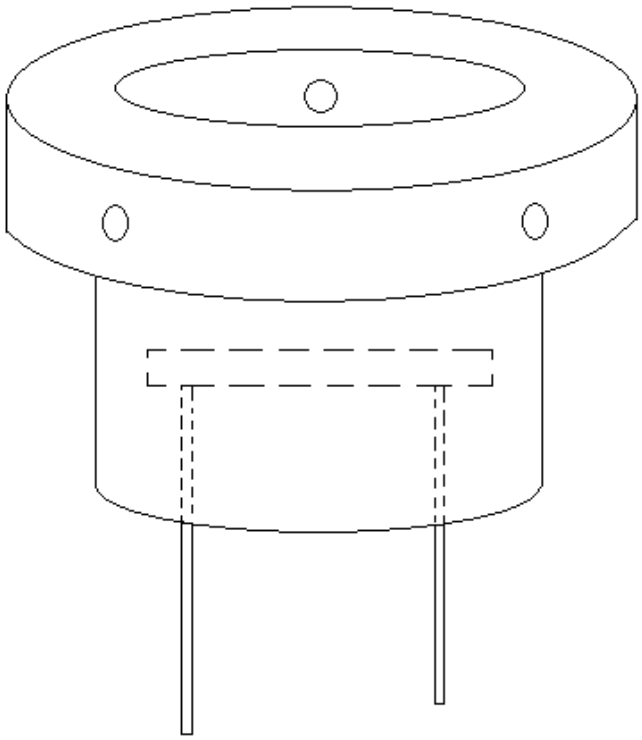

Figure 9. A well is constructed above a cylindrical transducer. The dashed line is the view of the transducer. The two wires below are the leads to the transducer. The solvent well is the hole open on top. The three small circles are holes for the insertion of the electrodes.

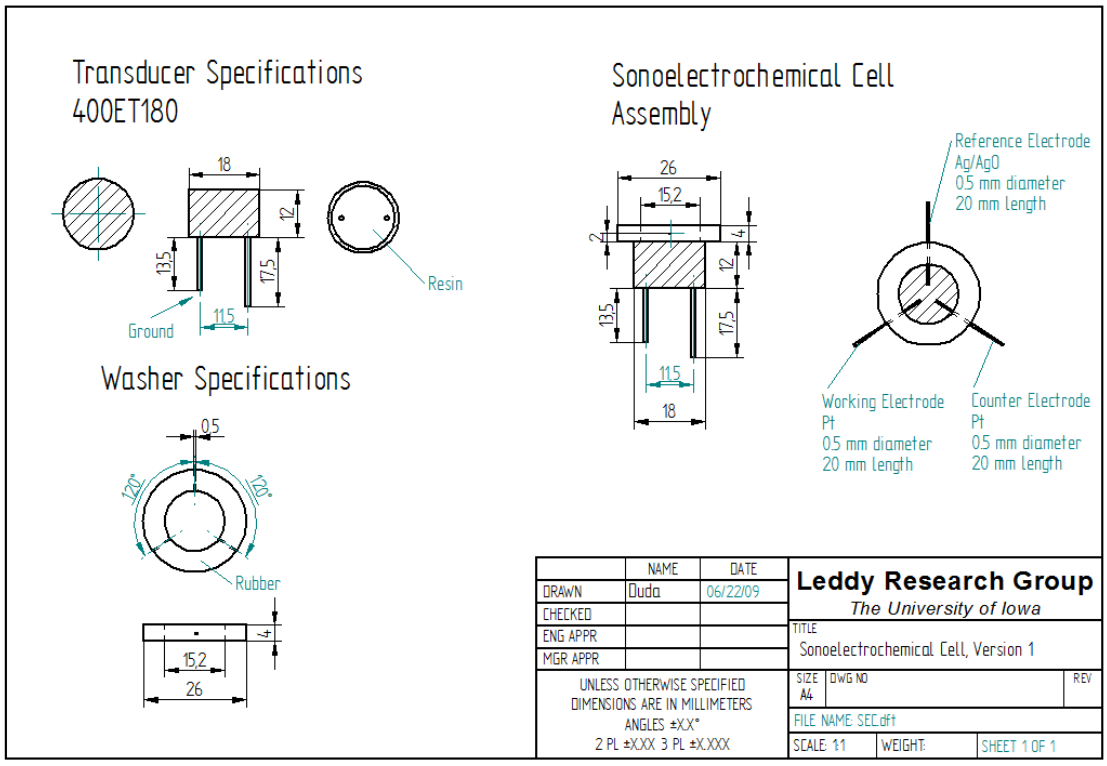

Figure 10. Blueprint of first generation sonoelectochemical cell

2.3.1 Original Configuration (Garden Hose Washer)

The original sonoelectrochemical cell was constructed with a garden hose washer composed of red rubber. Holes were punched through the edge of washer to accommodate the electrodes. The washer was then fastened to the face of the transducer with cyanoacrylate glue. See Figure 11.

2.3.2 Teflon Sheath with O-ring Seal

After the initial experiments were completed, a second cell was constructed.

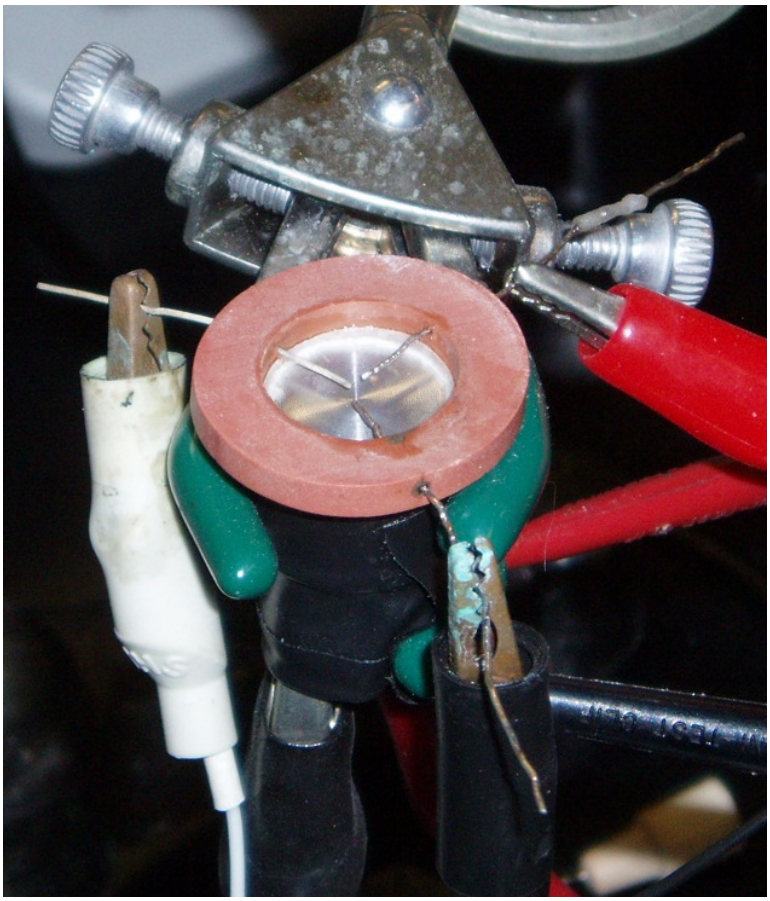

Figure 11. Photograph of the first generation sonoelectrochemical cell constructed from a garden hose washer glued to the face of the transducer. The working and counter electrodes are composed of platinum wires. The reference electrode is silver|silver oxide.

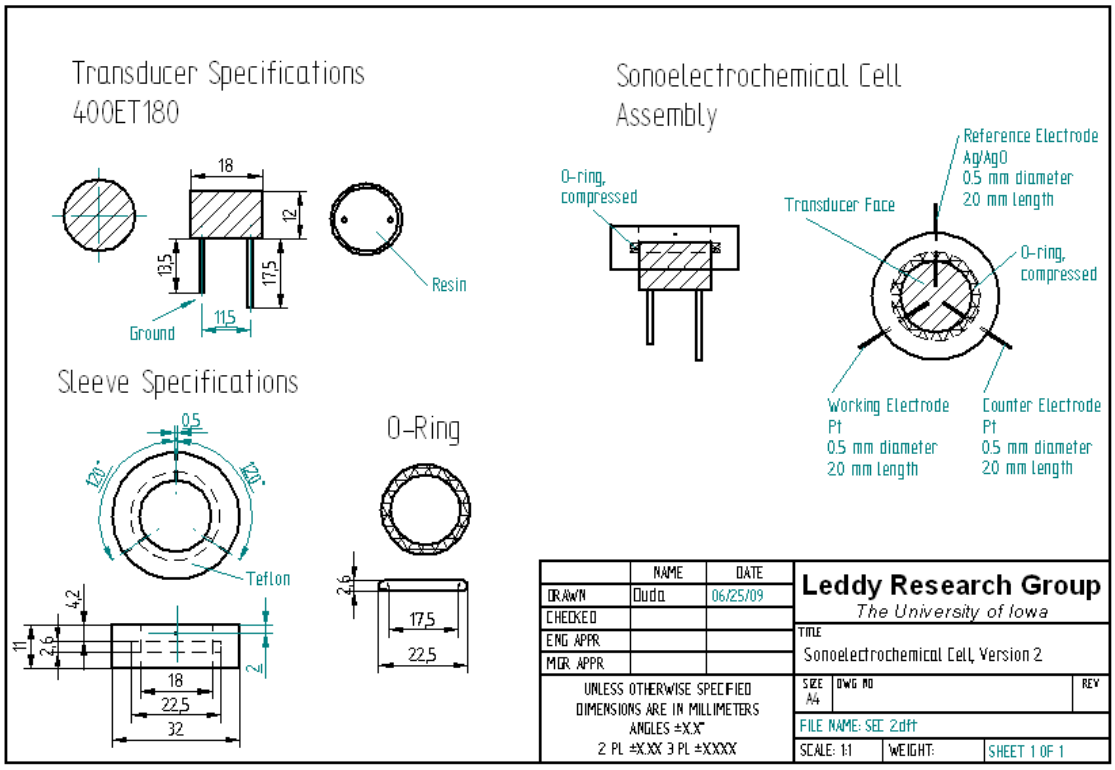

Figure 12. Blueprint of second generation sonoelectochemical cell. A hollow cyclindrical sleeve enshrouds the transducer in a manner similar to the garden hose washer.

Stock Teflon rod was machined to form a sleeve around the transducer. The Teflon structure replaces the rubber washer. The sleeve was sealed with an O-ring that rests below the face of the transducer. The sonoelectrochemical cell is held together by the snug fit of the components. No glue is used.

2.4 Relationship of Peak Voltage, V_p, to Pressure

The relationships between acoustic parameters and the input electrical signals that cause the piezoelectrical transducer to generate sound waves are numerous. To relate the acoustic forces generated by the transducer to the changes in the

Figure 13. Photograph of the second generation sonoelectrochemical cell constructed with a Teflon sleve to hold a thin layer of electrolyte above the transducer and around the wire electodes. The surface of transducer is the metallic disk seen below the three electrodes that are seperated by 120 degrees and pointed towared the center. All electrode are composed of platinum wire. The transducer is not in electrical contact with the electodes.

electrochemical reactions, a measurement of the signal driving the transducer must be related to the acoustic forces exerted at the electrode. The electrical input to drive the transducer is a sinusoidal voltage with a frequency of ∼41 kHz and amplitude of ∼10 volts. The peak voltage of the input signal can be converted to the sound pressure level data provided by the manufacturer. The sound pressure level measured at 30 cm in air, is related to the sound power level at the transducer which determines the acoustic forces at the electrode immersed in the solution. Steps and parameters are as follows.

2.4.1 V_p to V_{rms}

Peak voltage, V_p, is easily measured with an oscilloscope. A diagram of the oscilloscope trace and V_p is shown in Figure 14.

Because peak voltage is the measurement of a single point in a continuously varying signal that spans positive and negative values, it is not considered representative of the signal. The root mean square voltage (quadratic mean voltage), V_{rms} is used. Root mean square is calculated as the square root of the average of the sum of the square values of n terms. The V_{rms} reports the voltage signal that would be measured with a voltmeter.

$$X_{rms} = \sqrt{\frac{\sum_{i=1}^{n} x_i^2}{n}} \tag{3}$$

Many common waveforms have solutions that allow for direct conversion of peak amplitude (i.e., V_p) to root mean square voltage. The voltage signal used to drive

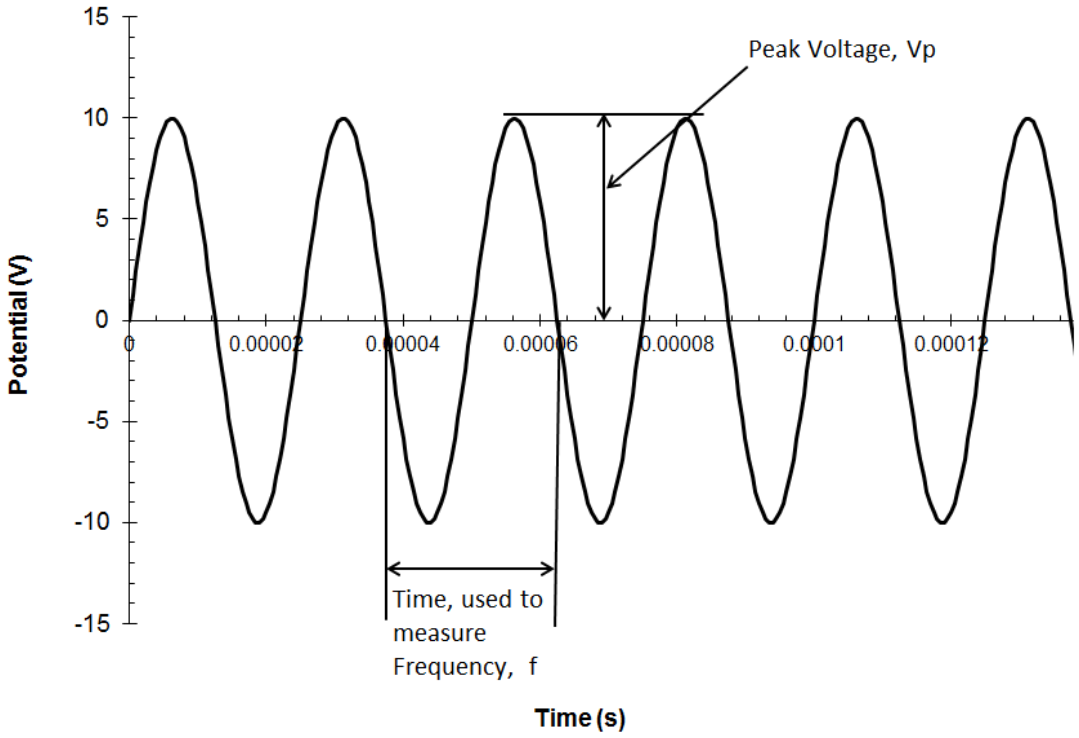

Figure 14. Plot of voltage as a function of time as would be measured with an oscilloscope. Sine wave shown is 40 kHz.

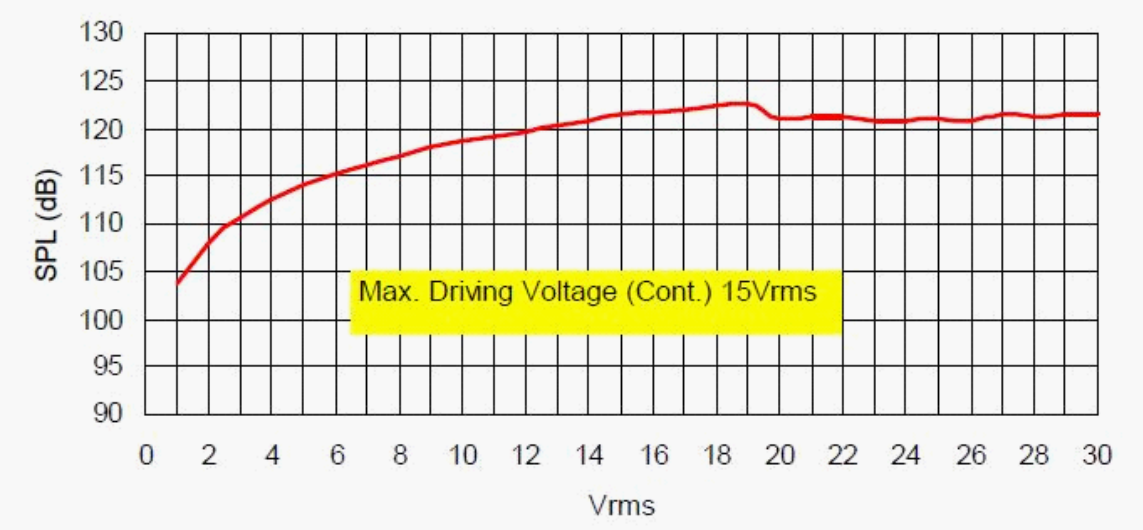

Figure 15. Manufacturer's plot of SPL as a function of V_{rms}. [1]

the transducer in this system is sinusoidal (i.e., sine wave), which allows the V_{rms} to be directly proportional to the V_p [33].

$$V_{rms} = \frac{V_p}{\sqrt{2}} \tag{4}$$

2.4.2 V_{rms} to SPL

The transducer manufacturer provides data that relates the root mean square voltage to the sound pressure level (SPL).

Sound pressure level, SPL, is measured in decibels (dB) and is defined as a logarithmic measure of the pressure of the sound relative to a standard as

$$SPL = 20 \log \left(\frac{p}{p_0} \right) \tag{5}$$

where p is the pressure exerted by the sound wave generated. The reference pressure

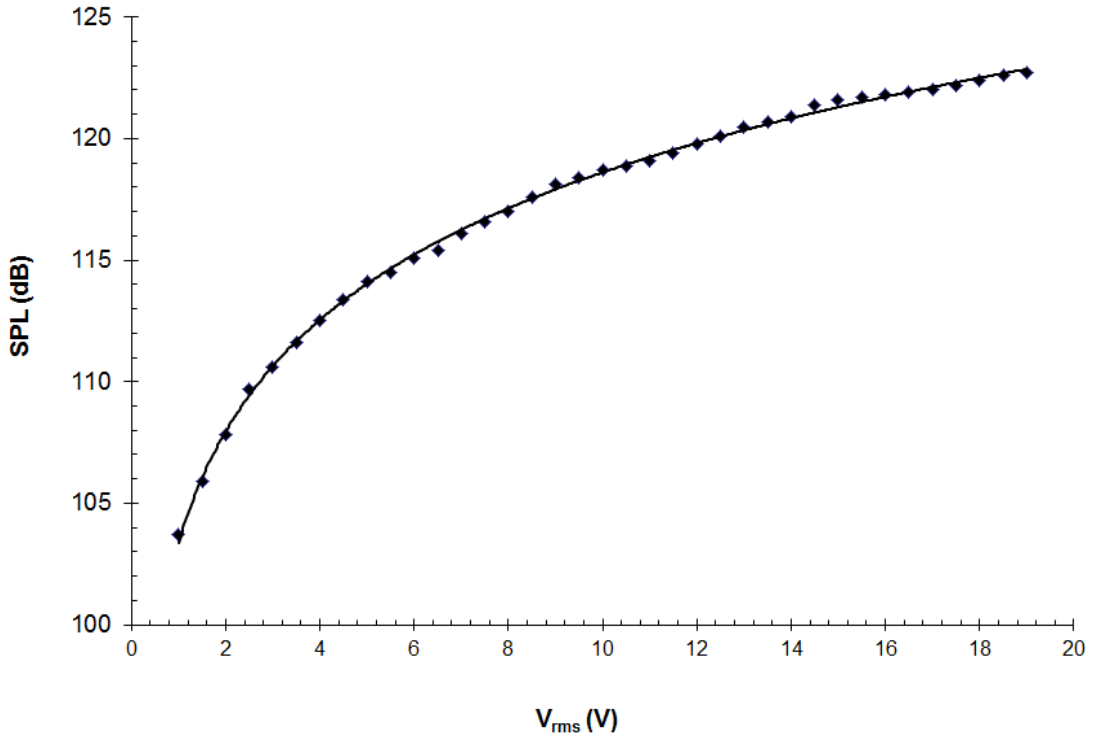

Figure 16. SPL as a function of V_{rms}. Points were taken from transducer manufacturer's data sheet. Logarithmic regression (solid line) yields $SPL = 6.6 \ln(V_{rms}) + 103.4$ with $R^2 = 0.999$.

level, p_o, is 20 μPa (rms), which is common in acoustics and is based on the threshold of human hearing [34, 35]. The decibel scale is commonly used in engineering, particularly acoustics, power, and electronics with references often determined by convention.

The data shown in Figure 15 are based on measurements taken in air at 30 cm distance from the transducer at 40 kHz [1].

Logarithmic regression of the manufacturer's data provides the relationship

$$SPL = 6.6 \ln(V_{rms}) + 103.4 \tag{6}$$

between V_{rms} and SPL. See Figure 16.

2.4.3 Relating Sound Pressure Level (SPL) to Sound Power Level (SWL)

To relate the manufacturer data (SPL, measured at distance) to the amount of acoustic energy at the electrode, the sound power level at the transducer must be determined so the changes in distance and medium from air to condensed fluid can be taken into account. Pressure is force per area and power is rate of energy delivery. Sound power level or sound watts level (SWL) is defined as a logarithmic measure of the sound power relative to a baseline standard. The formula is similar to that for sound pressure,

$$SWL = 10 \log \left(\frac{P}{P_0} \right) \tag{7}$$

where P is the frequency dependent sound power of the source in watts. The internationally accepted reference power level (P_0) is 1×10^{-12} W [35].

The relationship between SPL and SWL is dependent on the dimensionality of the source (i.e., point source, line source, or plane source) and the distance between the source and receiver, R. Here, the assumptions are a homogeneous medium and sound propagation from a single point source.

Acoustic Intensity Acoustic intensity is important in acoustics as a means of measuring SWL at a distance from the source (e.g., transducer). In a sound wave, acoustic intensity, $\overrightarrow{I}$, is a vector quantity that is the cross product of the pressure,

p, and the particle velocity, $\overrightarrow{v}$. Particle velocity should not be confused with either the speed of the wave (i.e., speed of sound) or molecular velocity. Particle velocity is essentially the speed at which particles oscillate around the initial position (rarefaction).

$$\overrightarrow{I} = p \times \overrightarrow{v} \tag{8}$$

Both acoustic intensity and particle velocity are vector quantities. The direction of the intensity is the average direction of energy flow. Average acoustic intensity is obtained by integration over time [36].

$$I = \frac{1}{T}\int_0^T p(t)v(t)dt \tag{9}$$

where T is the time, usually over the duration of a measurement or several wave cycles. The average acoustic intensity (also referred to, incorrectly, as instantaneous intensity) becomes power over unit area (e.g., W/m^2) and will be referred to as sound intensity, I, for the remainder of this document.

Characteristic acoustic impedance, z, is an intrinsic property of the medium defined as the product of the density, ρ, and the speed of sound, c, in the medium expressed in $N{\cdot}s/m^3$.

$$z = \rho c \tag{10}$$

Because the manufacturer's measurements were made in air and the electrodes in the sonoelectrochemical cell are immersed in solution characteristic acoustic impedance needs to be addressed. Water is 800 times denser than air and the speed of sound in water is 4.3 times greater. Thus, the characteristic acoustic impedance of water is 3500 times greater than air leading to 3500 times less intensity in water than air at

the same pressures. Physically, this means air molecules displace further from their original position than water molecules [3, 37].

Sound Intensity Sound intensity, I, derived from acoustic intensity above, is used as a measure of the rate of transport of kinetic energy through a medium, expressed in power per unit area (W/m^2).

$$I = \frac{P}{A} \tag{11}$$

where P is the sound power and A is the surface area through which the wave propagates.

Sound intensity can also be expressed as the square of the pressure over the characteristic acoustic impedance, z.

$$I = \frac{p^2}{z} \tag{12}$$

Sound pressure Sound pressure, p, can be related to the sound power, P, by combining Equations 11 and 12.

$$p^2 = \frac{Pz}{A} \tag{13}$$

This allows SPL to be related to SWL given [38]

$$P_0 = \frac{p_0^2}{z} \tag{14}$$

$$10\log\left(\frac{p^2}{p_0^2}\right) = 10\log\left(\frac{P}{P_0}\right) + 10\log\left(\frac{z}{z}\right) - 10\log(A) \tag{15}$$

$$10\log\left(\frac{z}{z}\right) = 0 \tag{16}$$

$$10\log\left(\frac{p^2}{p_0^2}\right) = 10\log\left(\frac{P}{P_0}\right) - 10\log(A) \tag{17}$$

This provides the SWL at the point of measurement, to find the SWL at the source dispersion and attenuation must be taken into account.

Dispersion The shape and distance from the source is contained in the area. For a point source with continuous output, the sound propagates out spherically through spherical concentric surface areas.

$$A = 4\pi R^2 \tag{18}$$

$$SPL = SWL - 10\log(4\pi R^2) \tag{19}$$

Sound from the transducer in the system radiates in a hemispherical fashion. To account for this, a geometric directivity factor, Q, is included in the area through which the sound propagates [39, 40].

$$SPL = SWL - 10\log\left(\frac{4\pi R^2}{Q}\right) \tag{20}$$

The geometric directivity factor, Q, is defined as the ratio of the intensity at some distance and angle from the source, I_θ, to the intensity at the same distance, if the total power from the source were radiated uniformly in all directions, I_u.

$$Q = \left(\frac{I_\theta}{I_u}\right)_R \tag{21}$$

The value for Q is unitless. For simple configurations where the field of intensity is either uniform or nonexistent, the value for Q is easily determined geometrically. In this case, because sounds propagates from surface of the transducer in a hemisphere, the value of Q is 2 [39, 40]. See Figure 17.

Attenuation Attenuation of the intensity of the sound wave is analogous to the Beer-Lambert law used for light [3]. Attenuation accounts for the acoustic energy

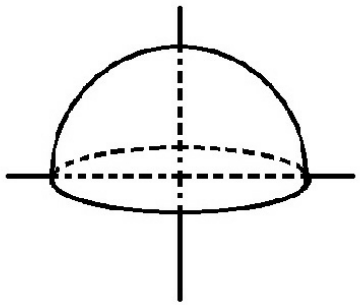

Figure 17. Sound propagates from the transducer surface in a hemisphere.

converted to heat and thus affects the pressure and temperature. For a sound wave

$$I = I_s \exp(-2\alpha R) \tag{22}$$

where I_s, is the intensity at the source, R is the distance from the receiver to the source and α is the attenuation coefficient. Note that the intensity at the source, I_s, is not the same as the reference intensity, I_0. The losses by attenuation are accounted in two components. Stokes deduced that frictional interactions from the translational movement of the molecules will result in conversion of some of the energy into heat [41]. Kirchhoff further added that there would be further losses due to thermal conduction within the medium. Because there are high and low pressure and temperature regions and heat will conduct from high to low temperature, the amount of work returned will be less that the amount needed to originally compress the medium [42]. Both of these effects are used to explain any acoustic energy that is converted into heat energy raising the temperature of the system. The corresponding equations for these two loss effects are combined to form

the attenuation coefficient [3]

$$\alpha = \frac{2\pi^2 f^2}{\rho c^3}\left\{\frac{4\eta}{3} + \frac{(\gamma-1)\,\kappa}{C_p}\right\} \tag{23}$$

where η is the viscosity of the medium, κ is the thermal conductivity of the medium, C_p is the molar heat capacity at constant pressure, and γ is the ratio of the heat capacity at constant pressure to constant volume. Note that attenuation is proportional to the square of the frequency. The effect of attenuation is inherent in any measurement of SPL. In that respect, losses from attenuation must be accounted in any attempt to relate the measurements made at a distance to the power at the source. To account for this, Equation 22 is rearranged and used as in additional term in Equation 20. Inclusion of the relationship in Equation 20 yields

$$10\log\left(\frac{I}{I_s}\right) = \frac{-20\alpha R}{2.3} \tag{24}$$

$$SPL = SWL - 10\log\left(\frac{4\pi R^2}{Q}\right) - \frac{20\alpha R}{2.3} \tag{25}$$

Combining Equations 4, 6 and 25 allows V_P to be used as a measure of the SWL.

$$SWL = 15.2\log\left(V_p\right) + 101.0 + 10\log\left(\frac{4\pi R^2}{2}\right) + \frac{20\alpha R}{2.3} \tag{26}$$

The manufacturer's data were taken at a distance, R, from the transducer of 0.30 m. The value for attenuation, α, in the air is 1.683 m^{-1} based on the values in Table 1.

This allows the plotting of both the P and SWL with relation to V_p. See Figure 18.

$$SWL = 15.2\log(V_p) + 98.6 \tag{27}$$

Table 1. Variables used to determine the attenuation coefficient in air.

Symbol	Constant	Value	Unit
f	Frequency	40,000	Hz
ρ	Density	1,161	g/m^3
c	Speed of sound	343.9	m/s
η	Viscosity	0.0186	g/m·s
C_p	Molar heat capacity, constant pressure	29.19	J/mol·K
C_v	Molar heat capacity, constant volume	20.85	J/mol·K
κ	Thermal conductivity	0.0262	W/K·m

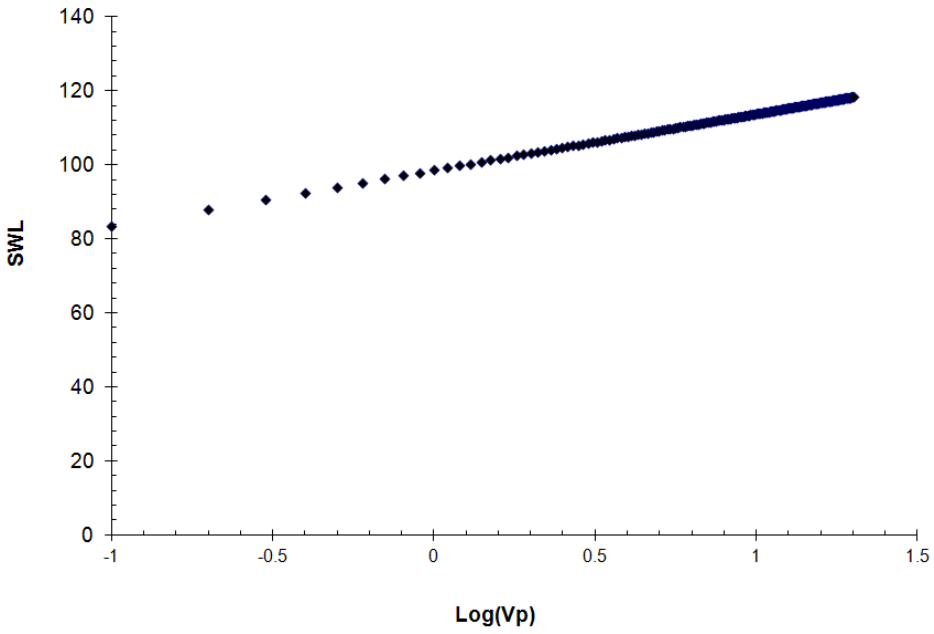

Figure 18. Plot of SWL versus $\log(V_p)$ as per Equation 27.

2.4.4 Estimated energy provided to the electrodes by acoustic forces

To calculate the acoustic energy at the electrode, the SWL at the source is used to calculate the SPL in the cell taking into account the change in medium and the affect of the change in distance. Equation 25 (below)

$$SPL = SWL - 10\log\left(\frac{4\pi R^2}{Q}\right) + \frac{-20\alpha R}{2.3} \qquad ((23))$$

is used to determine the SWL from the SPL based on the manufacturer's measurements made in air at a distance of 0.30 m. The same equation can be reversed to find the SPL at the electrodes by changing the terms used to compensate for dispersion and attenuation.

Dispersion Revisited Because the distance between the electrodes in relation to the source, R, is significantly shorter ($\sim$2.5 mm), the transceiver can no longer be treated as a point source. From the perspective of the electrodes, the transducer needs to be treated as a plane source because R is much smaller than the radius of the source, a, ($R<<a$). This calls for new terms accounting for radial dispersion of energy with a distance based term that accounts for the new configuration [38].

$$A = \frac{4\pi a^2}{\ln(1 + a^2/R^2)} \qquad (28)$$

$$SPL = SWL - 10\log\left(\frac{4\pi a^2}{\ln(1 + a^2/R^2)}\right) \qquad (29)$$

At short distances,

$$\ln\left(1 + \frac{a^2}{R^2}\right) \approx 2\ln\left(\frac{a}{R}\right) \qquad (30)$$

this simplifies Equation 29.

$$SPL = SWL - 10\log\left(\frac{2\pi a^2}{\ln(a/R)}\right) \tag{31}$$

It should be noted that the symbol a used for the determining dispersion in this section is different from the α that is used for the attenuation coefficient. The dispersion expressed in Equations 29 and 32 are based on the spatial relations between the source and receiver.

Attenuation Revisited The same principles of attenuation hold true for both point and planer sources. Expanding Equation 31 to non-logarithmic terms yields

$$\frac{p^2}{z} = P\frac{2\ln(a/R)}{4\pi a^2} \tag{32}$$

Because attenuation accounts for the acoustic energy converted to heat, inclusion of attenuation provides a relationship that demonstrates how the power, P, affects the pressure and temperature.

$$\frac{p^2}{z} = P\frac{2\ln(a/R)}{4\pi a^2}\exp[-2\alpha R] \tag{33}$$

Essentially, the attenuation term is fixed in a given medium. It represents the fraction of power that is retained to change the pressure in the medium. Whereas the amount of energy lost is dependent on distance from the source, the small values for α imply the amount of energy converted to heat is minimal at low frequencies. For air, α is 0.0168 that corresponds to a power loss of less than 0.01%. Water has an α of 1.00×10^{-5} based on the values in Table 2 that make attenuation in water negligible.

Table 2. Variables used to determine the attenuation coefficient in water.

Symbol	Constant	Value	Unit
f	Frequency	40,000	Hz
ρ	Density	995650	g/m^3
c	Speed of sound	1497	m/s
η	Viscosity	0.7977	g/m·s
C_p	Molar heat capacity, constant pressure	75.327	J/mol·K
C_v	Molar heat capacity, constant volume	74/53	J/mol·K
κ	Thermal conductivity	0.6154	W/K·m

Pressure at the Electrode Substitution of Equation 27 into Equation 31 with a value for a of 0.009 m and R of 0.0015 m provides a relationship between SPL as a function of V_p. Inclusion of Equation 5 allows expression directly in terms of pressure. The change in medium is accounted for by inclusion of the term $+10\log\left(\frac{z}{z}\right)$ to adjust for the change in characteristic acoustic impedance.

$$SWL = 15.2\log(V_p) + 98.6 \tag{34}$$

$$SPL = SWL + 10\log\left(\frac{z}{z}\right) - 10\log\left(\frac{2\pi a^2}{\ln(a/R)}\right) \tag{35}$$

$$SPL = 15.2\log(V_p) + 98.6 + 10\log\left(\frac{z}{z}\right) - 10\log\left(\frac{2\pi a^2}{\ln(a/R)}\right) \tag{36}$$

$$p = p_0 10^{0.05\left[15.2\log(V_p)+98.6+10\log\left(\frac{z}{z}\right)-10\log\left(\frac{2\pi a^2}{\ln(a/R)}\right)\right]} \tag{37}$$

This equation places the rms pressure generated by the unamplified system at 0.34 atm with a reasonably linear response over the working range of the system. See Figure 19.

2.4.5 Calculation of $V\Delta P$

To evaluate the data, the acoustic energy input is calcualted. The acoustic energy input ΔPV is taken as $V\Delta P$ because the acoustic energy will impart pressure to the

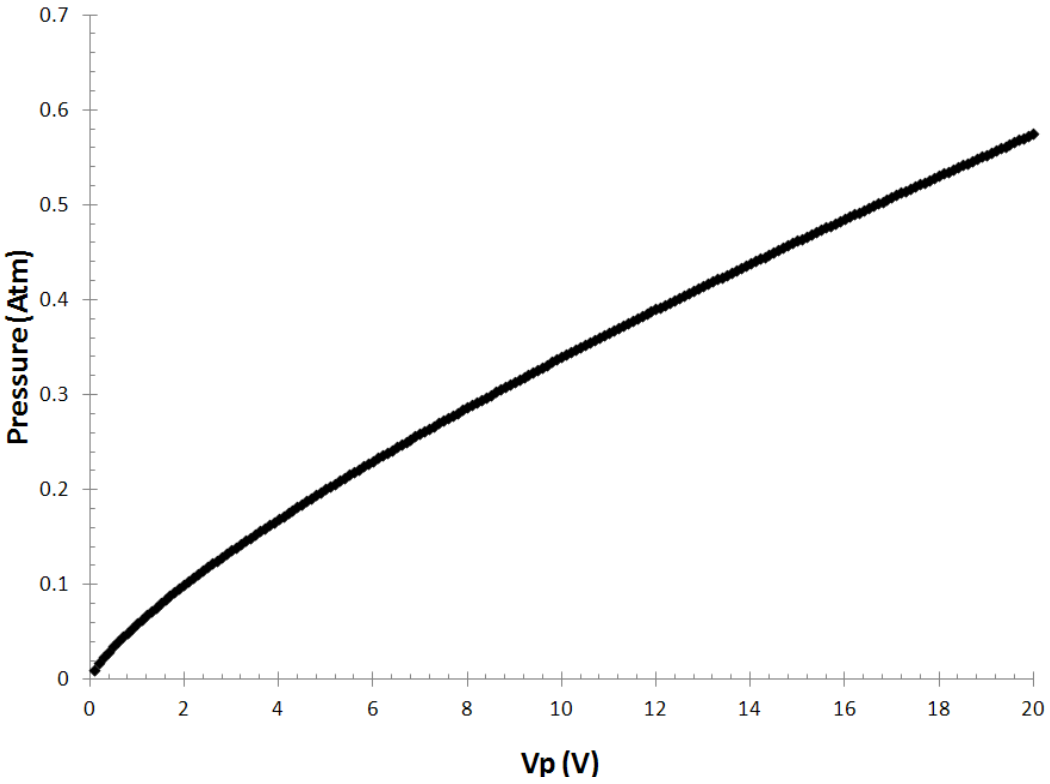

Figure 19. Plot of Equation 37 for the pressure at the transducer surface as a function of peak voltage.

solution but is not likely to impact volume. For ΔP in atmospheres and V in liters, the acoustic energy to the solution in J/mol is

$$Acoustic\ Energy\ to\ Solution = V\Delta P \times \frac{101.27\ J}{liter\ atm} \tag{38}$$

V is taken as the molar volume, 0.018 liters/liter. ΔP is calculated from equation 37 in pascals; the value 101.27 is part of the unit conversion.

$$p = p_0 10^{0.05\left[15.2\log(V_p)+98.6+10\log\left(\frac{z}{z}\right)-10\log\left(\frac{2\pi a^2}{\ln(a/R)}\right)\right]} \tag{39}$$

2.5 Electrochemical Measurements

Electrochemical measurements, specifically cyclic voltammetric sweeps, are performed in a standard three electrode configuration. Scan rate, electrode composition, probe concentration and sensitivity settings vary with experiment.

2.5.1 Potentiostat

Measurements were made with a BAS 100B Electrochemical Analyzer controlled with a HP pavilion 520W computer system under a Microsoft Windows 2000 operating system.

2.5.2 Electrode Generation

Unless otherwise specified, working and counter electrodes consisted of platinum wires 1.5 mm in diameter with 8 mm of length with all surfaces exposed to the solution. Reference electrodes were composed of either a similar piece of platinum wire (Pt|PtO) or 1.5 mm diameter silver wire reacted with concentrated nitric acid

($Ag|Ag_2O$).

2.5.3 Reference Stability

Sonication provides energy to the system. This energy can be used to enhance slow heterogeneous electron transfer kinetics. The energy can also be dissipated into the electrodes. Several electrode materials were found to be unstable. This included the current carrying electrodes as well as the reference electrode. Early measurements were undertaken with a silver | silver chloride reference electrode or a silver | silver oxide quasireference electrode. After the solution had been sonicated for several minutes, the silver | silver chloride reference electrodes were found occasionally to disintegrate. The silver deposited on the electrode and was stripped as the potential was scanned oxidatively. Because of the fragility of the silver reference electrodes and concerns about destroying the also fragile calomel reference electrodes, a platinum | platinum oxide quasireference electrode was used in all of the later studies.

2.6 General Measurement Protocol

The steps in the electrochemical protocol include preparation of the electrode surface and subsequent and electrochemical scans.

2.6.1 Preparation of System

Prior to every experiment, the cell was cleaned with nitric acid and rinsed with Millipore treated water. Platinum electrodes were soaked in concentrated nitric acid

and rinsed with deionized water (Milli Q). Silver | silver oxide reference electrodes were also regenerated with concentrated nitric acid. Prior to loading the system with solution, the acoustic system was started and checked for appropriate frequency and amplitude potential. The function generator was then turned off and solution was placed in the well forming a meniscus arching across the top of the well. Once solution was added to the cell, the bulk solution temperature was taken with a Fluke 62 Mini Infrared Thermometer.

2.6.2 Electrochemical Scans

Potential sweeps are proceeded by 5 second hold. Data were saved to a hard disk after each scan, after which acoustic settings were adjusted as individual experimental protocol required. Scans were typically conducted in sets of three to five for each sonication setting. Scan rates were typically set at 50 or 100 mV/s.

2.6.3 Maintenance

Electrical connections (e.g., alligator clips connecting the electrodes to the electrochemical analyzer) were regularly sanded and occasionally replaced to reduce electrical resistance. The transducer was replaced when inconsistent results were obtained.

CHAPTER 3

EFFECTS OF LOW INTENSITY SONICATION IN A THIN LAYER ON HETEROGENEOUS ELECTRON TRANSFER KINETICS

3.1 Introduction

In this study, it is demonstrated that the application of acoustic energy to thin layer electrochemical systems increases the standard heterogeneous electron transfer rate, k^0. This is the rate of electron transfer between the electrode and a redox species in solution at the electrode surface. Two one electron transfer probes are compared; one with a fast (reversible) heterogeneous electron transfer rate and one with an electron transfer rate comparable to the rate of voltage perturbation (quasireversible).

Tris(2,2'-bipyridyl)ruthenium(II) chloride hexahydrate, $Ru\,(bpy)_3^{2+}$ (Sigma-Aldrich) is a classic example of an outer sphere redox probe with fast heterogeneous electron transfer kinetics at platinum electrodes. Outer sphere electron transfers require no structural alteration on electon transfer.

$$Ru\,(bpy)_3^{3+} + e \rightleftharpoons Ru\,(bpy)_3^{2+} \tag{40}$$

Demonstration of the reversibility under cyclic voltammetric perturbation requires linear variation of the peak current with the square root of the scan rate and no change in peak splitting with scan rate [43]. These are verified for $Ru\,(bpy)_3^{2+}$data. The diffusion coefficient is determined by combination of the cyclic voltammetric

scan rate study and a rotating disk voltammetry at different rotation rates.

For comparison, ferric ion was chosen because $Fe^{3+} \mid Fe^{2+}$ is a classic example of a redox couple with slower heterogeneous electron transfer rates at platinum electrodes. The iron couple undergoes near outer sphere electron transfer and is typically regarded as an outer sphere electron transfer process.

$$Fe^{3+} + e \rightleftharpoons Fe^{2+} \tag{41}$$

Simple heterogeneous electrochemical reactions at an electrode have two components: mass transport where the reactant moves to the electrode surface and product moves away and electron transfer where an electron is transferred across the electrode solution interface between the electrode and the substrate that is at the electrode surface. Heterogenous electron transfer is illustrated in Figure 20.

3.1.1 Arrhenius Equation

Most rate constants, k, follow the Arrhenius equation that expresses the rate constant as a function of temperature, T (K),

$$k = A \exp\left(\frac{-E_A}{RT}\right) \tag{42}$$

where E_A (J/mol) is the activation energy, R is the gas constant and A is the frequency factor. The classical potential energy curve for a chemical reaction is shown in Figure 21. The energy of activation is the height of the energy barrier between reactants and the complex, here [X]. The exponential term characterizes the energy to bring the reactants to the top of the barrier. The frequency factor, A,

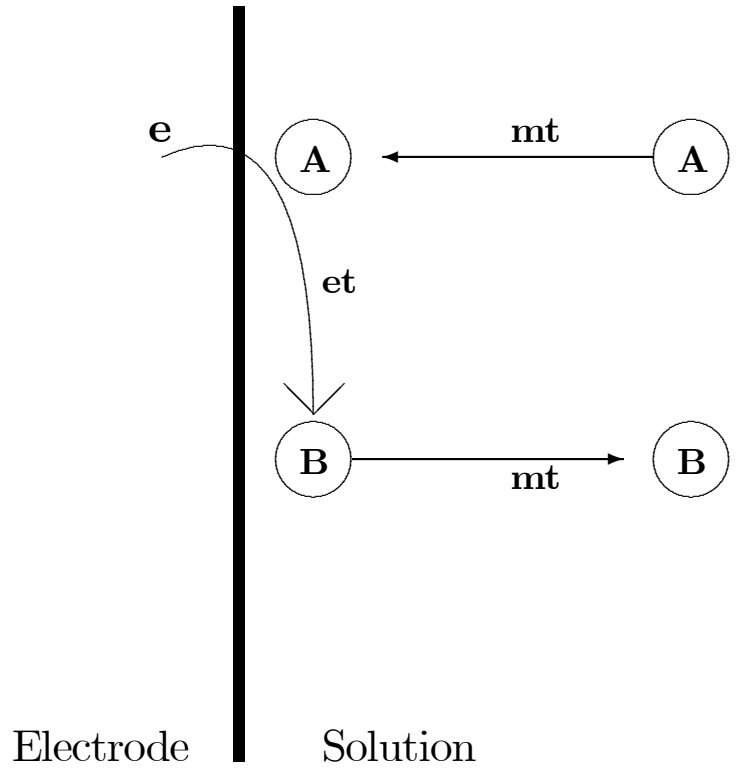

Figure 20. Heterogeneous electron transfer occurs across the electrode solution interface. Here, the reaction is $A + e \rightleftharpoons B$. The process of electron transfer involves mass transport (mt) of reactant to the electrode where it undergoes electron transfer (et) at the electrode surface to form product that then undergoes mass transport to the bulk of the solution.

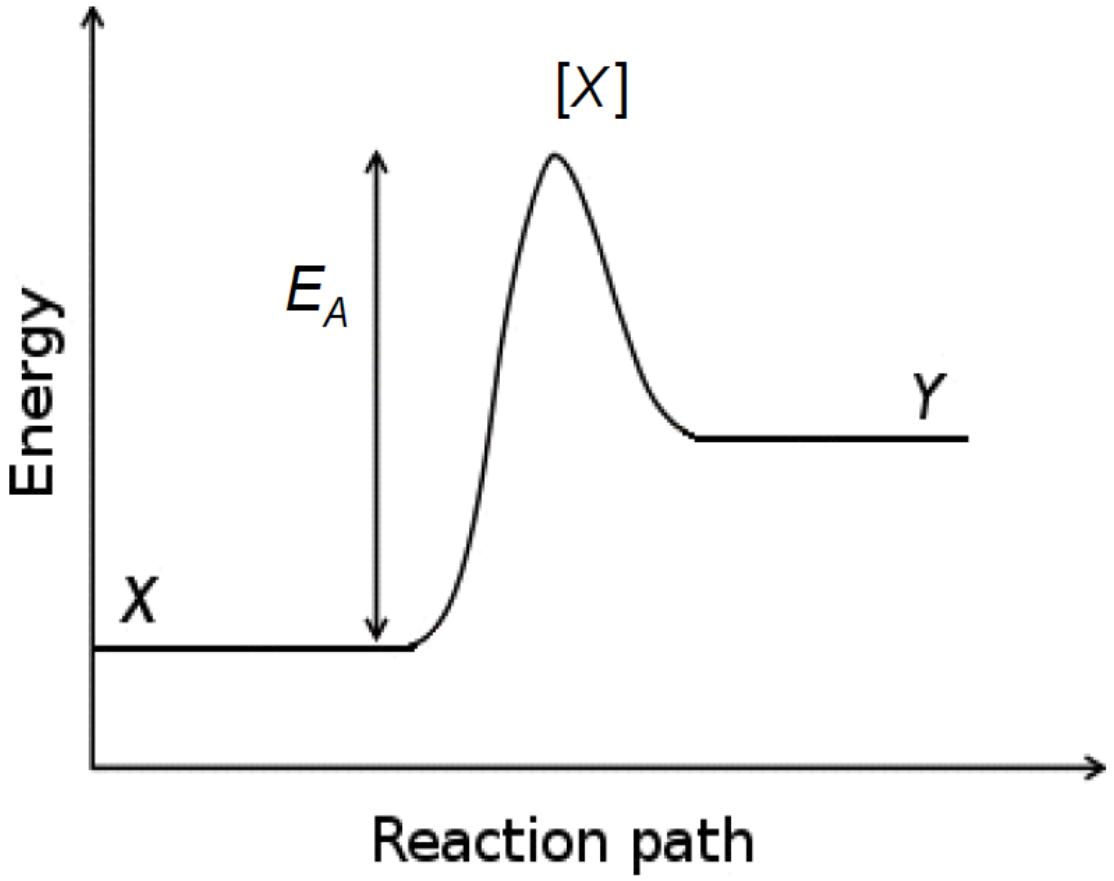

Figure 21. The energy along the reaction coordinate for the generic reaction $X \rightleftarrows Y$ is shown. The energy of activation, E_A, is measured from the reactant to the energy at the top of the curve where the complex $[X]$ is formed.

can represent the number of attempts on the barrier.

The rate of the reaction is expressed as

$$k = A \exp\left[-\frac{\Delta G^{\ddagger}}{RT}\right] \tag{43}$$

in activated complex theory and transition state theory where the free energy of activation, $\Delta G^{\ddagger}$, characterizes the enthalpy and the entropy of the reaction. The Gibb relationship relates $\Delta G^{\ddagger}$ to the enthalpy of activation, $\Delta H^{\ddagger}$, and entropy of

activation, $\Delta S^{\ddagger}$, as

$$\Delta G^{\ddagger} = \Delta H^{\ddagger} - T\Delta S^{\ddagger} \tag{44}$$

such that

$$k = A \exp\left[-\frac{\Delta H^{\ddagger}}{RT}\right] \exp\left[\frac{\Delta S^{\ddagger}}{R}\right] \tag{45}$$

For a system of fixed volume and pressure, $\Delta H^{\ddagger}$ sets the height of the barrier. The entropy describes the disorder or probability of states for the reaction. The width of the energy curve characterizes the entropy. Activated complex theory is illustrated in Figure 22 by the solid line where a complex [X] is formed that can fall back down the barrier to either reactant or product.

3.1.2 Effect of Sonication

In condensed phases of quiescent solutions, there is no change in pressure and volume of the bulk phase during a reaction. Sonication of a solution induces rarefaction and a concomitant change in pressure and volume. Classically, changes in pressure and volume are observed in gas phase reactions. When a gas expands, work is done such that energy is removed from the system and expelled into the surroundings; work, $w < 0$. When a condensed fluid is sonicated such that it undergoes rarefaction, work on the fluid induces significant changes in pressure. In rarefaction, work done on the system introduces energy into the system and $\omega > 0$.

In the context of the activation complex theory, the change in pressure volume lowers the height of the barrier $\Delta H^{\ddagger}$ by $\Delta\left(PV\right)^{\ddagger}$. For the condensed fluid, sonication provides sufficient energy to induce rarefaction. The energy lowers the barrier height as shown in Figure 22. Sound energy increases the reaction rate by decreasing the

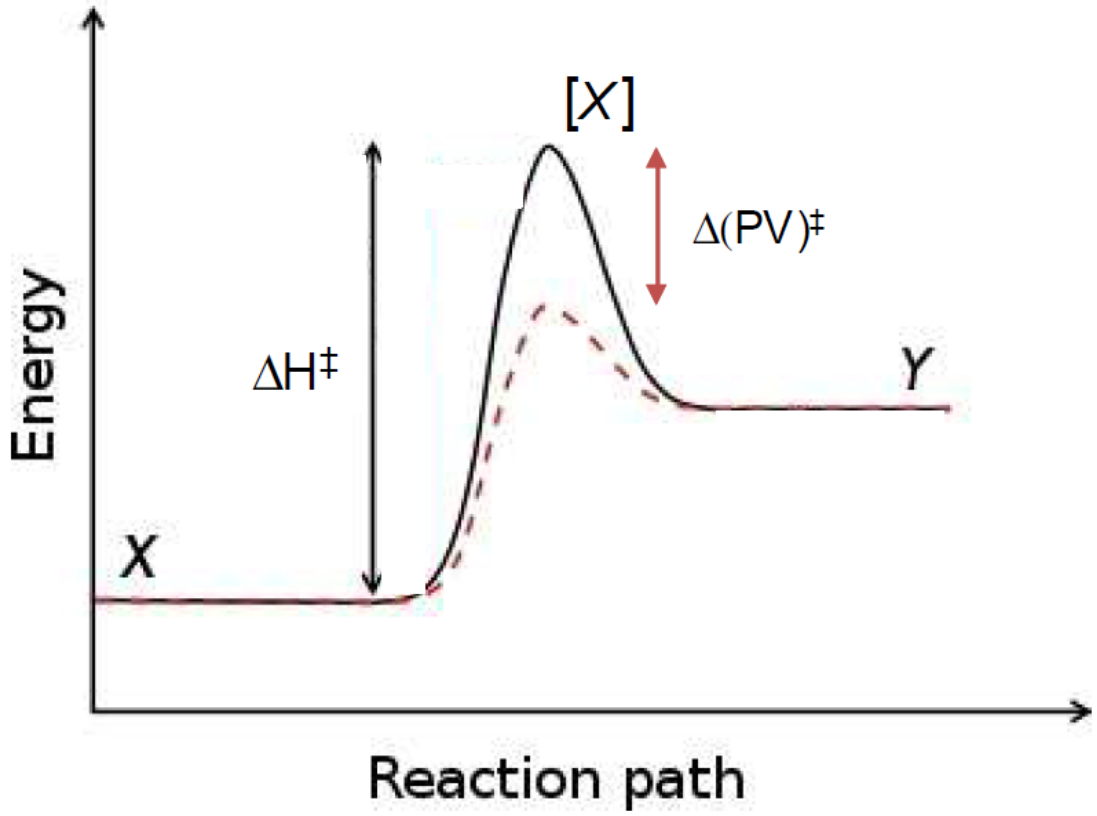

Figure 22. The energy along the reaction coordinate for the generic reaction $X \rightleftarrows Y$ is modified to account for the impact of acoustic energy provided to the reaction. The impact is to lower the energy of the barrier. The height of the barrier is now lowered by the acoustic energy as it is transformed into a change in pressure volume of activation, $\Delta\left(PV\right)^{\ddagger}$.

enthalpy.

The impact of sonication on kinetics manifests in the reduced energy barrier. In the rate equation, the enthalpy term in Equation 45 reflects the change in pressure volume in the condensed phase. Let the free energy of activation, enthalpy, and entropy in the absence of sonication are denoted $\Delta G_{\emptyset}^{\ddagger}$, $\Delta H_{\emptyset}^{\ddagger}$, and $\Delta S_{\emptyset}^{\ddagger}$. At this

point, it is assumed the entropy is not altered by sonication.

$$k = A\exp\left[-\frac{\left(\Delta H_{\emptyset}^{\ddagger} - \Delta\left(PV\right)^{\ddagger}\right)}{RT}\right]\exp\left[\frac{\Delta S_{\emptyset}^{\ddagger}}{R}\right] \quad (46)$$

$$= A\exp\left[\frac{\Delta\left(PV\right)^{\ddagger}}{RT}\right]\exp\left[-\frac{\Delta H_{\emptyset}^{\ddagger}}{RT}\right]\exp\left[\frac{\Delta S_{\emptyset}^{\ddagger}}{R}\right] \quad (47)$$

$$= A\exp\left[\frac{\Delta\left(PV\right)^{\ddagger}}{RT}\right]\exp\left[-\frac{\Delta G_{\emptyset}^{\ddagger}}{RT}\right] \quad (48)$$

Thus, the rate is expected to increase exponentially with $\Delta\left(PV\right)^{\ddagger}$ as sonication lowers the enthalpy.

3.1.3 Electron Transfer Kinetics and Impacts of Sonication

The kinetic model for one electron transfer is outlined by Bard and Faulkner [2]. A single electron transfer is characterized by a formal potential, $E^{0'}$.

$$O + e \rightleftarrows R \qquad E^{0'} \quad (49)$$

The process can be considered as two reactions, each the reverse of the other.

$$O + e \xrightarrow{k_{red}} R \quad (50)$$

$$R \xrightarrow{k_{ox}} O + e \quad (51)$$

Consider the parabolic potential energy surfaces shown in Figure 23, taken from reference [2]. The curve on the left corresponds to reactant $O + e$ and the curve on the right to product R. The intersection of the parabolas forms the energy barrier analogous to that illustrated in Figure 22. At applied potential $E^{0'}$, the height of the barrier is the same for the reactants and products. Let the barrier height be

represented as $\Delta G^{\ddagger}_{0c}$ and $\Delta G^{\ddagger}_{0a}$ for the reactants and product, respectively. The zero subscript corresponds to standard conditions where the applied potential is equal to $E^{0'}$. The symmetry of the intersection of the reactant and product curves at the top of the barrier is characterized by a symmetry factor, the transfer coefficient, α. Values of α are defined between 0 and 1 with values most typically $\alpha = 0.5$; corresponds to a symmetric intersection at the top of the barrier.

A unique advantage of electrochemistry is that control of the applied potential E corresponds to control of the free energy of activation. The applied potential alters the reactant and product activation free energies as

$$\Delta G^{\ddagger}_{c} = \Delta G^{\ddagger}_{0c} + \alpha F(E - E^{0'}) \tag{52}$$

$$\Delta G^{\ddagger}_{a} = \Delta G^{\ddagger}_{0a} - (1-\alpha) F(E - E^{0'}) \tag{53}$$

where F is Faraday constant, 96485 C/mole. The rate constants are of an Arrhenius form and expressed as

$$k_{red} = A \exp\left(\frac{-\Delta G^{\ddagger}_{c}}{RT}\right) \tag{54}$$

$$= A \exp\left(\frac{-\Delta G^{\ddagger}_{0c}}{RT}\right) \exp\left[\frac{-\alpha F}{RT}(E - E^{0'})\right] \tag{55}$$

$$k_{ox} = A \exp\left(\frac{-\Delta G^{\ddagger}_{a}}{RT}\right) \tag{56}$$

$$= A \exp\left(\frac{-\Delta G^{\ddagger}_{0a}}{RT}\right) \exp\left[\frac{(1-\alpha) F}{RT}(E - E^{0'})\right] \tag{57}$$

Because $\Delta G^{\ddagger}_{0c} = \Delta G^{\ddagger}_{0a} = \Delta G^{\ddagger}_{0}$, the rates are expressed in terms of a standard heterogeneous rate constant, k^0 (cm/s). When the potential applied to the electrode

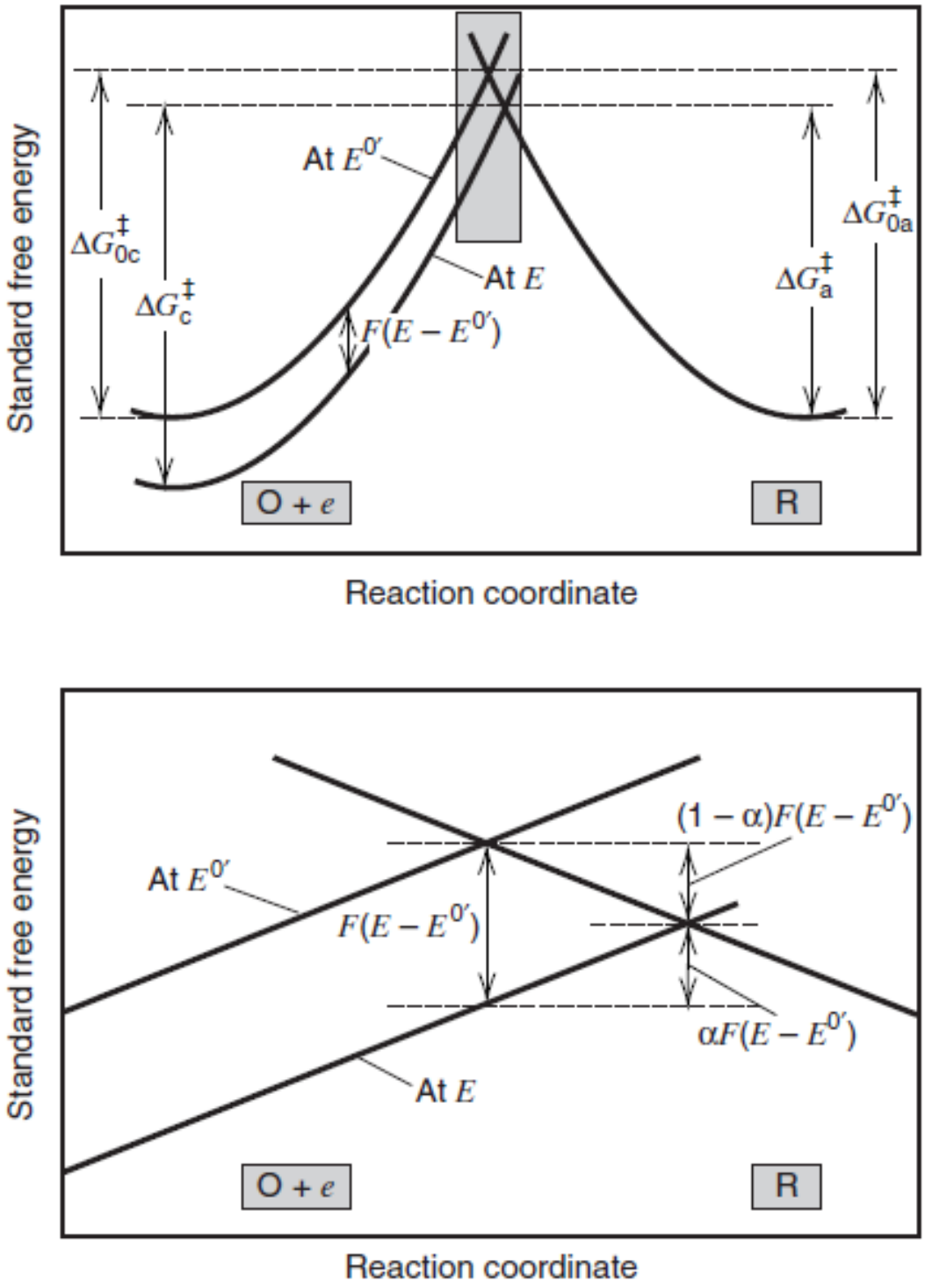

Figure 23. The potential energy surface for an electron transfer at the electrode surface is shown. This schematic includes effects of changes in the electrode potential on the energy surface and thus the energetics of the electron transfer process. The image is Figure 3.2.2 in Reference [2].

is $E^{0'}$, $k_{red} = k_{ox} = k^0$.

$$k_{red} = k^0 \exp\left[\frac{-\alpha F}{RT}(E - E^{0'})\right] \tag{58}$$

$$k_{ox} = k^0 \exp\left[\frac{(1-\alpha) F}{RT}(E - E^{0'})\right] \tag{59}$$

The flux at the electrode surface is expressed as $i\,(t)\,/nFA$ where $i\,(t)$ is the current at time t, n is the number of electrons transferred typically one, and A is the area of the electrode surface (cm^2). For concentrations of O and R at the electrode surface, $C_O\,(0,t)$ and $C_R\,(0,t)$, the rate of electrolysis is expressed [2] as the difference in the rates of reduction and oxidation.

$$\frac{i(t)}{nFA} = k_{red} C_O(0,t) - k_{ox} C_R(0,t) \tag{60}$$

Substitution into equation 60 of equations 58 and 59 yields an expression, the current potential characteristic.

$$i = FAk^0 \left[C_O(0,t) \exp\left(\frac{-\alpha F}{RT}(E - E^{0'})\right) - C_R(0,t) \exp\left(\frac{(1-\alpha)F}{RT}(E - E^{0'})\right)\right] \tag{61}$$

k^0 is of Arrhenius form.

$$k^0 = A \exp\left(\frac{-\Delta G_0^{\ddagger}}{RT}\right) \tag{62}$$

It is anticipated that sonication will impact heterogeneous electron transfer in a manner analogous to that outlined in section 3.1.2. By analogy to equation 48, equation 61 is

$$i = FAk^0 \exp\left(\frac{\Delta (PV)^{\ddagger}}{RT}\right) \begin{bmatrix} C_O(0,t) \exp\left(\frac{-\alpha F}{RT}(E - E^{0'})\right) \\ -C_R(0,t) \exp\left(\frac{(1-\alpha)F}{RT}(E - E^{0'})\right) \end{bmatrix} \tag{63}$$

Other impacts of sonication on the heterogeneous electron transfer rate are possible.

3.1.4 Mass Transport

In cyclic voltammetry for a species O in solution, potential is swept from a potential several hundred millivolts positive of $E^{0'}$ to a potential several hundred millivolts negative of $E^{0'}$. At early potentials, the driving force for conversion of O to R is small and little or no current passes. As the potential is swept closer to $E^{0'}$, the conversion of O to R at the electrode surface is enhanced. At applied potential $E^{0'}$, half of the O immediately at the electrode surface is electrolyzed for a high k^0. As potential is swept negative of $E^{0'}$, the electrolysis of O is mass transport limited and the concentration of O at the electrode surface goes to zero. On the reverse sweep, the R generated on the forward sweep is electrolyzed back to O analogously to the forward sweep.

The concentration of O and R on the forward sweep is perturbed over a thickness, the diffusion length that is dependent on the time of electrolysis. For a sweep at 100 mV/s over a 1 V range, the electrolysis of O is effective for approximately half the forward sweep, or about 5 s. The diffusion length, ℓ, is calculated as

$$\ell = \sqrt{Dt} \tag{64}$$

where D is the diffusion coefficient for O. Allow $D \sim 5 \times 10^{-6}$ cm^2/s. The diffusion length is about 5×10^{-3} cm or 50 μm.

Under mild sonication that does not cause bulk turbulence, sound waves cause

displacement of fluid over a domain where the fluid is moved back and forth about the fluids initial position. There is no net transport of fluid as would be observed in, for example, rotating disk voltammetry and other voltammetric methods where forced fluid flow yields net fluid displacement. Under mild sonication, the fluid is oscillated about an initial point. The fluid displacement can be roughly approximated as

$$\Delta \sim \sqrt{D/f} \tag{65}$$

where f is the frequency of the oscillator. Oscillators are commonly 40 kHz or 4×10^4/s. For $D \sim 5 \times 10^{-6}$ cm^2/s, $\Delta \sim 1 \times 10^{-5}$ cm or 0.1 μm.

On a cyclic voltammetric time scale, $\ell \sim 500\Delta$. Sonication will not significantly alter the diffusion length and therefore under mild sonication, impacts on mass transport observed under force transport that yield net solvent displacement are not anticipated. For voltammetry in a quiescent solution, the concentration profile at the electrode surface is characterized by erf $\left[x/\sqrt{4Dt}\right]$ that has a gradually rising and slightly rounded functional form that drops over a thickness approximated by ℓ. Sonication may tend to generate local homogenization of the concentration profile such that the concentration profile is somewhat linearized. If the concentration profile is linearized in this manner, the avian cyclic voltammetric shape observed in quiescent solution may assume some sigmoidal character.

No substantial increase in mass transport is anticipated under mild sonication. Some linearization of the concentration profile caused by fluid oscillation but not net fluid displacement may shift the voltammetric response from avian toward sigmoidal. No large increases in current are anticipated.

3.2 Experimental

The experimental protocols are as follows.

3.2.1 Cyclic voltammetry and rotating disk

Electrochemical Cell The electrochemical cell is a 100 mL beaker with the working, counter and reference electrode suspended in solution. The electrodes are arranged as to be equidistant and to remain out of contact with the beaker.

Working Electrode A glassy carbon electrode with a Teflon sheath (Pine Instruments, 0.437 cm^2) was rinsed with deionized water (Millipore Model Milli Q plus 18.2 MΩ) and polished by hand with a polishing pad and successive 1, 0.5 and 0.05 alumina oxide polishing powers (Buehler). The electrode surface was again rinsed with deionized water.

Counter and Reference Electrodes The counter electrode was a platinum mesh wire (Sigma-Aldrich, 52 mesh, 1 in^2). Prior to use, the electrode was immersed in concentrated nitric acid (Fisher Scientific) for two minutes and rinsed in deionized water. The reference electrode was a saturated calomel electrode (SCE) cleaned with a brief rinse with deionized water (Millipore Model Milli Q plus 18.2 MΩ).

Electrolyte A solution of 0.100 M nitric acid (Fisher Scientific) in deionized water (Millipore Model Milli Q plus 18.2 MΩ) was used as the electrolyte.

Materials Unless otherwise noted, all chemicals used were obtained from Sigma-Aldrich Chemical Co. and were used as received. Tris(2,2'-bipyridyl)dichlororuthenium(II) hexahydrate ($Ru\,(bpy)_3^{2+}$) is a commercially

available redox probe. A 1.00 mM solution of $Ru\,(bpy)_3^{2+}$ in 0.100 M nitric acid electrolyte was used to study a fast electron transfer.

Rotation The working electrode was rotated with an adjustable speed analytical rotor (Pine Research Instrumentation, model AFASR) at rotation speeds of 600, 700, 800, 900 and 1000 rpm. To eliminate bias of sequence of rotation rate, voltammetric scans were taken in random order of rotation rate.

Voltammetry A BAS 100B Electrochemical Analyzer was used to collect all voltammetry measurements. Voltammograms were recorded at scan rates of 0.1, 0.2, 0.3, 0.4, and 0.5 V/s. To eliminate bias of scan rate sequence, voltametric scans were taken in random order of scan rate.

3.2.2 Sonoelectrochemical cell with $Ru\,(bpy)_3^{2+}$ or Fe^{3+}

Electrochemical Cell A second generation sonoelectrochemical cell as described in Chapter 2 was cleaned with concentrated nitric acid (Fisher Scientific) and deionized water (Millipore Model Milli Q plus 18.2 MΩ). Unless otherwise noted, a nitrogen blanket was set up to surround the sonoelectochemical cell.

Working and Counter Electrodes The working and counter electrodes consisted of 0.5 mm platinum wire (Sigma-Aldrich) inserted 8 mm into the solution. Prior to use, the electrode was immersed in concentrated nitric acid (Fisher Scientific) for four minutes and rinsed in deionized water (Millipore Model Milli Q plus 18.2 MΩ).

Reference Electrodes The reference electrode used with the $Ru\,(bpy)_3^{2+}$ solution was a silver | silver oxide electrode constructed from 0.5 mm silver wire

(Sigma-Aldrich) dipped in nitric acid (Fisher Scientific) for 1 minute and rinsed with deionized water (Millipore Model Milli Q plus 18.2 MΩ). The reference electrode used with the Fe^{3+} solution consisted of 0.5 mm platinum wire (Sigma-Aldrich) inserted 8 mm into the solution. Prior to use the electrode was immersed in concentrated nitric acid (Fisher Scientific) for four minutes and rinsed in deionized water (Millipore Model Milli Q plus 18.2 MΩ).

Electrolyte A solution of 0.500 M nitric acid (Fisher Scientific) in deionized water (Millipore Model Milli Q plus 18.2 MΩ) was used as the electrolyte.

Materials Unless otherwise noted, all chemicals used were obtained by Sigma-Aldrich Chemical Co. and were used as received. Tris(2,2'-bipyridyl)dichlororuthenium(II) hexahydrate ($Ru\,(bpy)_3^{2+}$) and iron (III) nitrate nonahydrate (Fe^{3+}) are commercially available redox probes. A 8.50 mM solution of $Ru\,(bpy)_3^{2+}$ in 0.500 M nitric acid electrolyte and a 0.500 mM solution of Fe^{3+} in 0.500 M nitric acid electrolyte were used as a redox probes. Unless otherwise noted, all solutions were degassed with nitrogen gas for 15 minutes. 1 mL of either solution was placed in the sonoelectochemical cell well with a disposable pipet creating a meniscus approximately 3 mm above the top of the well.

Sonication Sound waves were generated in the sonoelectrochemical cell at a frequency of 41 kHz. Unless otherwise noted, intensity was varied from 100 % (maximum) down to approximately 30 % in roughly 10 % increments. Unsonicated scans were run before and after the sonication sets. Peak voltage (V_p) of the transducer was monitored with an oscilloscope. Where noted, sonication intensity was set in random order to eliminate bias.

Voltammetry A BAS 100B Electrochemical Analyzer is used to collect all voltammetry measurements. Voltammograms are recorded at scan rates of 0.05 or 0.1 V/s as noted.

3.3 Voltammetric Results for $Ru\,(bpy)_3^{2+}$ and Fe^{3+} Redox Probes with and without Sonication

The experimental results are as follows.

3.3.1 Determination of the Diffusion Coefficient of $Ru\,(bpy)_3^{2+}$

Cyclic voltammetric scans run at scan rates of 0.1, 0.2, 0.3, 0.4, and 0.5 V/s are shown in Figure 24. With the same stock solution and electrodes, rotating disks scans are run with the rotation speeds of 600, 700, 800, 900, and 1000 rpm at a scan rate of 0.1 V/s. The rotating disk voltammetry results are presented in Figure 25.

From the cyclic voltammetric scans a plot of peak current as a function of the square root of the scan rate was generated. A plot was made for the rotating disk data of limiting current as a function of the square root of the rotation speed. In cyclic voltammetry, the peak current for a reversible system is given by the Randles-Sevcik equation [2]:

$$i_p = (2.69 \times 10^5) n^{\frac{3}{2}} A D_o^{1/2} C_o^* \upsilon^{\frac{1}{2}} \tag{66}$$

where n is the number of electrons, C^* is the bulk concentration and υ is the scan rate. Figure 24 shows that the difference in peak potentials, ΔE_p, does not change with scan rate, υ. Furthermore, Figure 26 shows a linear relationship

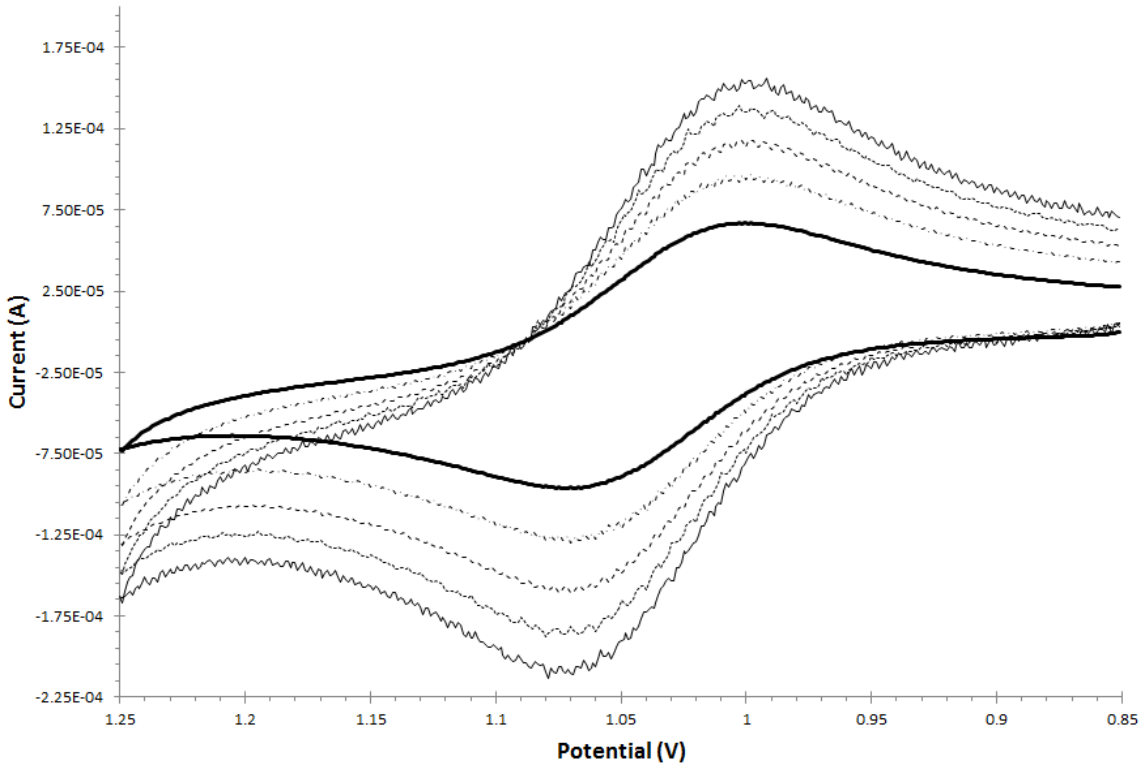

Figure 24. Cyclic voltammetry scans of 1.00 mM $Ru\,(bpy)_3^{2+}$ taken at different scan rates: (lowest maximum peak to highest) 0.1, 0.2, 0.3, 0.4, and 0.5 V/s. Note the difference in peak potentials do not change with scan rate.

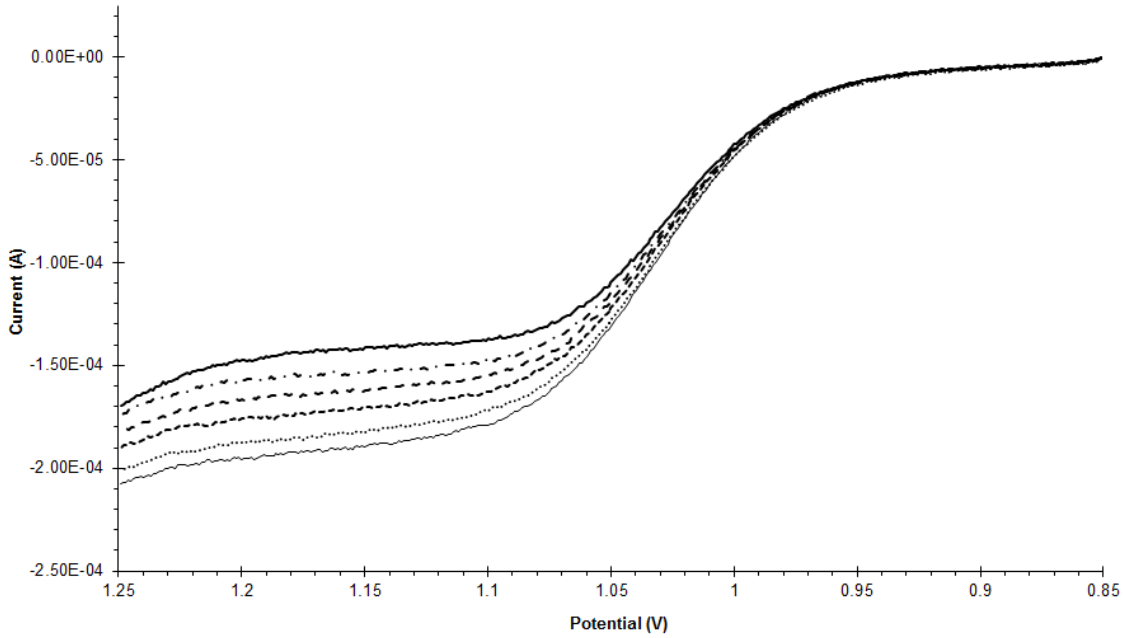

Figure 25. Rotating disk scans of 1.00 mM $Ru\,(bpy)_3^{2+/3+}$ taken at different rotation speeds: (lowest maximum peak to highest) 600, 700, 800, 900, and 1000 rpm.

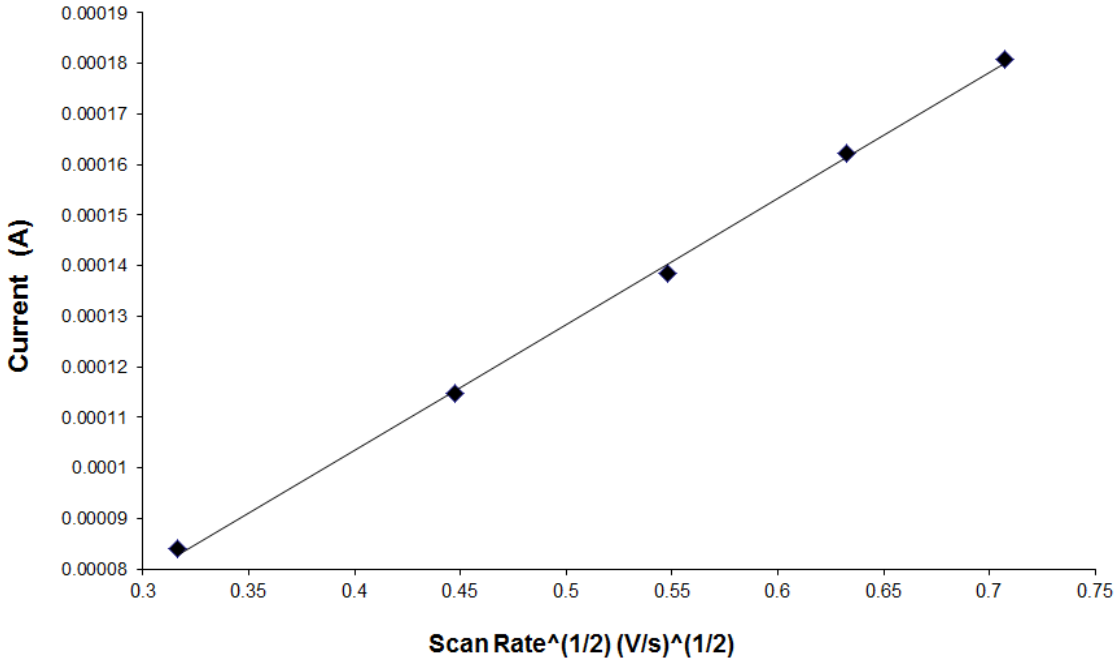

Figure 26. Plot of peak current of cyclic voltammetry scans of 1.00 mM $Ru\,(bpy)_3^{2+}$ as a function of the square root of the scan rate. Regression: $i_l = (2.5 \pm 0.1) \times 10^{-4}\sqrt{v} + (4 \pm 2) \times 10^{-6}$. R^2= 0.99.

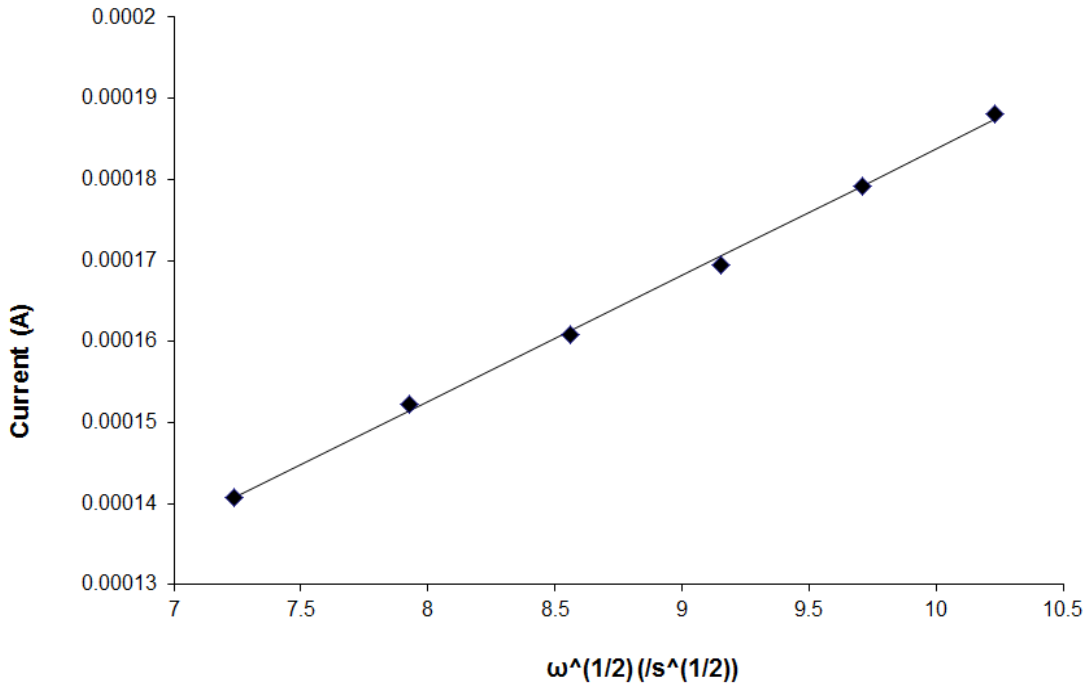

Figure 27. Plot of limiting current of rotating disk scans of 1.00 mM $Ru\,(bpy)_3^{2+}$ as a function of the square root of the rotation speed. Regression: $i_l = (1.5 \pm 0.1) \times 10^{-5}\sqrt{\omega} + (2.8 \pm 0.3) \times 10^{-5}$. R^2= 0.99.

between i_p and $v^{\frac{1}{2}}$, which is consistent with Equation 66. Data are typical of the $Ru\,(bpy)_3^{2+} \mid Ru\,(bpy)_3^{3+}$ reaction is fast (reversible).

For rotating disk, the limiting current is expressed at the Levich equation [2]:

$$i_{l,c} = 0.62nFAD_o^{\frac{2}{3}}\omega^{\frac{1}{2}}v^{-\frac{1}{6}}C_o^* \tag{67}$$

where F is Faraday's constant, ω is the angular frequency of rotation, and v is the kinematic viscosity. From the slopes of the plots, A, the area of the electrode and D_o, the diffusion coefficient can be solved for simultaneously. This resulted in a diffusion coefficient of $(4.5 \pm 0.1) \times 10^{-6}$ cm^2/s. This diffusion coefficient is used later to determine the electrode area of the sonoelectrochemical cell.

3.3.2 Determination of Electrode Area

The data set collected from sonicated cyclic voltammetry scans in section 3.3.3 was used to determine the area of the electrode of the sonoelectochemical cell. Physically, the working electrode consists of a piece of 0.5 mm platinum wire that is inserted 8 mm into the solution. This calculated geometric electrode area is 0.13 cm^2.

To determine the electrode area electrochemically, the peak height of each scan was found and data plotted according to Equation 66. This produced and average of 0.12 ± 0.01 cm^2.

3.3.3 $Ru\,(bpy)_3^{2+}$ with and without Sonication

A series of cyclic voltammetry scans were run in the sonoelectrochemical cell for

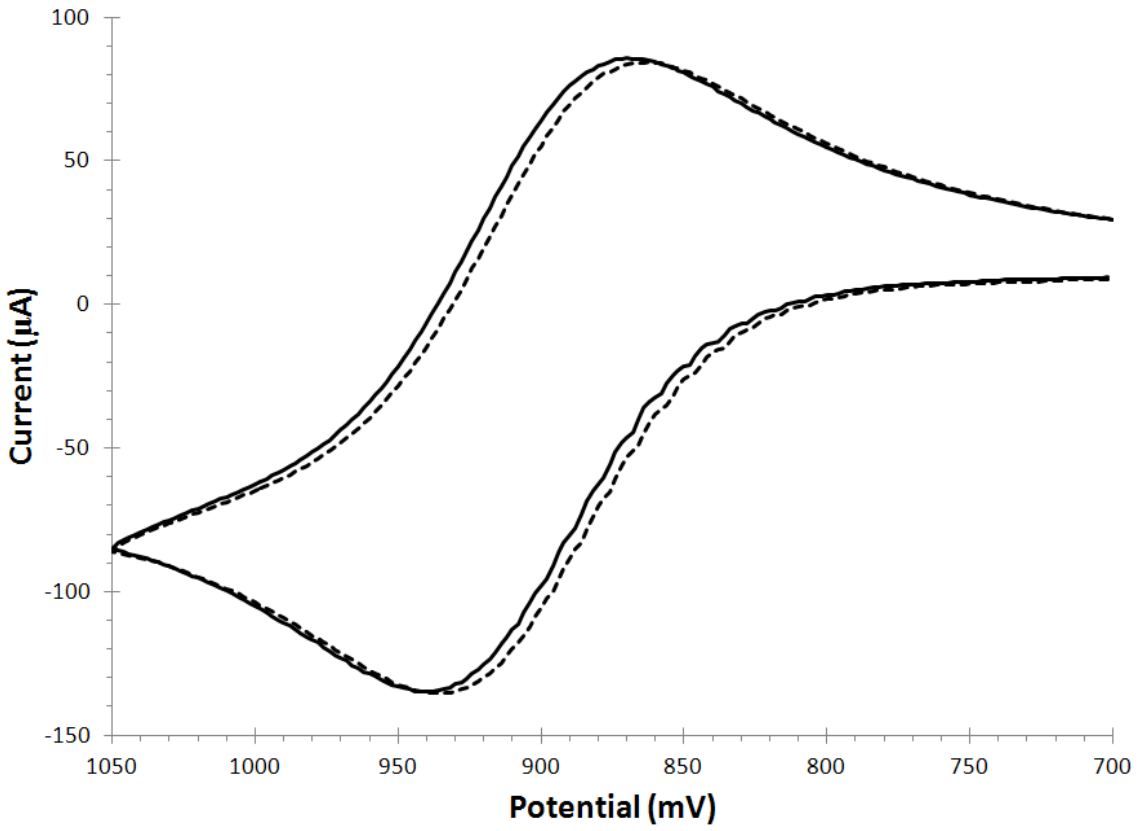

Figure 28. Comparative cyclic voltammograms of 8.50 mM $Ru\,(bpy)_3^{2+}$ in 0.100 M nitric acid taken with and without sonication. Scan rate is 0.05 V/s. Sonicated (maximum intensity, dashed), Unsonicated (solid).

8.50 mM $Ru\,(bpy)_3^{2+}$ in 0.100 M HNO_3. An initial set of three scans is run without sonication, followed by 8 sets of three scans each. The scan sets are separated by approximately 10 % increments of sonic intensity and are performed in random order of intensity. A final set of three scans is taken without sonication. Scan rate is 50 mV/s. Figure 28 is a plot showing representative scans.

The difference between the potential at peak reduction current and the potential at peak oxidation current, E_{pred} and E_{pox} respectively, often referred to as ΔE_p, is

Table 3. Tabulation of cyclic voltammetry data for 8.50 mM $Ru(bpy)_3^{2+}$ in 0.100 M nitric acid taken at various levels of sonication.

Sonication Intensity (%)	E_{pred} (mV)	i_{pred} (μA)	E_{pox} (mV)	i_{pox} (μA)	ΔE_p (mV)
none (pre)	932 (± 0)	-133.6 (± 0.5)	870 (± 1)	93.6 (± 0.3)	61 (± 1)
100	935 (± 1)	-133.8 (± 0.9)	873 (± 2)	93.8 (± 0.4)	60 (± 3)
90	934 (± 1)	-133 (± 1)	875 (± 1)	94 (± 1)	60 (± 0)
80	939 (± 1)	-132.7 (± 0.6)	880 (± 2)	96.9 (± 0.4)	59 (± 2)
70	939 (± 1)	-132.5 (± 0.9)	877 (± 3)	95.2 (± 0.6)	61 (± 3)
60	941 (± 2)	-132.3 (± 0.6)	877 (± 2)	96.7 (± 0.4)	63 (± 4)
50	937 (± 1)	-133.1 (± 0.6)	877 (± 2)	95.4 (± 0.3)	60 (± 1)
40	938 (± 2)	-132.2 (± 0.7)	879 (± 1)	97.0 (± 0.6)	59 (± 3)
30	933 (± 1)	-134 (± 1)	873 (± 2)	93.6 (± 0.3)	60 (± 3)
none (post)	941 (± 2)	-132.3 (± 0.3)	879 (± 2)	97.7 (± 0.5)	62 (± 4)

Note: Potentials recoreded versus a silver oxide reference. Data include peak potentials and currents as well as the difference in potentials. Each point is the average of three replicates.

used as a diagnostic of a reversible reaction.

$$\Delta E_p = E_{pred} - E_{pox} \tag{68}$$

ΔE_p is a function of the switching potential to a minor extent, but ΔE_p is always close to $2.3RT/nF$ or $59/n$ mV at 25°C [2]. An average for the sonicated samples produces ΔE_p of 61 ± 3 mV. The unsonicated samples yield ΔE_p is 62 ± 3 mV. This demonstrates that the reaction is reversible and that sonication has little effect on the reaction rate of an already fast electron transfer rate. A summary of the voltammetric data, E_{pred}, E_{pox} and ΔE_p. for various sonication intensities are given in Table 3.

3.3.4 Fe^{3+} with and without sonication

A second series of cyclic voltammetry scans were run in the sonoelectrochemical cell with a 5.00 mM Fe^{3+} in 0.500 M nitric acid electrolyte. An initial set of three scans were run without sonication, followed by 7 sets of three scans each at

assorted levels of sonic intensity. The scans were separated by approximately 10 % increments of sonic intensity and performed in random order. A final set of three scans was taken without sonication. The scan rate was 100 mV/s. Figure 29 is a plot of representative scans. Figure 30, which shows the reverse wave, was taken from another set under similar conditions (sonicated and unsonicated). The increase in the slope of the reductive waves between 0 and -200 mV between sonicated and unsonicated scans in Figure 29 indicates increased heterogenous electron transfer kinetics with increased sonic intensity. The difference in the slope of the reductive waves between 0 and -200 mV between the unsonicated scans (before and after sonication) indicate that the increased heterogenous electron transfer kinetic persist after sonication, possibly due to changes in the electrode surface.

3.3.5 Determination of k^0 and α

The determination of k^0 from the cyclic voltammetric data presents some unique challenges in that the scans tend to be a hybrid of avian and sinusoidal morphology. Traditional analysis methods are derived from the assumption that there will be a limiting current based on a flux of redox material limited only by the rate of mass transport. Equation 67 (Levich equation) for steady state mass transport for sigmodial current versus potential curves or Equation 66 (Randles-Sevcik equation) for diffusion in aqueous solutions for avian current versus potential curves. The data collected shifts from wave type to the other with the application of acoustic energy.

To address this issue, a model to fit the data was developed from the current

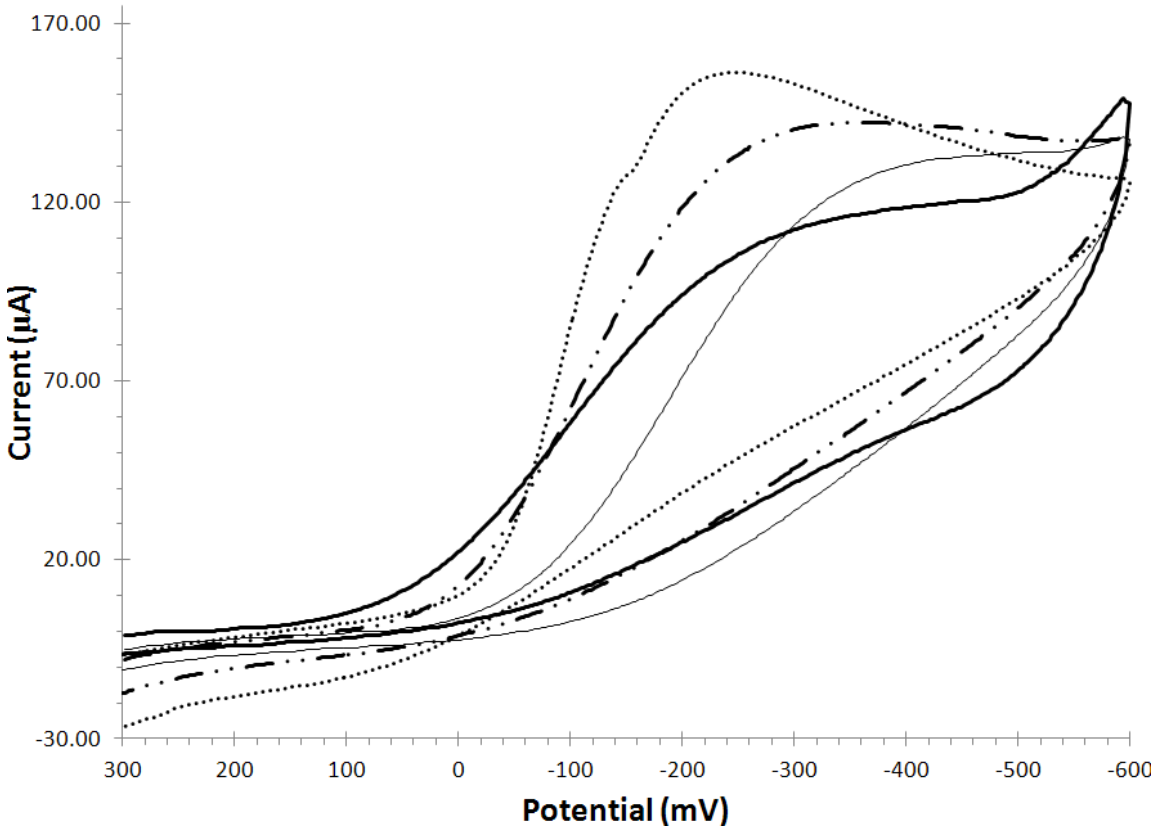

Figure 29. Comparative cyclic voltammograms of 5.00 mM Fe^{3+} in 0.500 M nitric acid taken at assorted levels of sonication. Initial Unsonicated (heavy solid); Sonicated , maximum intensity (dotted); Sonicated , 30 % intensity (dashed); Final Unsonicated (light solid).

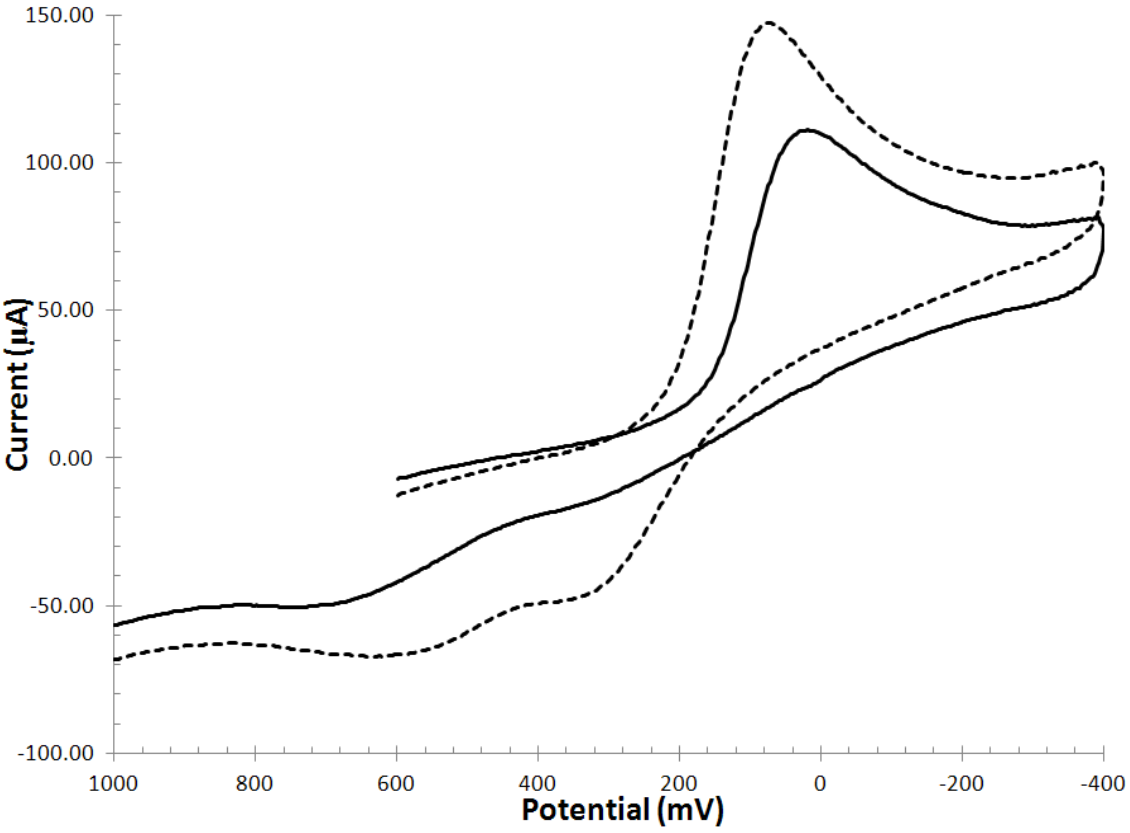

Figure 30. Comparative cyclic voltammograms of 5.00 mM Fe^{3+} in 0.500 M nitric acid with reverse scan extended to show backwave. Performed with and without sonication. Solution was degassed with N_2 and run under a nitrogen blanket. Unsonicated (solid), Sonicated (dashed).

potential equation [2].

$$\frac{i\left(t\right)}{nFAk^{0}} = C_{O}\left(0,t\right)\exp\left[-\alpha f\eta\right] - C_{R}\left(0,t\right)\exp\left[\left(1-\alpha\right)f\eta\right] \tag{69}$$

where η, the overpotential, is $E - E^{0'}$. When $D_O = D_R$

$$C_{O}\left(0,t\right) + C_{R}\left(0.t\right) = c^{*} \tag{70}$$

If only is O present at the start, which is the case with the iron (III) data,

$$C_{R}\left(0,t\right) = C^{*} - C_{O}\left(0,t\right) \tag{71}$$

Substitution of $C_R\left(0,t\right)$ from equation 71 into equation 69,

$$\frac{i\left(t\right)}{nFAk^{0}} = C_{O}\left(0,t\right)\exp\left[-\alpha f\eta\right] - \left[C^{*} - C_{O}\left(0,t\right)\right]\exp\left[\left(1-\alpha\right)f\eta\right] \tag{72}$$

Equation 72 is then normalized by C^*,

$$\frac{i\left(t\right)}{nFAk^{0}C^{*}} = \frac{C_{O}\left(0,t\right)}{C^{*}}\exp\left[-\alpha f\eta\right] - \left[1 - \frac{C_{O}\left(0,t\right)}{C^{*}}\right]\exp\left[\left(1-\alpha\right)f\eta\right] \tag{73}$$

For a linearized concentration profile,

$$\frac{C_{O}\left(0,t\right)}{C^{*}} = 1 - \frac{i\left(t\right)}{i_{\lim}} \tag{74}$$

$$\begin{aligned}\frac{i\left(t\right)}{nFAk^{0}C^{*}} &= \left\{1 - \frac{i\left(t\right)}{i_{\lim}}\right\}\exp\left[-\alpha f\eta\right] - \left[1 - \left(1 - \frac{i\left(t\right)}{i_{\lim}}\right)\right]\exp\left[\left(1-\alpha\right)f\eta\right] &(75)\\ &= \left\{1 - \frac{i\left(t\right)}{i_{\lim}}\right\}\exp\left[-\alpha f\eta\right] - \frac{i\left(t\right)}{i_{\lim}}\exp\left[\left(1-\alpha\right)f\eta\right] &(76)\end{aligned}$$

The exchange current i_0 expresses the standard hetergeneous rate in terms of known system parameters.

$$i_{0} = nFAk^{0}C^{*} \tag{77}$$

$$\frac{i\left(t\right)}{i_0} = \left\{1 - \frac{i\left(t\right)}{i_{\lim}}\right\} \exp\left[-\alpha f\eta\right] - \frac{i\left(t\right)}{i_{\lim}} \exp\left[\left(1-\alpha\right) f\eta\right] \tag{78}$$

The object is to find i_0 (which can be used to determine k^0) and α. $\eta = E - E^{0'}$ is based on $E^{0'}$. Hence, with the quasireference used here, $E^{0'}$is not well determined. Equation 78 is used to fit three variables: i_0, α, and $E^{0'}$. To fit data, Equation 78 is rearranged.

$$\begin{aligned}
\frac{i\left(t\right)}{i_0} &= \left\{1 - \frac{i\left(t\right)}{i_{\lim}}\right\} \exp\left[-\alpha f\eta\right] - \frac{i\left(t\right)}{i_{\lim}} \exp\left[\left(1-\alpha\right) f\eta\right] && (79)\\
\frac{i\left(t\right)}{i_0} \exp\left[+\alpha f\eta\right] &= 1 - \frac{i\left(t\right)}{i_{\lim}} - \frac{i\left(t\right)}{i_{\lim}} \exp\left[f\eta\right] && (80)\\
&= 1 - \frac{i\left(t\right)}{i_{\lim}} \left(1 + \exp\left[f\eta\right]\right) && (81)
\end{aligned}$$

No simple plot is obvious that simplifies analysis. It is noted that when $\eta = 0$,

$$\begin{aligned}
\frac{i\left(t\right)}{i_0} &= 1 - 2\frac{i\left(t\right)}{i_{\lim}} && (82)\\
i_0 &= i_{\lim} \frac{i\left(E^{0'}\right)}{i_{\lim} - 2i\left(E^{0'}\right)} && (83)
\end{aligned}$$

Equation 81 is solved for $i\left(t\right)$ so as to plot $i\left(t\right)$ with E amd allows i_0, α, and $E^{0'}$ as adjustable parameters.

$$\begin{aligned}
\frac{i\left(t\right)}{i_0} \exp\left[\alpha f\eta\right] &= 1 - \frac{i\left(t\right)}{i_{\lim}} \left(1 + \exp\left[f\eta\right]\right) && (84)\\
i\left(t\right) \left\{\frac{\exp\left[\alpha f\eta\right]}{i_0} + \frac{1 + \exp\left[f\eta\right]}{i_{\lim}}\right\} &= 1 && (85)\\
i\left(t\right) &= \frac{1}{\frac{\exp[\alpha f\eta]}{i_0} + \frac{1+\exp[f\eta]}{i_{\lim}}} && (86)\\
\frac{i\left(t\right)}{i_{\lim}} &= \frac{i_0}{i_{\lim} \exp\left[\alpha f\eta\right] + i_0 \left(1 + \exp\left[f\eta\right]\right)} && (87)\\
&= \frac{\frac{i_0}{i_{\lim}}}{\exp\left[\alpha f\eta\right] + \frac{i_0}{i_{\lim}} \left(1 + \exp\left[f\eta\right]\right)} && (88)
\end{aligned}$$

Note from equation 77 the standard rate constant, k^o, can be determined from the

fit. given A, C^* and n.

3.3.6 Fitting of Fe^{3+} Data

An example of this fitting is shown in Figure 31. The forward scan of the data (from the baseline to i_{lim}) is used to fit the model using the Solver tool embedded into Microsoft Office Excel. The Solver tool uses the Generalized Reduced Gradient (GRG2) nonlinear optimization code, which was developed by Leon Lasdon, University of Texas at Austin, and Alan Waren, Cleveland State University. Ultimately, it is the rising portion of the slope that corresponds to the electron transfer rate. A χ^2 comparison of the data and the model was generated after initial guesses for i_0/i_{lim}, α and $E^{0'}$. A χ^2 test for goodness of fit compares points generated by the model to data points with the following equation:

$$\chi^2 = \sum_{i=1}^{n} \frac{(O_i - E_i)^2}{E_i} \tag{89}$$

where E_i is the expected value (model), O_i is the observed value (data), and n is the number of data points. The Solver tool is the used to adjust i_0/i_{lim}, α and $E^{0'}$ so as to minimize the value of χ^2. A χ^2 value of 1 or less is considered a good fit for most models. Values for α were constrained between 1 and 0 and values for $E^{0'}$ were constrained between -0.2 and 0.1 volts. None of the fittings reached these constraints for the final values. Various initial guesses were used for each fitting so as to avoid local minimums. Typical values of χ^2 were below 0.1.

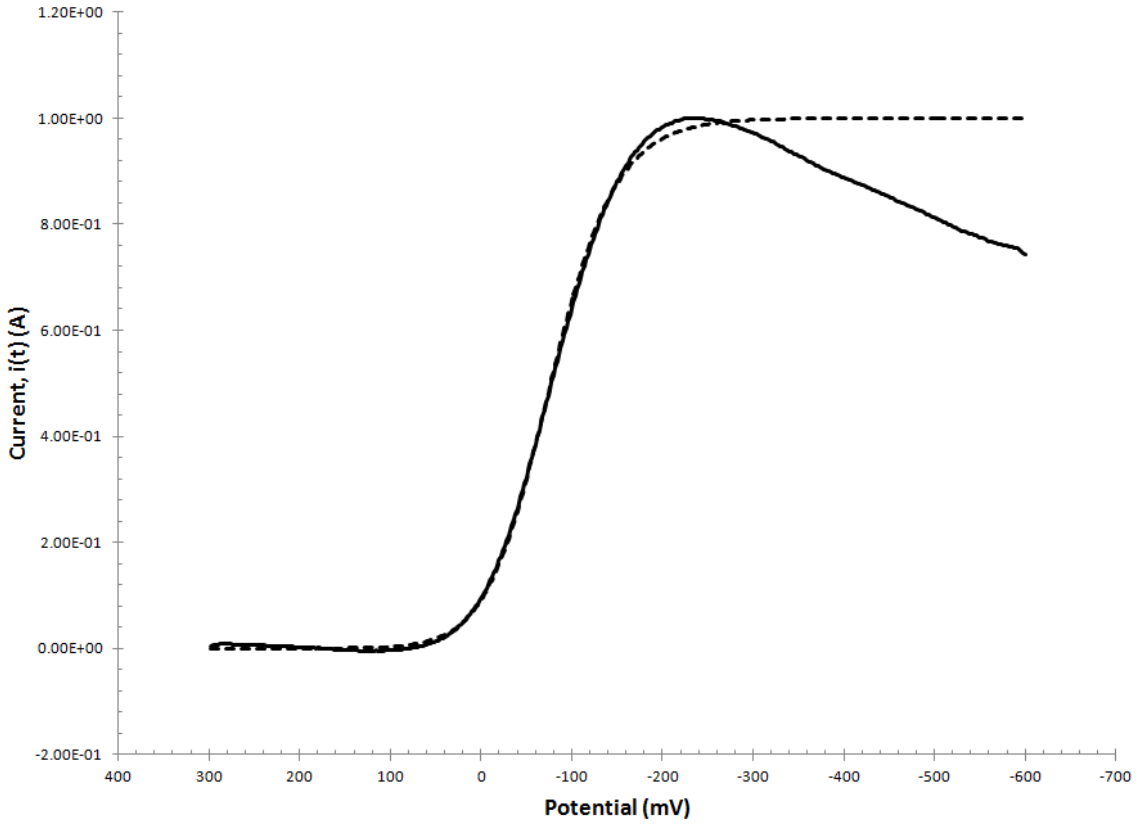

Figure 31. Example of fitted sonicated Fe^{3+} cyclic voltammetric data to current overpotential model. $\chi^2 = 0.0329$. Data (solid); Model (Dashed)

3.3.7 Calculation of $V\Delta P$

To evaluate the data, the acoustic energy input is calculated. The acoustic energy input ΔPV is taken as $V\Delta P$ because the acoustic energy will impart pressure to the solution but is not likely to impact volume. For ΔP in atmospheres and V in liters, the acoustic energy to the solution in J/mol is

$$Acoustic\ Energy\ to\ Solution = V\Delta P \times \frac{101.27\ J}{liter\ atm} \tag{90}$$

V is taken as the molar volume, 0.018 liters/liter. ΔP is calculated from equation 37 in pascals; the value 101.27 is part of the unit conversion for pascals to atomspheres. The pressure in pascals is calculated from the peak voltage, V_p as described in Section 2.4.

$$p = p_0 10^{0.05\left[15.2\log(V_p)+98.6+10\log\left(\frac{z}{z}\right)-10\log\left(\frac{2\pi a^2}{\ln(a/R)}\right)\right]} \tag{91}$$

Then, $\Delta G_A^0 = V\Delta P$ in J/mol.

Once all the curves are fit, plots of k^0 as a function of $V\Delta P$ and α as a function of $V\Delta P$ are generated. See Figures 32 and 33 for Fe^{3+} data. A summary of the voltammetric data, k^0, α and $E^{0\prime}$ for various sonication intensities is given in Table 4.

Replicates of the Fe^{3+} experiments were performed on different days. Figures 34 and 37 are representative plots of the cyclic voltammograms of these experiments. Figures 35, 36, 38, and 39 are plots of k^0 as a function of $V\Delta P$ and α as a function of $V\Delta P$ and Tables 5 and 6 are a summary of the voltammetric data, k^0, α and $E^{0\prime}$ for various sonication intensities.

All three sets of experiments demonstrate a similar trend with respect to the

Table 4. Tabulation of cyclic voltammetric data set 1 for 5.00 mM Fe^{3+} in 0.100 M nitric acid taken at various levels of sonication.

Sonication Intensity (%)	k_0 (cm/s)	α	$E^{0'}$ (mV)	$V\Delta P$ (J/mol)
none (pre)	0.00028 (± 0.00003)	0.38 (± 0.01)	40 (± 20)	0
100	0.011 (± 0.001)	0.40 (± 0.04)	-80 (± 20)	0.24
90	0.0088 (± 0.0004)	0.48 (± 0.04)	-79 (± 7)	0.22
80	0.0031 (± 0.0009)	0.69 (± 0.02)	-50 (± 10)	0.21
70	0.0025 (± 0.0007)	0.61 (± 0.01)	-53 (± 5)	0.19
60	0.0014 (± 0.0001)	0.58 (± 0.01)	-45 (± 2)	0.18
50	0.0011 (± 0.0001)	0.54 (± 0.01)	-44 (± 5)	0.17
40	0.0007 (± 0.0001)	0.48 (± 0.01)	-50 (± 9)	0.14
none (post)	0.0004 (± 0.0001)	0.42 (± 0.01)	-70 (± 20)	0

Note: Potentials recored versus a platinum | platinum oxide reference. Data include standard heterogeneous electron transfer rate, α, $E^{0'}$ and VΔP. Each point is the average of three replicates. Overall average $E^{0'}$ is -59 (± 1) mV.

standard rate constant, k^0, increasing with sonic intensity, albeit the magnitude of the effect varies with each experiment. The inconsistency in magnitude of effect between experiments may be attributed to the degradation of the transducer over time and minor variations in position of electrodes and height of the meniscus. The commercial transducers were not originally designed for use in solution and tend to loose efficiency over time. It should also be noted that whether a system shows reversible, quasireversible and irreversible kinetics as a function of scan rate. Because a scan rate of 0.1 V/s was used for all scans for all of the Fe^{3+} experiments, all values for k^0 above 0.09 cm/s will appear reversible [43] thus limiting analysis.

The transfer coefficient, α, has no consistent trend across the three replicate experiments; α increases with sonic intensity with the original set, decreases with sonic intensity in the second set and is invariant with the third set. While no trend is apparent, α is consistently higher than the literature value, 0.42 [44].

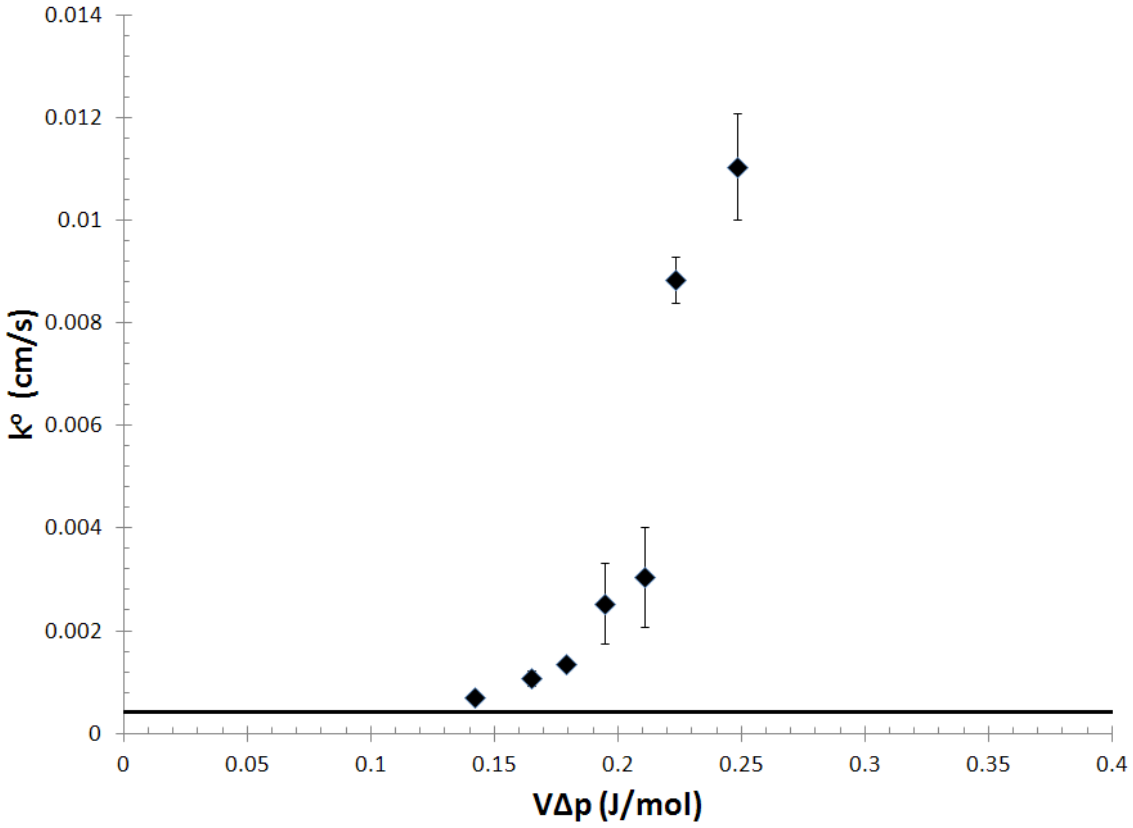

Figure 32. Plot of the standard heterogeneous electron transfer rate constant, k^0, as a function of $V\Delta P$ for sonicated Fe^{3+} cyclic voltammetric data set 1. Error bars represent standard deviations. Each point is an average of three scans. Solid line represents the standard rate constant, k^0, of unsonicated scans.

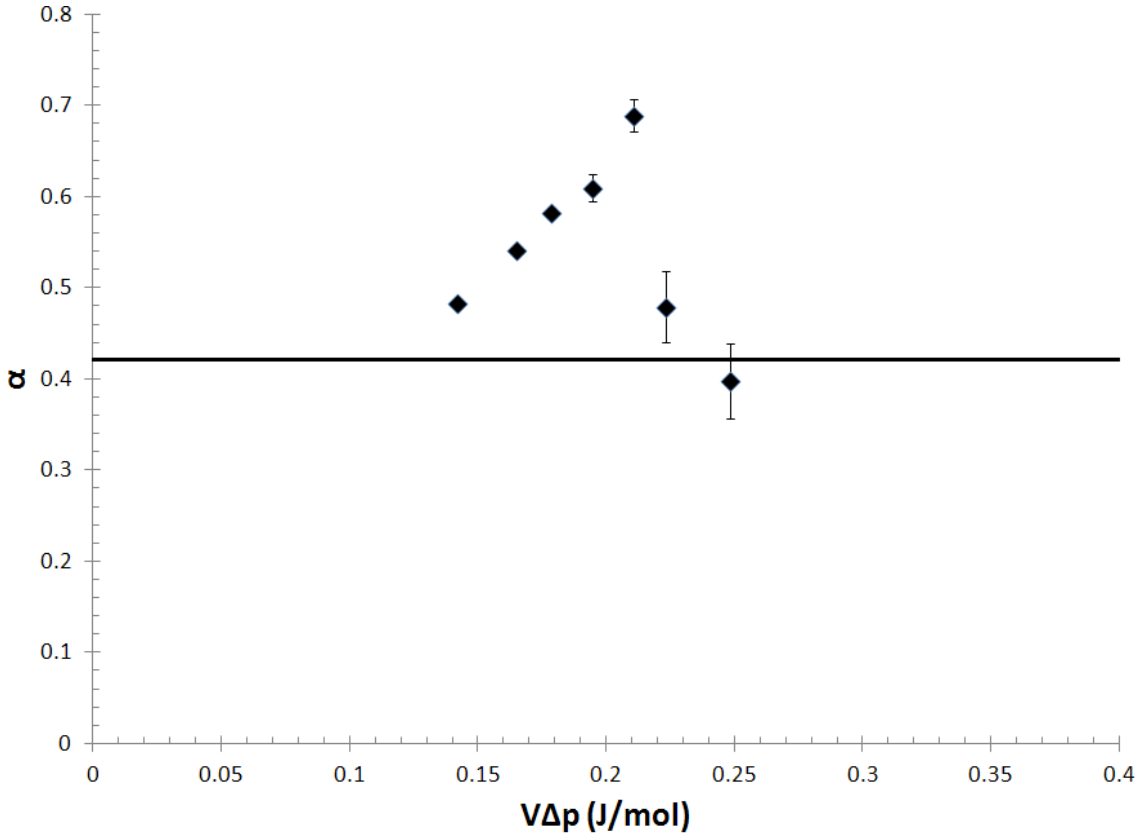

Figure 33. Plot of the transfer coefficient, α, as a function of $V\Delta P$ for sonicated Fe^{3+} cyclic voltammetric data set 1. Error bars represent standard deviations. Each point is an average of three scans. The solid line represents the transfer coefficient, α, of unsonicated scans.

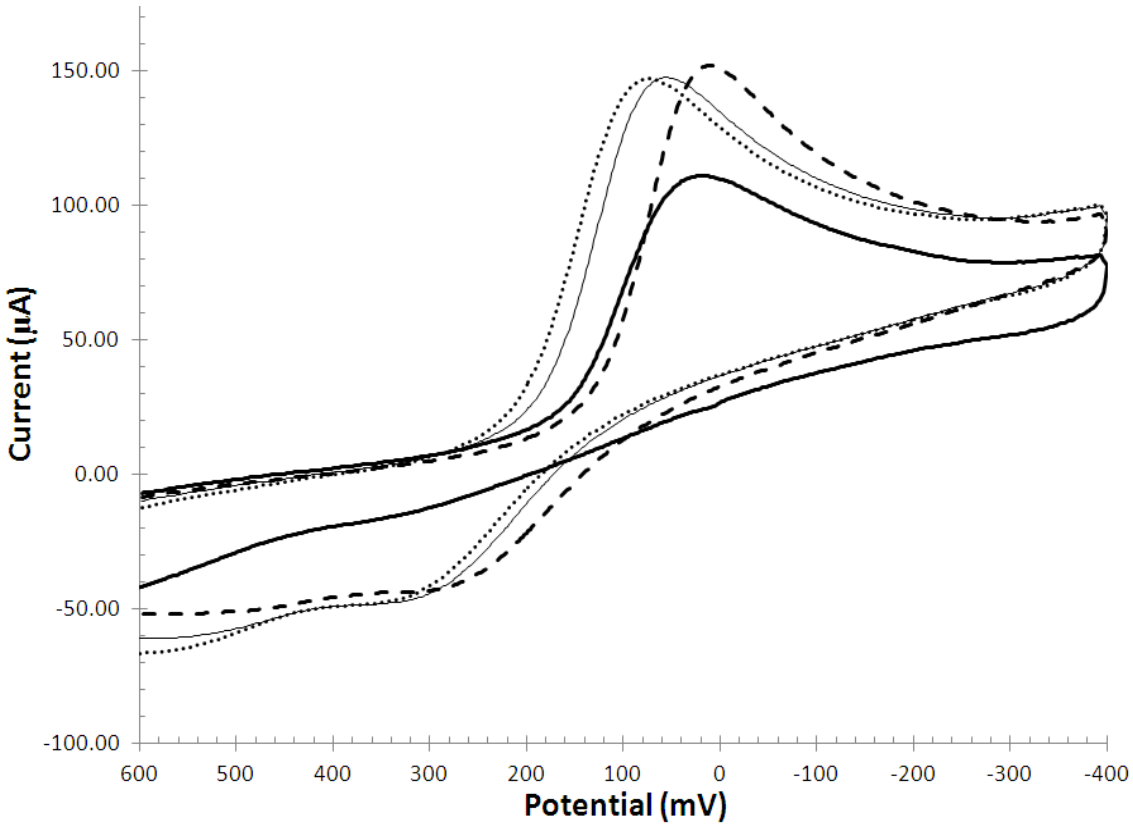

Figure 34. Comparative cyclic voltammograms of 5.00 mM Fe^{3+} in 0.100 M nitric acid taken at assorted levels of sonication for data set 2. Initial Unsonicated (heavy solid); Sonicated , maximum intensity (dotted); Sonicated , 50 % intensity (dashed); Final Unsonicated (light solid).

3.4 Discussion

Impacts on the rates of heterogeneous electron transfer are evaluated by considering two redox probes. These experiments are intended to compare the quasireversible ferric ion and the reversible $Ru\,(bpy)_3^{2+}$ complex to demonstrate the impacts of cavitation free sonication on heterogeneous electron transfer kinetics. One probe, ferric ion, exhibits a slower rate of heterogeneous electron transfer, whereas, ruthenium tris-bipyridal, exhibits reversible or rapid rate of heterogeneous

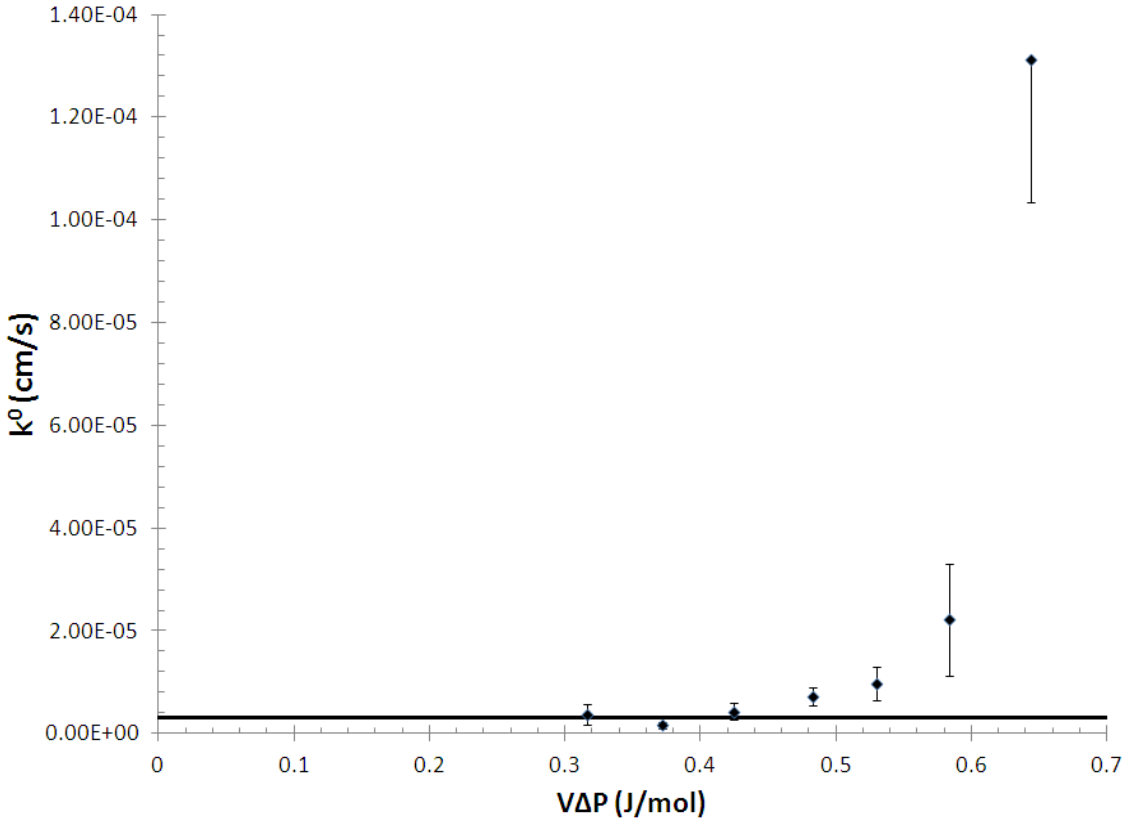

Figure 35. Plot of the standard heterogeneous electron transfer rate constant, k^0, as a function of $V\Delta P$ for sonicated Fe^{3+} cyclic voltammetric data set 2. Error bars represent standard deviations. Each point is an average of three scans. Solid line represents the standard rate constant, k^0, of unsonicated scans.

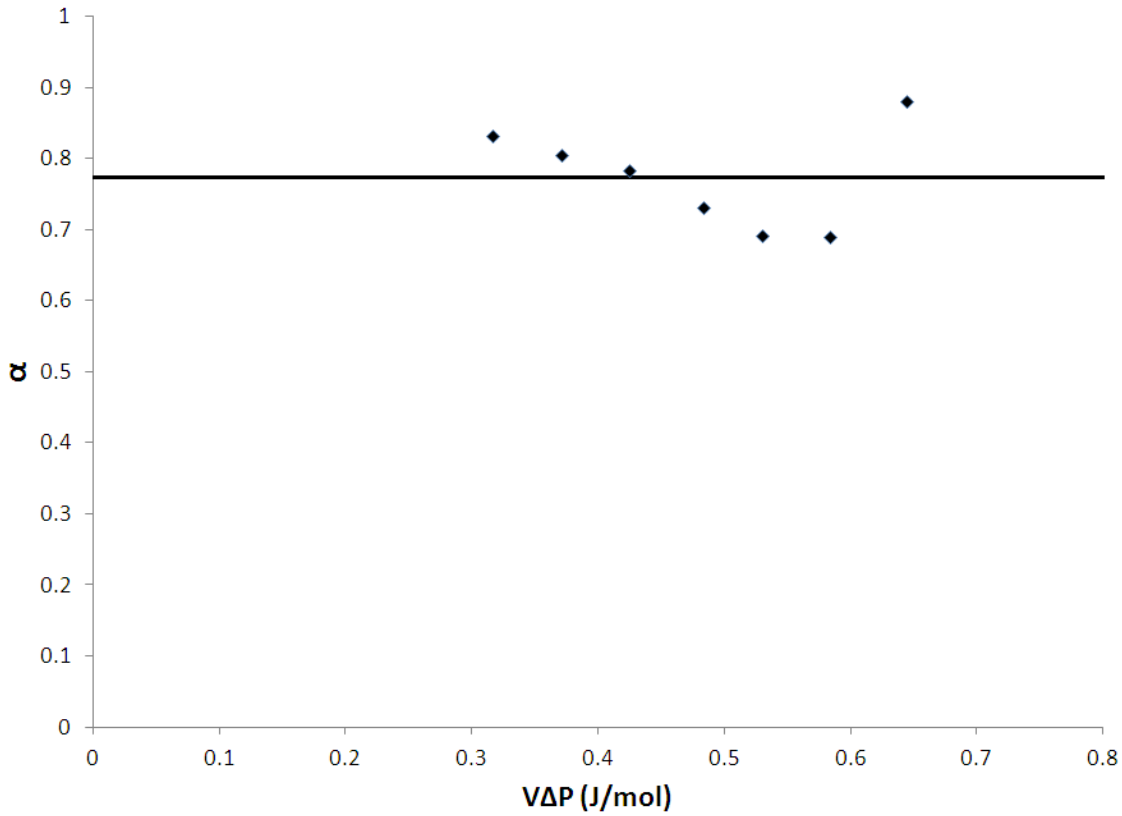

Figure 36. Plot of the transfer coefficient, α, as a function of $V\Delta P$ for sonicated Fe^{3+} cyclic voltammetric data set 2. Error bars represent standard deviations. Each point is an average of three scans. The solid line represents the transfer coefficient, α, of unsonicated scans.

Table 5. Tabulation of cyclic voltammetry data Set 2 for 5.00 mM Fe^{3+} in 0.100 M nitric acid taken at various levels of sonication.

Sonication Intensity (%)	k_0 (cm/s)	α	$E^{0'}$ (mV)	$V\Delta P$ (J/mol)
none (pre)	3.0 ($\pm$ 0.7) $\times 10^{-6}$	0.77 ($\pm$ 0.01)	327 ($\pm$ 3)	0
100	1.7 ($\pm$ 0.4) $\times 10^{-4}$	0.71 ($\pm$ 0.02)	250 ($\pm$ 10)	0.64
90	2 ($\pm$ 1) $\times 10^{-5}$	0.69 ($\pm$ 0.03)	327 ($\pm$ 3)	0.58
80	1.0 ($\pm$ 0.3) $\times 10^{-5}$	0.69 ($\pm$ 0.01)	250 ($\pm$ 10)	0.53
70	7 ($\pm$ 1) $\times 10^{-6}$	0.73 ($\pm$ 0.04)	280 ($\pm$ 10)	0.48
60	4 ($\pm$ 2) $\times 10^{-6}$	0.78 ($\pm$ 0.01)	290 ($\pm$ 20)	0.42
50	1.6 ($\pm$ 0.6) $\times 10^{-6}$	0.80 ($\pm$ 0.01)	329 ($\pm$ 9)	0.37
40	4 ($\pm$ 2) $\times 10^{-6}$	0.83 ($\pm$ 0.02)	320 ($\pm$ 20)	0.31
30	6 ($\pm$ 3) $\times 10^{-6}$	0.84 ($\pm$ 0.03)	311 ($\pm$ 9)	0.26
none (post)	1.3 ($\pm$ 0.1) $\times 10^{-5}$	0.86 ($\pm$ 0.01)	303 ($\pm$ 10)	0

Note: Potentials recored versus a platinum | platinum oxide reference. Data include standard heterogeneous electron transfer rate, α, $E^{0'}$ and VΔP. Each point is the average of four replicates. Overall average $E^{0'}$ is -280 ($\pm$ 40) mV.

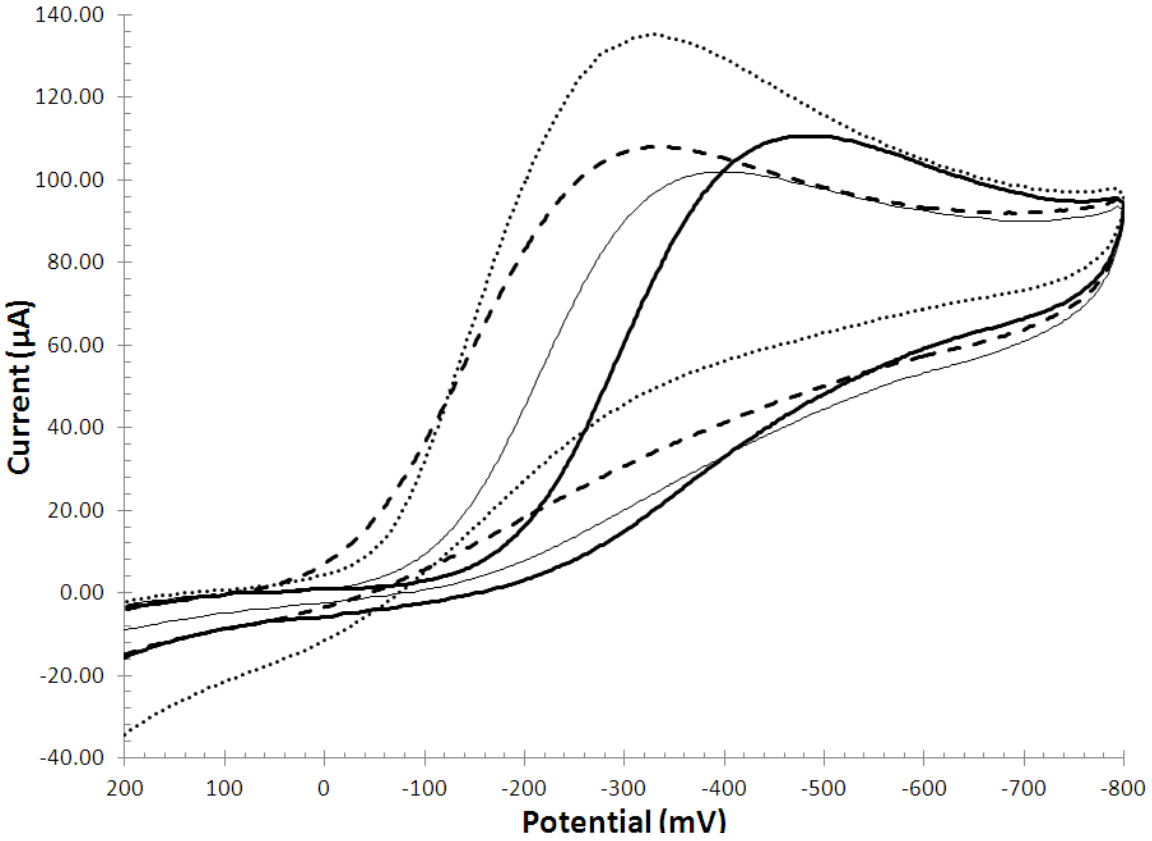

Figure 37. Comparative cyclic voltammograms of 10.00 mM Fe^{3+} in 0.500 M nitric acid taken at assorted levels of sonication for data set 3. Initial Unsonicated (heavy solid); Sonicated , maximum intensity (dotted); Sonicated , 50 % intensity (dashed); Final Unsonicated (light solid).

Table 6. Tabulation of cyclic voltammetry data Set 3 for 10.00 mM Fe^{3+} in 0.500 M nitric acid taken at various levels of sonication.

Sonication Intensity (%)	k_0 (cm/s)	α	$E^{0'}$ (mV)	$V\Delta P$ (J/mol)
none (pre)	1.9 (± 0.4) $\times 10^{-6}$	0.52 (± 0.01)	12 (± 1)	0
100	6.8 (± 0.8) $\times 10^{-4}$	0.57 (± 0.01)	-107 (± 7)	0.24
90	1.8 (± 0.6) $\times 10^{-4}$	0.59 (± 0.01)	-40 (± 20)	0.22
80	2.0 (± 1) $\times 10^{-5}$	0.56 (± 0.01)	63 (± 40)	0.20
70	1.7 (± 0.7) $\times 10^{-5}$	0.53 (± 0.01)	70 (± 20)	0.18
60	8.8 (± 0.5) $\times 10^{-6}$	0.54 (± 0.01)	82 (± 3)	0.15
50	1.1 (± 0.2) $\times 10^{-5}$	0.55 (± 0.01)	54 (± 3)	0.14
40	8.1 (± 0.8) $\times 10^{-6}$	0.57 (± 0.01)	41 (± 6)	0.12
none (post)	6.3 (± 3) $\times 10^{-6}$	0.59 (± 0.01)	12 (± 1)	0

Note: Potentials recored versus a platinum | platinum oxide reference. Data includes standard heterogeneous electron transfer rate, α, $E^{0'}$ and VΔP. Each point is the average of three replicates. Overall average $E^{0'}$ is 16 (± 6) mV.

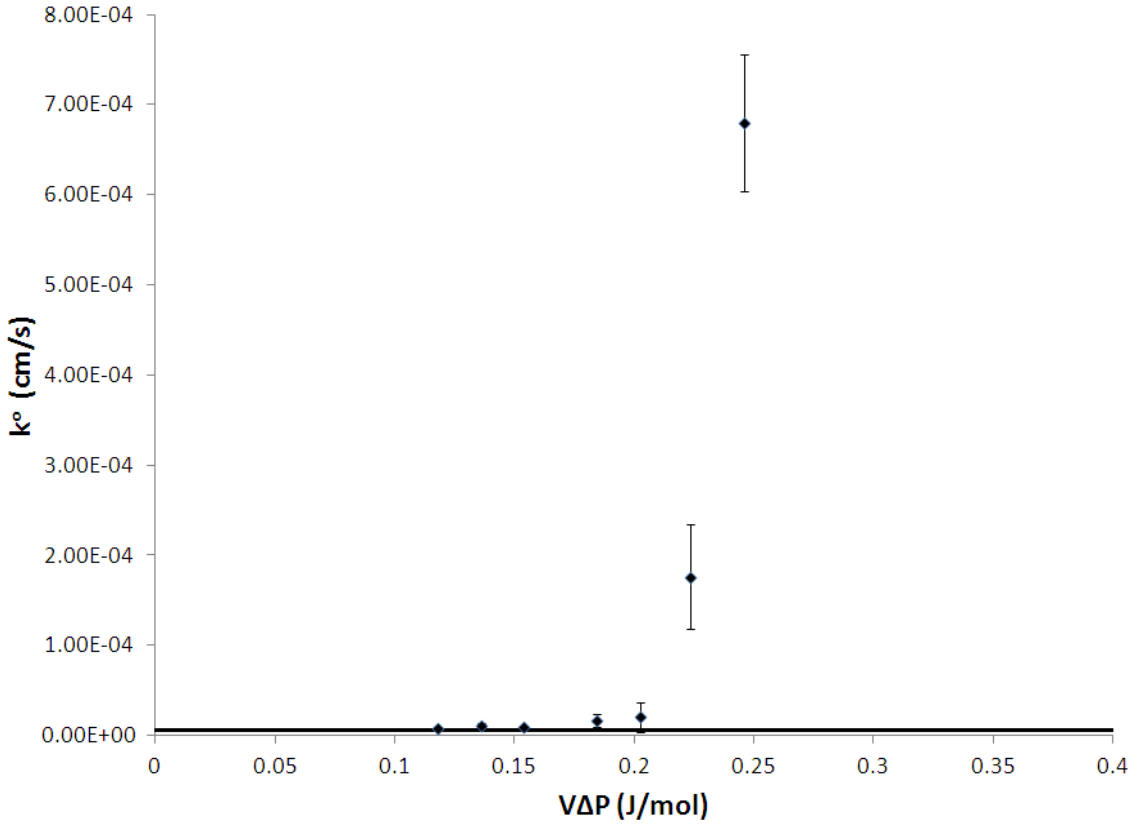

Figure 38. Plot of the standard rate constant, k^0, as a function of $V\Delta P$ for sonicated 10.00 mM Fe^{3+} cyclic voltammetric data set 3. Error bars represent standard deviations. Each point is an average of three scans. Solid line represents the standard rate constant, k^0, of unsonicated scans.

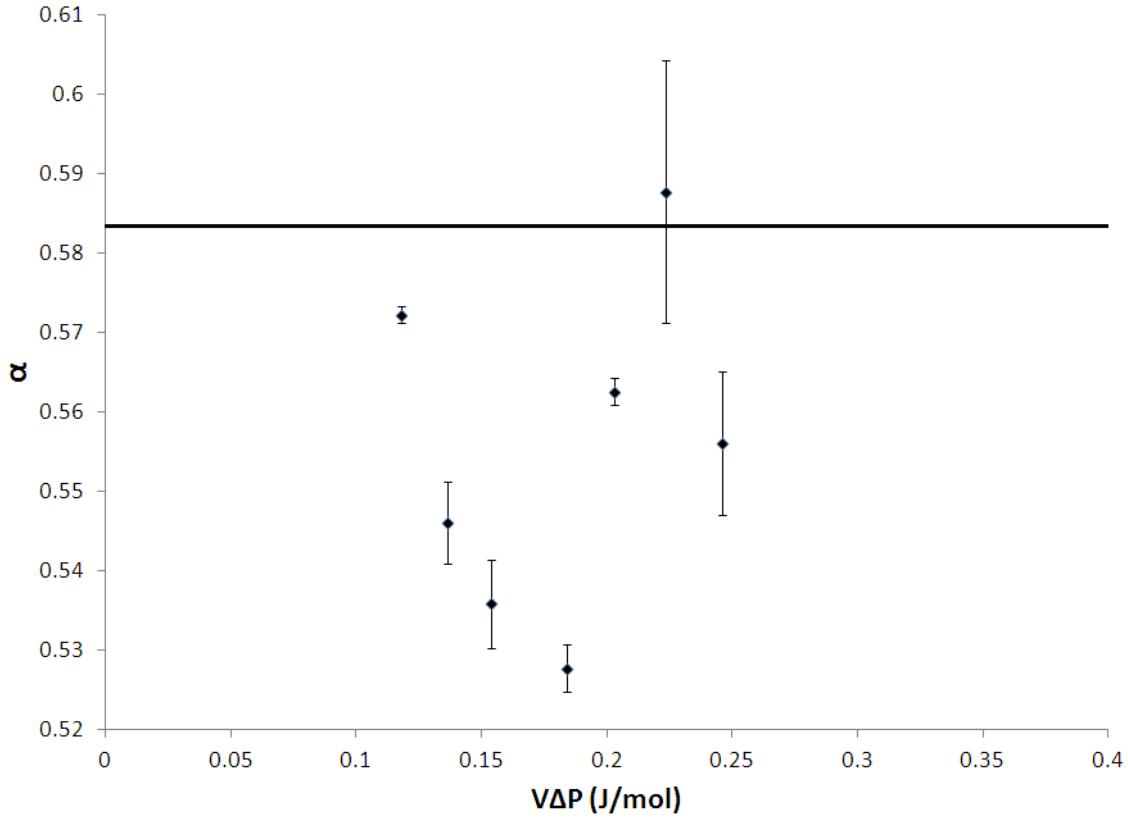

Figure 39. Plot of the transfer coefficient, α, as a function of $V\Delta P$ for sonicated 10.00 mM Fe^{3+} cyclic voltammetric data set 3. Error bars represent standard deviations. Each point is an average of three scans. The solid line represents the transfer coefficient, α, of unsonicated scans.

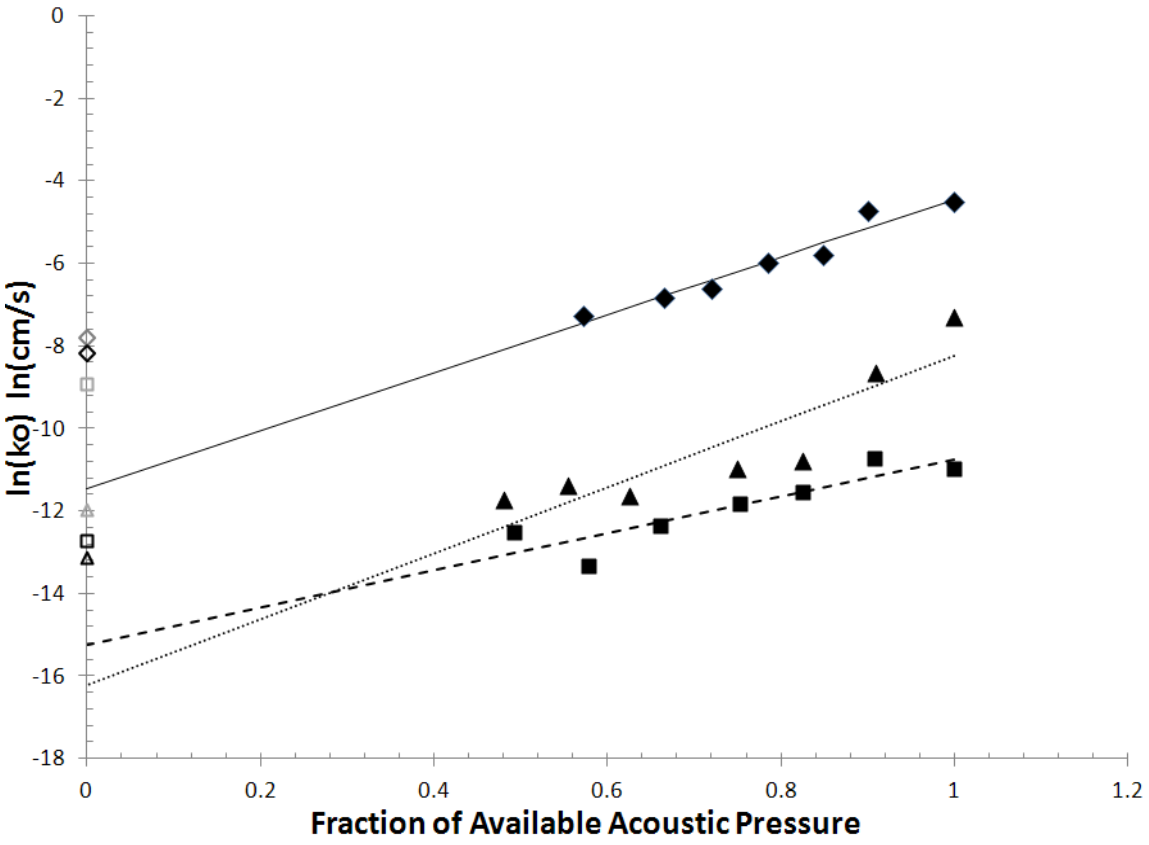

Figure 40. The natural log of standard heterogeneous electron transfer constant. $ln(k^0)$ as a function of the fraction of available acoustic pressure, F_p, for the reduction of Fe^{3+}in all three data sets. For all three data sets, the $ln(k^0)$ at zero acoustic pressure is denoted with unfilled data points. Dark markers were taken before sonication, light markers were taken after sonication. Data set 1 (♦) has a linear regression (solid line) of: $ln(k^0) = (7.0 \pm 0.7) \times F_p - (11.4 \pm 0.6)$ with $R^2 = 0.94$. Data set 2 (■) has a linear regression (dotted line) of: $ln(k^0) = (4.5 \pm 1) \times F_p - (15.4 \pm 0.6)$ with $R^2 = 0.80$. Data set 3 (▲) has a linear regression (dashed line) of: $ln(k^0) = (8.0 \pm 2) \times F_p - (16 \pm 1)$ with $R^2 = 0.79$.

electron transfer. Evaluation of the two probes by cyclic voltammetry showed that the rate of heterogeneous electron transfer for ferric ion is dramatically increased with sonic intensity. The already rapid electron transfer species, ruthenium tris-bipyridal, shows no impact of sonication.

For ferric ion, the heterogeneous electron transfer rate increases on sonication as shown by the shape of the cyclic voltammograms that become more consistent with consistent with faster electron transfer. See Figures 29, 34 and 37. Fitting of the data yields increases in the standard heterogenous rate constant, k^0, and changes in the transfer coefficient, α, that are gradually increasing. This is in contrast to the $Ru\,(bpy)_3^{2+}$ system, which has fast kinetics and does not change voltammetric morphology with sonication. See Section 3.3.3.

The data in Table 6 have the highest k^0, 108 times higher than the unsonicated solution after the system has been sonicated. For the data in Tables 4 and 5 the k^0 at maximum sonic intensity is 27.5 and 12.1 fold higher. There is a consistent increase in k^0 of greater than one order of magnitude across the data sets. The inconsistency in magnitude of effect between experiments is most likely attributable to the degradation of the transducer over time. The commercial transducers were not originally designed for use in solution and tend to loose efficiency over time.

As a result of transducer degradation with use, when $V\Delta P$ is calculated from the fraction of maximum intensity, the absolute energy of sonication is not specified, but rather a relative intensity. This is because the efficacy of the transducer can differ at the maximum intensity. Data are considered as a fraction of maximum intensity but the values are relative to the quality of the transducer at the time the experiment

is undertaken. Thus, the data for the three iron experiments differ with respect to the values of $V\Delta P$ but the behavior is the same across all three experiments. The standard heterogeneous rate increases monotonically with intensity of sonication.

The literature value of the transfer coefficient is 0.42 for the unsonicated system [44]. The transfer coefficient and ranges from 0.40 to 0.69 for the sonicated system and increases with sonic intensity in data set 1. This trend is reversed for the second data set that ranges from 0.69 to 0.84 for the sonicated system and decreases with sonic intensity. The transfer coefficient for the third data set has no trend with respect to sonic intensity and averages 0.55 ± 0.02 across all sonic intensities. The lack of a consistent trend could also be the result of degradation of the transducer with stronger variation of alpha observed at the higher absolute intensities. Given the lack of consistent variation in alpha with intensity, more attention was focused on understanding the behavior of k^0 than on α.

These effects are consistent with effective transfer of acoustic energy at the electrode surface as a means to accelerate the rate of heterogeneous electron transfer when the rate without sonication is slow. For $O + e^- \rightleftharpoons R$, the forward and backward rates of electron transfer are

$$k_f(E) = k^0 \exp\left[\frac{-\alpha F}{RT}(E - E^{0'})\right] \quad (92)$$

$$k_b(E) = k^0 \exp\left[\frac{(1-\alpha) F}{RT}(E - E^{0'})\right] \quad (93)$$

With increased sonic intensity, k^0 increases. It is noted that increases in α tend to decrease $k_f(E)$ and increase $k_b(E)$. It should also be noted that ferric ion has at least some component of inner sphere reorganization energy (about 29 % of the total

reorganization energy) whereas $Ru\,(bpy)_3^{2+}$ is not considered to have an inner sphere component to its reorganization energy [44].

The effect on k^0 appears surprising when the amount of acoustic energy put into the system ($\sim$ 0.25 J/mol) in comparison to $\Delta G^{\ddagger}$ ($\sim$ 74.2 kJ/mol) is considered [45]. Consider the change in k^0 between sonicated and unsonicated reactions. If all of the acoustic energy is directed at lowering $\Delta G^{\ddagger}$ to increase k^0, the relationship

$$k = A \exp\left[\frac{\Delta\,(PV)^{\ddagger}}{RT}\right] \exp\left[-\frac{\Delta G^{\ddagger}}{RT}\right] \tag{94}$$

yields an expected $V\Delta P$ of 11.3 J/mol. This is misleading in several ways. First, the values calculated for $V\Delta P$ are based solely upon the effect of the initial pass of the sound wave and do not take into account any reflections. In Section 1.1.4, the advantages of reducing the third dimensional component such that the three dimensional bulk energy is confined to two dimensions is discussed. For simplicity, this effect is not included in the values provided for $V\Delta P$. Inclusion of the reflections would increase $V\Delta P$. A similar argument can also be made for the effect of the meniscus upon focusing of the reflected sound waves. Further, these energies are energies per volume where the sonication effects may arise as energy is dropped from three dimensions across the two dimensional surface of the electrode.

Equation 94 is a theoretical relationship between k and changes in pressure and volume. If the relationship in Equation 94 is correct, then $\ln(k^0)$ as a function of $V\Delta P$ should be linear. Figure 40 is a plot of natural log of standard heterogeneous electron transfer constant. $ln(k^0)$ as a function of the fraction of available acoustic pressure, $F_p = I/I_{max}$ where I is the intensity normalized by the maximum intensity

I_{max} as measured on the oscilloscope,for the reduction of Fe^{3+}in all three data sets.

The values for $V\Delta P$ do not take into account the degradation of the transducer over time. Newer transducers tend to show lower measured peak driving voltages than older ones when covered in solution. The used transducers show higher voltages, but appear to have less effect as the piezoelectric material integrity declines. To compare across data sets, $V\Delta P$ is normalized to the highest $V\Delta P$ value in each set, reflecting the fraction of available acoustic pressure, $F_{\dot{p}}$.

In Figure 40 data set 1 has a linear regression of: $ln(k^0) = (7.0 \pm 0.7) \times F_p - (11.4 \pm 0.6)$ with $R^2 = 0.94$, data set 2 has a linear regression of: $ln(k^0) = (4 \pm 1) \times F_p - (15.4 \pm 0.6)$ with $R^2 = 0.80$, and data set 3 has a linear regression of: $ln(k^0) = (8 \pm 2) \times F_p - (16 \pm 1)$ with $R^2 = 0.79$. The coefficient of determination, R^2, shows a moderate degree of goodness of fit to the linear regression for each data set. The slopes for data sets 1 and 3 are similar and the intercepts for data sets 2 and 3 are similar. This demonstrates that there is empirical validity to Equation 94. The data are insufficient to discriminate as to whether the standard enthalpy of activation alone is impacted by sonication or whether the entropy is also impacted.

However, it is clear that sonication increases the rate of heterogeneous electron transfer kinetics with substantial increases in excess of an order of magnitude for the standard heterogeneous rate, k^0. Whether only the standard enthalpy of activation is effect or if the standard entropy of activation is also effected.

CHAPTER 4

IMPACT OF ACOUSTIC ENERGY ON ELECTRODE SURFACES

4.1 Introduction

In early experiments on Fe^{3+} and O_2, the cyclic voltammetric morphologies of initial scans taken prior to sonication and final unsonicated scans taken after sonication differ. The post-sonication scans retained some morphology of sonication without active sonication that is characteristic of improved heterogenous electron transfer rates. This raised the question of whether sonication changes the electrode surface.

Classically, one means of electrode passivation is the formation of oxides on metal electrode surfaces. On platinum, the formation of platinum (IV) oxide is considered a three step process [46]. First, platinum is oxidized with water to form a platinum (I) hydroxide, PtOH. (Equation 95). Second PtOH undergoes a place exchange into the crystal structure a second oxidation step to form platinum (II) oxide, PtO. (Equation 96). Third and final, oxidation of PtO with another water forms platinum (IV) oxide, PtO_2. (Equation 97). Overall, oxidation of Pt to PtO_2 is a four electron, four proton process.

$$Pt + H_2O \rightarrow PtOH + H^+ + e^- \qquad 0.85 - 1.10\ V \tag{95}$$

$$PtOH \xrightarrow{place\ exchange} PtO + H^+ + e^- \qquad 1.10 - 1.40\ V \tag{96}$$

$$PtO + H_2O \rightarrow PtO_2 + 2H^+ + 2e^- \qquad > 1.40\ V \tag{97}$$

The observed potentials are measured with regular hydrogen electrode (RHE) reference. The PtO layer typically limits at two monolayers with a platinum (IV) oxide overlayer of unrestricted thickness [46]. The rate of oxide formation is dependent on the crystal surface of the platinum [47]. The initial growth of the two monolayers of PtO and the first monolayer of PtO_2 is a slow process [47].

Once formed, the passivated layers are $Pt \mid 2PtO \mid nPtO_2$. The removal of the oxide layers by reduction is thought to start with the reduction of platinum (II) oxide. That is followed by the reduction of the platinum (IV) oxide.

$$Pt \quad | \quad 2PtO \mid nPtO_2 + 4H^+ + 4e^- \rightarrow Pt \mid nPtO_2 + 2H_2O \qquad 0.60 - 0.30\ V \quad (98)$$

$$Pt \quad | \quad nPtO_2 + 4nH^+ + 4ne^- \rightarrow Pt + 2nH_2O \qquad 0.30 - 0.10\ V \quad (99)$$

The observed potentials are measured with an RHE reference. Oxide layer formation and reduction on platinum is potential dependant and slow. If the kinetics are improved to the extent that the clean platinum surface is available for reaction, high rates of electrolysis at the platinum electrocatalyst are available than at the oxide passivated platinum surface.

Another effect that may explain the persistence of improved kinetics post-sonication is the surface reconstruction of platinum. This involves the rearrangement of the platinum crystal matrix such that a different facet of the crystal is exposed. Pt(100) and (Pt111) often provide different electrocatalytic efficiencies. The energy required for surface reconstruction of platinum is not well established because measurements are difficult, but literature models fine a relatively low energy, on the order of 1.99×10^{-20} J/Å^2 [47]. Changes in the crystal

structure face can have a significant impact on reaction rate. For example, studies have shown that initial surface oxide formation is significantly faster on Pt(100) than on Pt(111) and is attributed to the ease with which the arriving oxygen is integrated into the platinum matrix [46, 47].

In the first experiment, the persistence of the change in the rates of heterogeneous electron transfer are evaluated by comparing unsonicated scans before and after sonication. This experiment expands up the Fe^{3+} experiments in chapter 3 by adding an additional set of post-sonication, unsonicated scans after the system rests for five minutes. This is intended to provide insight as to the persistence of the change in morphology.

The second experiment involves scanning the platinum oxide reduction peak with and without sonication. Sonicated and unsonicated scans consist of repeated sweeps used to monitor the platinum oxide reduction peak to see if it changes during sonication.

4.2 Experimental

Two experiments are of interest: 5.00 mM Fe^{3+} in 0.100 M nitric acid and blank electrolyte 0.100 M nitric acid

Electrochemical Cell A second generation sonoelectrochemical cell as described in Chapter 2 is cleaned with concentrated nitric acid (Fisher Scientific) and deionized water (Millipore Model Milli Q plus 18.2 MΩ). A nitrogen blanket is set up to surround the sonoelectochemical cell.

Working and Counter Electrodes The working and counter electrodes consist

of 0.5 mm platinum wire (Sigma-Aldrich) inserted 8 mm into the solution. Prior to use the electrode is immersed in concentrated nitric acid (Fisher Scientific) for four minutes and rinsed in deionized water (Millipore Model Milli Q plus 18.2 MΩ).

Reference Electrode The quasireference electrode used consists of 0.5 mm platinum wire (Sigma-Aldrich) inserted 8 mm into the solution. Prior to use, the electrode is immersed in concentrated nitric acid (Fisher Scientific) for four minutes and rinsed in deionized water (Millipore Model Milli Q plus 18.2 MΩ).

Electrolyte A solution of 0.100 M nitric acid (Fisher Scientific) in deionized water (Millipore Model Milli Q plus 18.2 MΩ) is used as the electrolyte.

Materials Unless otherwise noted, all chemicals used are obtained by Sigma-Aldrich Chemical Co. and are used as received. Iron (III) nitrate nonahydrate (Fe^{3+}) is used to form a 0.500 mM solution of Fe^{3+} in the aforementioned 0.100 M nitric acid electrolyte is used as a redox probe. All solutions are degassed with nitrogen gas for 15 minutes. 1 mL of solution is placed in the sonoelectochemical cell well with a disposable pipette; this creates a meniscus that peaks about 3 mm above the edge of the well. The studies of platinum in nitric acid electrolyte are the same as the ferric ion experiments except no redox probe is used and there is no nitrogen blanket.

Sonication Sound waves are generated in the sonoelectrochemical cell at a frequency of 41 kHz. Unless otherwise noted, intensity is varied from 100 % (maximum) down to approximately 40 % in roughly 10 % increments for Fe^{3+} and 20 % increments for blank electrolyte. Unsonicated scans are run before and after the sonication sets. Peak voltage (V_p) is monitored with an oscilloscope.

Table 7. Tabulation of cyclic voltammetry data set 2 for 5.00 mM Fe^{3+} in 0.100 M nitric acid taken before and after sonication.

Sonication Intensity (%)	k^0 (cm/s)	α
Pre-sonication	3.0 ($\pm$ 0.7) $\times 10^{-6}$	0.77 ($\pm$ 0.01)
Initial Post-sonication	1.3 ($\pm$ 0.3) $\times 10^{-4}$	0.87 ($\pm$ 0.01)
Final Post-sonication	1.4 ($\pm$ 0.1) $\times 10^{-5}$	0.86 ($\pm$ 0.02)

Note: Potentials recored versus a platinum | platinum oxide reference. Data includes standard heterogeneous electron transfer rate and α. Each average is of four replicates. Postsonication scan sets are seperated by about five minutes. Overall average E^0 is -280 ($\pm$ 40) mV.

Voltammetry A BAS 100B Electrochemical Analyzer is used to collect all voltammetry measurements. Voltammograms are recorded at scan rates of 0.1 V/s.

4.3 Voltammetric Results for Platinum Electrode before and after Sonication

Two experiments demonstrate that impact on the sonoelectochemical system persists after sonication ceases.

4.3.1 Platinum Electrode with Fe^{3+} Redox Probe in Nitric Acid Solution before and after Sonication

A series of cyclic voltammetric scans are run in the sonoelectrochemical cell with a 5.00 mM Fe^{3+} in 0.100 M nitric acid electrolyte. A set of three scans, each scan consisting of a forward and backward sweep, are run without sonication, followed by 7 sets of three scans each at assorted levels of sonic intensity. The scans are separated by approximately 10 % increments and performed in random order. After sonication, two sets of scans are taken without sonication approximately five minutes apart. Figure 41 is a plot of representative silent scans.

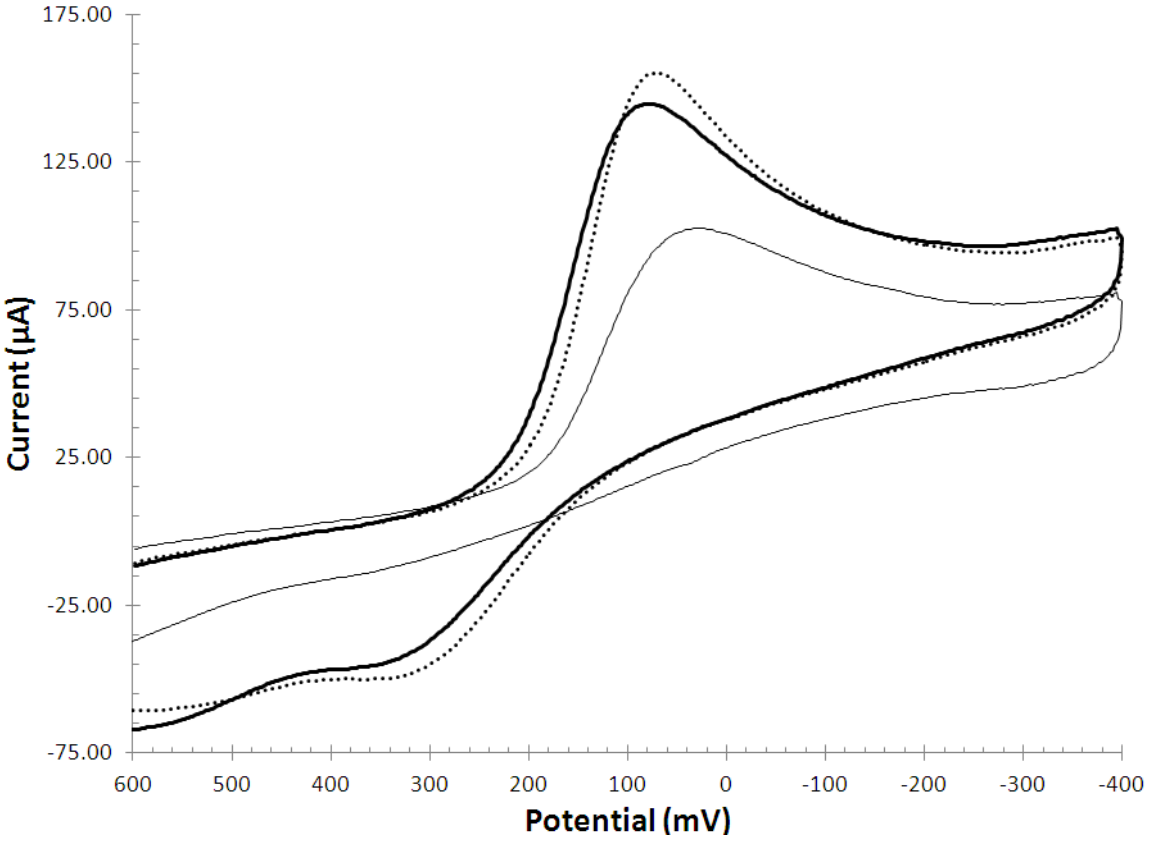

Figure 41. Comparative cyclic voltammograms of 5.00 mM Fe^{3+} in 0.100 M nitric acid taken before and after sonication. Initial Unsonicated (light solid); Unsonicated ($\sim$ 5 minutes after sonication, dotted); Unsonicated ($\sim$ 15 minutes after sonication, heavy solid).

4.3.2 Platinum Electrode in Nitric Acid Solution with and without Sonication

A series of cyclic voltammetry scans are run in the sonoelectrochemical cell with 0.100 M nitric acid solution. An initial set of fifty scans are run without sonication. This is followed by 4 sets of 10 scans under sonication with intensity varied from 100 % (maximum) down to approximately 40 % in roughly 20 % increments. A final set of 10 scans are taken without sonication immediately thereafter. Figure 42 is a plot of representative the initial silent scans and sonicated scans sonicated at 80 % approximately one minute apart. The platinum oxide reduction occurs near 0.2 V versus a platinum wire reference. Replicate initial scans prior to sonication overlay the solid line in Figure 42 and are not plotted. The average peak current of these initial scans is $68.0 \pm 5\mu A$. Repeated sonicated scans follow the same trend as shown in Figure 42 and are not plotted. The post sonication scans have a trend similar to the sonicated scans shown in Figure 42.

In Figure 42, reduction in the peak current for platinum oxide is found under sonication. The reduced platinum oxide current does not persist post sonication. Figure 43 is a plot of the peak current of platinum oxide reduction wave versus forward (reductive) sweep number before, after and at assorted acoustic intensities. The oxide peak diminishes with scan number (time) and sonic intensity. Figures 44 and 46 are plot of cyclic voltammetric data illustrating the last reductive sweep at each sonic intensity and the last three reductive sweeps a maximum intensity, respectively.

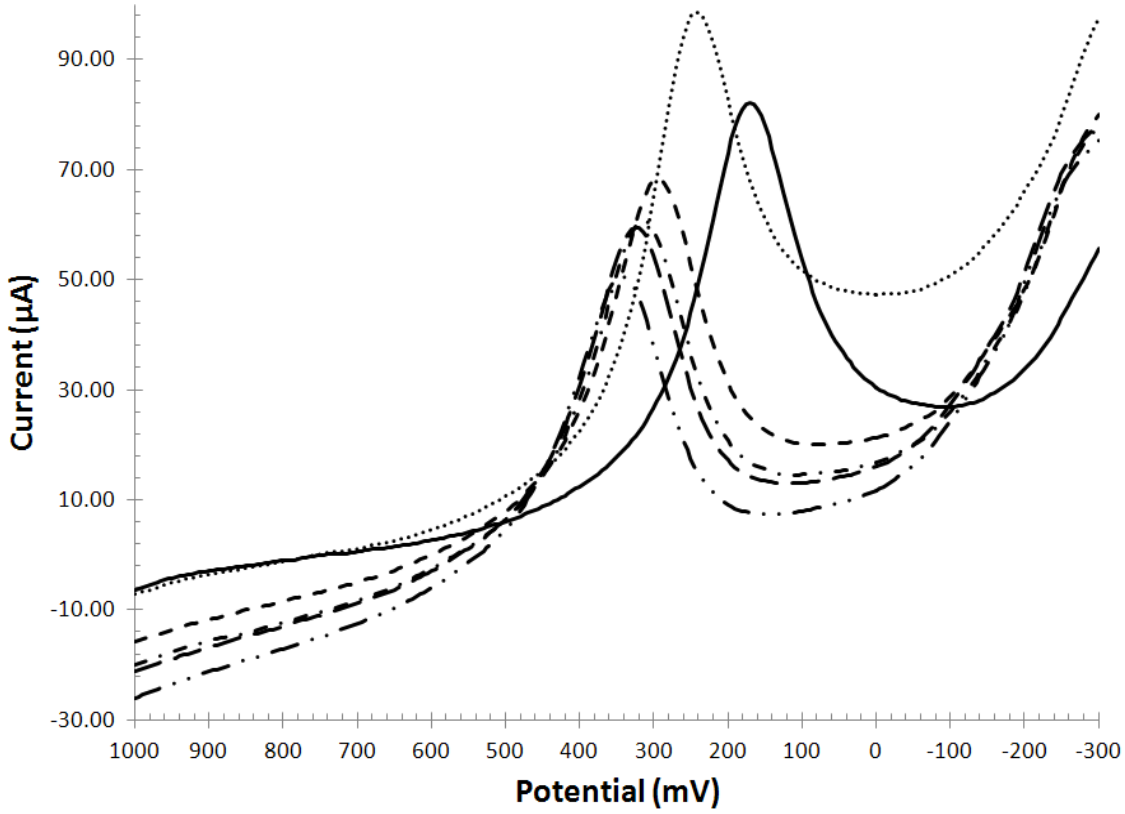

Figure 42. Comparative cyclic voltammograms of a platinum electrode in 0.100 M nitric acid taken before and at 80 % sonication. Voltammetric morphology indicates decreases in the platinum oxide wave. Initial Unsonicated (solid); Sonicated ($\sim$ 30 seconds of sonication, dotted); Sonicated ($\sim$ 90 seconds of sonication, short dashed); Sonicated ($\sim$ 150 seconds of sonication, dash-dot); Sonicated ($\sim$ 210 seconds of sonication, long dashed); Sonicated ($\sim$ 270 seconds of sonication, dash-dot-dot).

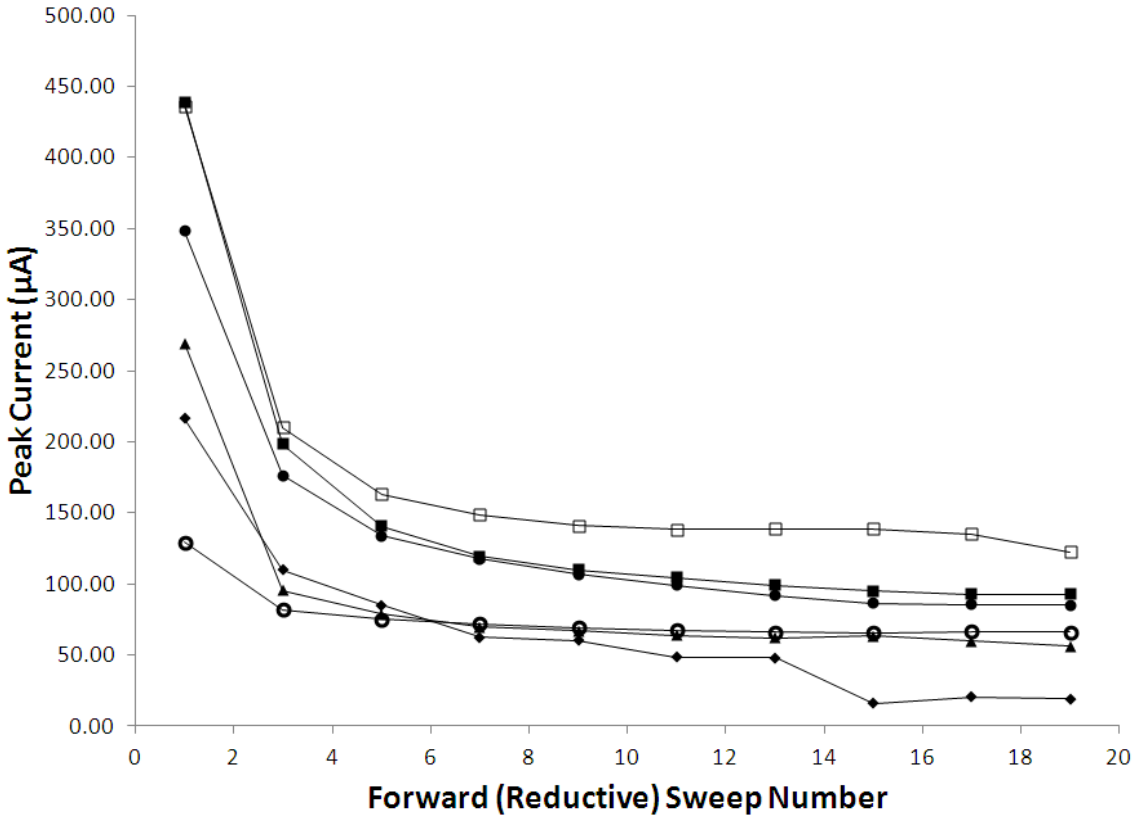

Figure 43. Plot of peak current of platinum oxide reduction wave versus forward (reductive) sweep number unsonicated and at assorted acoustic intensities. Pre-unsonicated (◯);100 % (♦); 80 % (▲); 60 % (●); 40 % (■); Post-unsonicated (□).

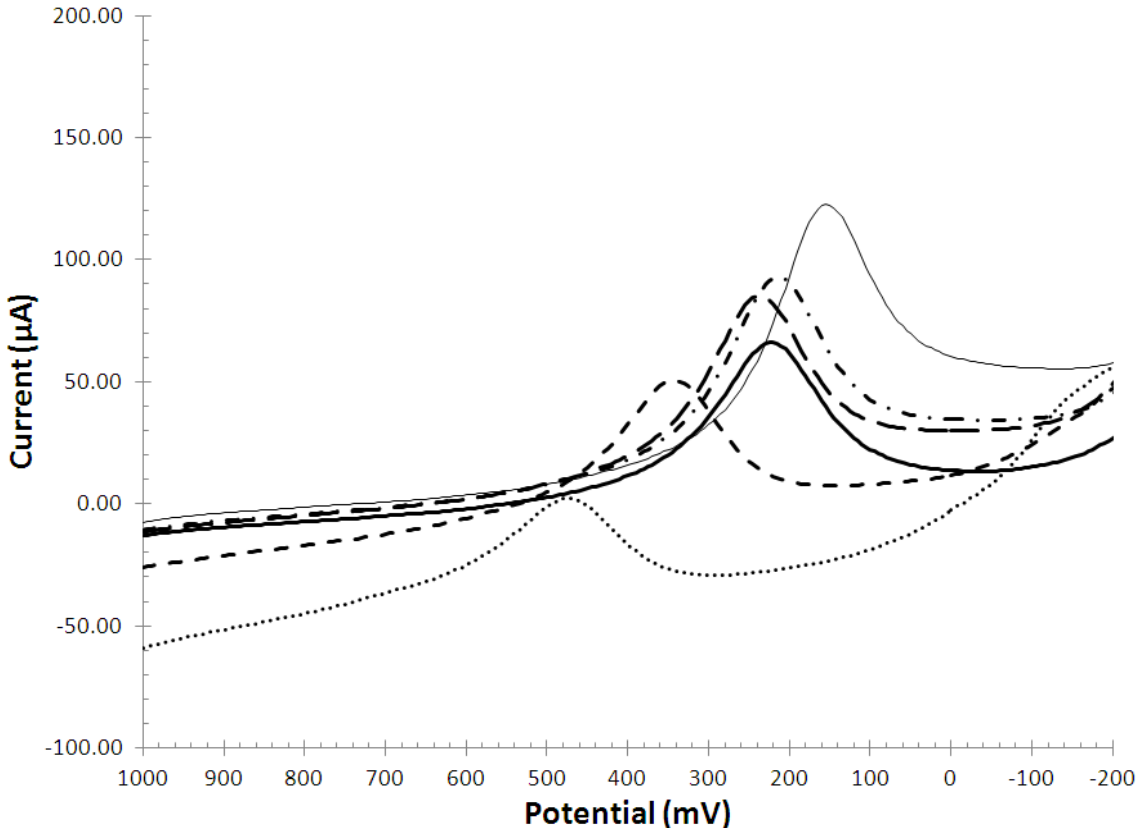

Figure 44. Comparative cyclic voltammograms of a platinum electrode in 0.100 M nitric acid, sonicated and unsonicated. Each wave is the 19^{th} sweep (10^{th} reductive sweep) of a 20 sweep scan. Sonicated scans were exposed to acousitc energy for $\sim$ 270 seconds. Initial Unsonicated (heavy solid); Sonicated, 100 % intensity (dotted); Sonicated, 80 % intensity (short dashed); Sonicated, 60 % intensity (long dashed); Sonicated 40 % intensity (dash-dot); Final Unsonicated (light solid).

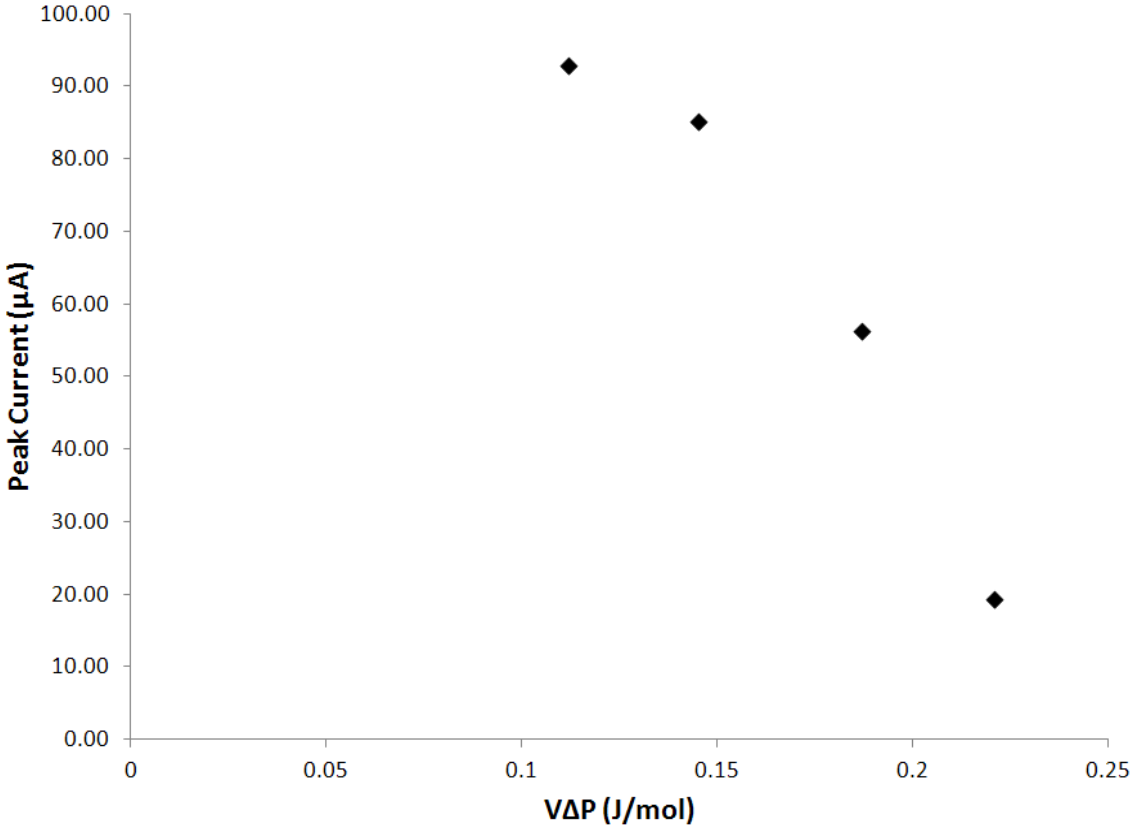

Figure 45. Plot of peak current of platinum oxide reduction wave as a function of $V\Delta P$. Each point is from the 19^{th} segment (10^{th} reductive sweep) of a 20 segment scan. Points are shown for sonication intensities of 100, 80, 60, and 40 % with higher currents at lower sonication intensity. Data were recorded in order of sonication intensity from high to low. The system was exposed to acousitc energy for $\sim$ 270 seconds for each scan.

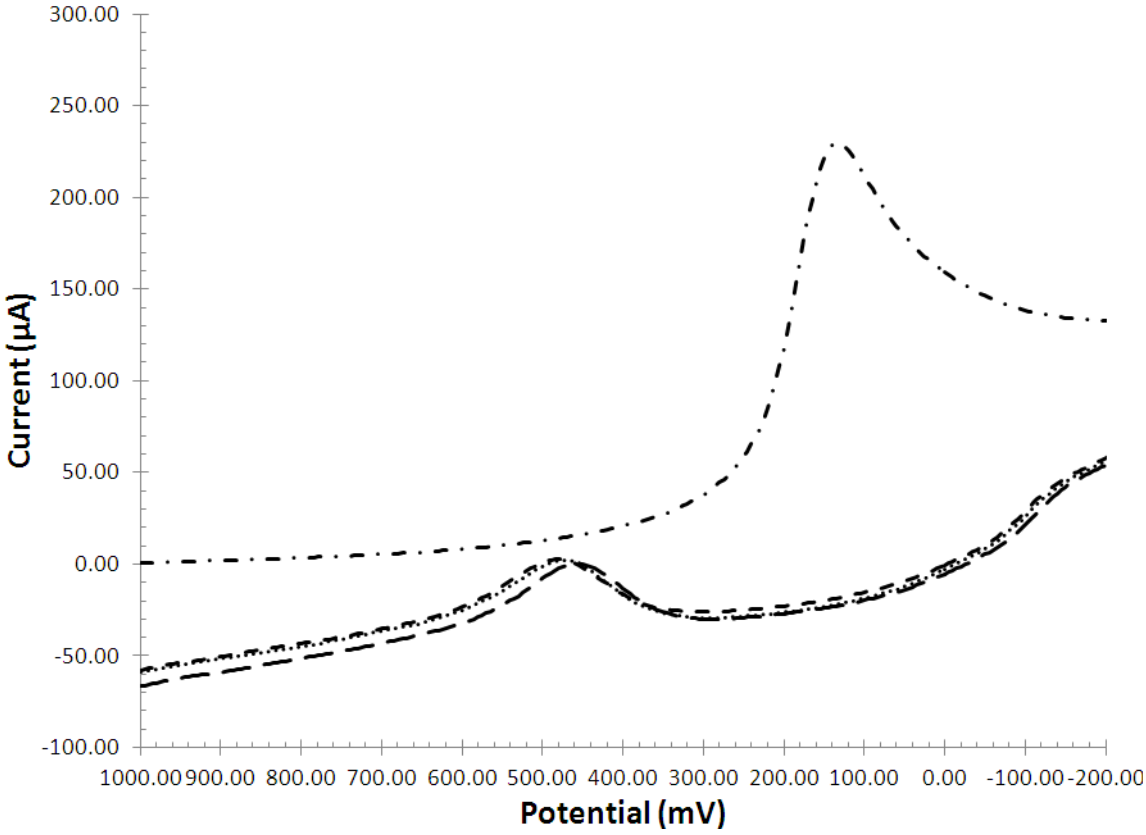

Figure 46. Comparative cyclic voltammograms of a platinum electrode in 0.100 M nitric acid taken at 100 % sonication. Voltammetric morphology indicates decreases in the platinum oxide wave. Initial Sonicated (0 seconds of sonication, dash-dot); Sonicated ($\sim$ 210 seconds of sonication, long dashed); Sonicated ($\sim$ 240 seconds of sonication, short dashed); Sonicated ($\sim$ 270 seconds of sonication, dotted).

4.4 Discussion

The persistence of increased heterogeneous electron transfer rates are evaluated by comparing unsonicated scans before and after sonication. The persistence of improved kinetics post sonication was first observed in early experiments when the initial and final unsonicated scans did not overlay and has been observed in most subsequent experiments. Evidence of the persistence of facile kinetics post sonication is shown in Figure 41 for Fe^{3+}. The standard heterogenous rate, k^0, and transfer coefficient, α, for these voltammograms are shown in Table 7. The representative data show a 48 fold increase in k^0 and a 0.1 increase in α, between the initial unsonicated scans and the unsonicated scans immediately post sonication. Five minutes postsonication, k^0 diminishes 10 fold but is greater than k^0 presonication. From a practical standpoint, this implies that constant sonication may not be necessary for all systems.

The catalytic effect of platinum is attributed to a platinum surface cleaned of oxide. Oxide layers impede heterogenous electron transfer. That improved kinetics persist postsonication may be the result of changes in the electrode surface (removal of the platinum oxides) and of change in the crystal face of the platinum (change in the crystal face from Pt(100) to Pt(111)). The energy required to break a Pt-O bond is reported as 391.6 ± 41.8 kJ/mol [45] and is in excess of the apparent acoustic energy added to the system on a volume basis, as calculated in Chapter 2. This effect may be explained by the trapping of energy in irregularities in the electrode surface. Similar phenomena allows for cavitation below the expected

theoretical acoustic energy levels in some systems. (See Section 1.1.2.) Note that this system does not produce enough acoustic energy for cavitation, even with surface irregularities.

The energy required for the surface reconstruction of platinum is not well defined experimentally, however models indicate the required energy is relatively low, on the order of 1.99×10^{-20} J/Å^2 [47] or 44.2 kJ/mol. This would imply an initial input of 2.4×10^{-5} J would be required to initially change the surface crystallinity of one working electrode in the system. Such changes in the crystal structure face can have a significant impact on rate of oxide formation. For example, studies have shown that initial surface oxide formation is significantly faster on Pt(100) than on (Pt111) and is attributed to the ease with which the arriving oxygen is integrated into the platinum matrix [47].

The second experiment evaluates the amount of platinum oxide as a function of intensity and time of sonication, as shown in Figures 42, 43, 44, 45, and 46. Prior to sonication, the platinum oxide reduction has an average peak current of 68.0 ± 0.5 μA. Over the course of sonication, the peak height diminishes as the platinum oxide is removed and more active electrode area is exposed, as shown in Figure 43. The first sonicated scan is at maximum acoustic intensity and has a peak current of 216.5 μA for the first sweep. After 160 seconds of maximum intensity sonication, the peak current is reduced to 60.4 μA indicating a reduction in the amount of available oxide. By 270 seconds, the peak current is 19.3 μA. The second sonicated scan behaves in a similar manner with an initial peak current of 269 μA which decreases to 56.2 μA after 270 seconds of sonication. Each successive

scan, run at a lower acoustic intensity, shows a steady decrease in the peak current of platinum oxide reduction between the initial and final sweep, indicating removal of the oxide layers. Whenever the acoustic intensity was decreased, the peak current increases in comparison to corresponding sweeps at higher acoustic intensities. Figure 45 is a plot of peak current of platinum oxide reduction wave as a function of $V\Delta P$. Each point is from the 19^{th} segment (10^{th} reductive sweep) of a 20 segment scan. At each point the system was exposed to acoustic energy for $\sim$ 270 seconds. As the level of sonication increases, there is less available oxide at the end of each scan. The peak current diminished with higher intensity of sonication indicates the energy input by sonication is sufficient to modify the platinum oxide layers.

In summary, the platinum oxide wave in cyclic voltammetric data decreases with sonication intensity, consistent with removal of the oxide layer. The removal of the oxide layer is consistent with increased kinetics of electron transfer with higher intensity of sonication. The removal of the oxide layer is also consistent with persistence of a sonication impact post sonication.

CHAPTER 5

IMPACT OF LOW INTENSITY SONICATION IN A THIN LAYER ON OXYGEN KINETICS

5.1 Introduction

The reduction of oxygen is a multistep process that requires four protons and four electrons. The first reduction step is thought to be the slow step kinetically.

The slow kinetics of oxygen reduction prevent spontaneous combustion and ensure mitigation of biological damage by reactive oxygen species, but limit performance of air batteries, fuel cells and other power sources. The inherently poor kinetics of oxygen severely limits the efficiency of the electrochemical reactions where oxygen reduction is part of the process. Direct thermal decomposition of oxygen is less selective; but in internal combustion engines, the moving parts limit efficiency to below 40 %. The ability to increase the rate of oxygen reduction kinetics in a electrochemical system can improve the efficiency of electrochemical power sources. Because of the high demand for compact power sources, the thin layer sonoelectrochemical cell is appealing.

In this study, acoustic energy is applied to a thin layer electrochemical systems to increase the apparent standard heterogeneous electron transfer rate, k^0, of the reduction of oxygen. Molecular oxygen is used as a sonoelectrochemical probe in a saturated solution. Furthermore, because the thin layer sonoelectochemical system

$$O_{2,absorbed}$$

$$\downarrow\uparrow H^+, e$$

$$HO^{\bullet}_{2,absorbed}$$

$$\downarrow\uparrow H^+, e$$

$$H_2O_{2,absorbed} \rightleftarrows H_2O_{2,solution}$$

$$\downarrow\uparrow$$

$$2HO^{\bullet}_{absorbed}$$

$$\downarrow\uparrow 2H^+, 2e$$

$$2H_2O_{absorbed} \rightleftarrows 2H_2O_{solution}$$

Figure 47. Reaction scheme for the reduction of oxygen to water. Note this is a complex 4 proton, 4 electron process.

profoundly increases the rate of ferric ion electrolysis, ferric ion was added to an oxygenated solution.

5.2 Experimental

Electrochemical Cell A second generation sonoelectrochemical cell as descibed in Chapter 2 is cleaned with concentarted nitric acid (Fisher Scientific) and deionized water (Millipore Model Milli Q plus 18.2 MΩ) .

Working and Counter Electodes The working and counter electrodes consisted of 0.5 mm platinum wire (Sigma-Aldrich) inserted 8 mm into the solution. Prior to use the electode is immersed in concentrated nitric acid (Fisher Scientific) for four minutes and rinsed in deionized water (Millipore Model Milli Q plus 18.2 MΩ).

Reference Electrode The reference electrode consists of a silver | silver oxide electode constructed from 0.5 mm silver wire (Aldrich) dipped in nitric acid (Fisher Scientific) for 1 minute and rinsed with deionized water (Millipore Model Milli Q plus 18.2 MΩ).

Electrolyte A solution of 0.100 M nitric acid (Fisher Scientific) in deionized water (Millipore Model Milli Q plus 18.2 MΩ) is used as the electrolyte.

Materials Unless otherwise noted, all chemicals used were obtained by Sigma-Alderich Chemical Co. and were used as received. Iron (III) nitrate nonahydrate (Fe^{3+}) is a commerically available redox probe. A 5.00 mM solution of Fe^{3+} in the aforementioned 0.500 M nitric acid electrolyte is used as a redox probe where mentioned. All solutions are saturated with O_2 using a needle based gassing

system for 20 minutes. At laboratory temperatures, this created a 0.28 mM solution of oxygen[48]. Saturation was maintained with an oxygen blanket surrounding the sonoelectochemical cell. 1 mL of either solution was placed in the sonoelectochemical cell well with a disposable pipet creating a meniscus approximately 3 mm above the top of the well.

Sonication Sound waves are generated in the sonoelectrochemical cell at a frequency of 41 kHz. Unless otherwise notes, intensity was varied from 100 % (maximum) down to approximately 40 % in roughly 10 % incriments. Unsonicated scans were run before and after the sonication sets. Peak voltage (V_p) was monitored with an oscilloscope. Where noted, sonication intensity was set in random order to eliminate bias.

Voltammerty A BAS 100B Electrochemical Analyzer is used to collect all voltammerty measurements. Voltammograms are recorded at scan rates of 0.1 V/s.

5.3 Voltammetric Results for O_2 and O_2 with Fe^{3+} Redox Probes with and without Sonication

Oxygen kinetics examined with and without ferric ion. The prinicple focus is on the oxygen reaction in the absence of iron ion.

5.3.1 Oxygen with and without Sonication

A series of cyclic voltammetric scans is run in the thin layer sonoelectrochemical cell with solutions of 100 mM nitric acid saturated with O_2 at room temperature, 0.28 mM. An initial set of three scans are run without sonication, followed by 7 sets

of three scans each at various intensities of sonication. A set of unsonicated scans are performed after sonication. Figure 48 is a plot of representative scans. Note that as the intensity increases, the voltammetric wave forms shift to a more erect morphology consistent with more rapid kinetics.

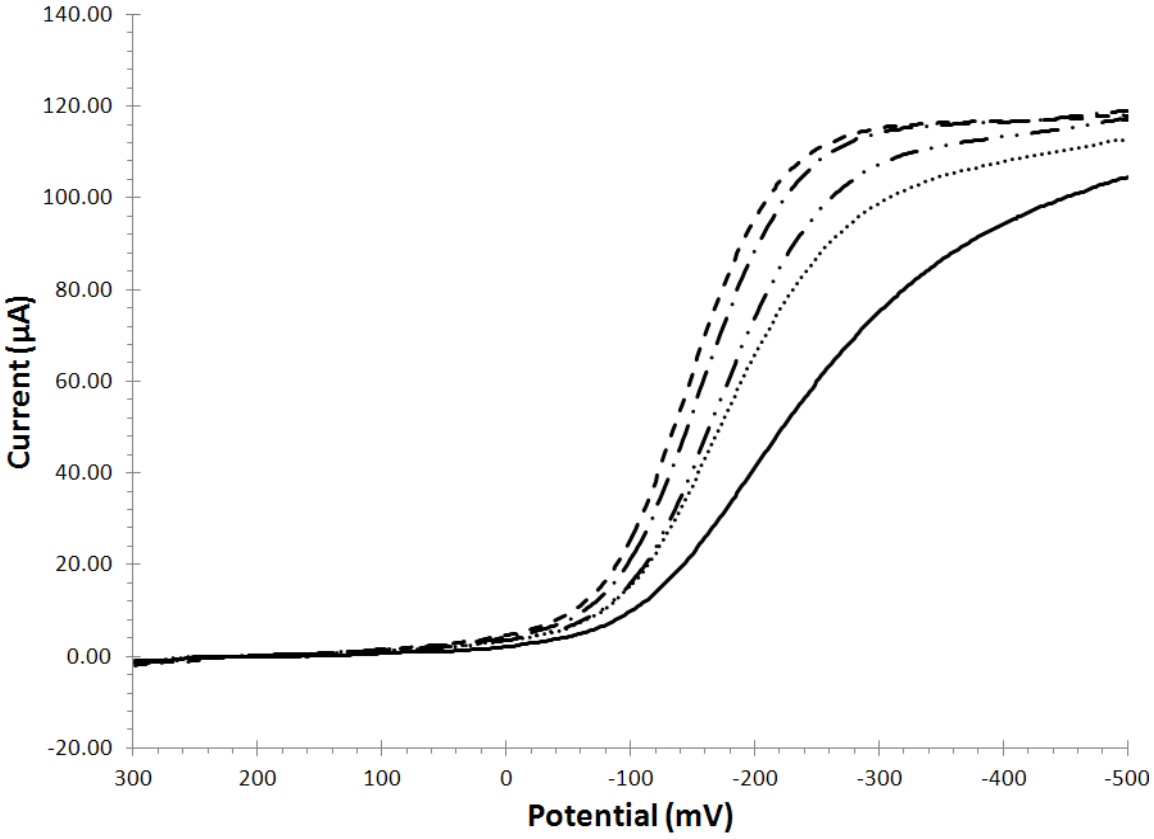

Figure 48. Cyclic voltammograms of 0.28 mM O_2 in 0.100 M nitric acid taken at assorted levels of sonication for data set 1. Sonicated 100 % intensity (dashed); Sonicated 80 % intensity (dash dot); Sonicated 60 % intensity (dash dot dot); Sonicated 40 % intensity (dotted); Unsonicated (post sonication) (solid). Scans were taken in the order listed.

Analyses of the oxygen data are performed in the same manner as the ferric ion data, as described in Section 3.3.5. An example of this fitting for oxygen is shown in Figure 49. The forward scan of the data (from the baseline to i_{lim}) is used to fit

the model using the Solver tool embedded into Microsoft Office Excel. A chi-square comparison of the data and the model was generated using initial guesses for $i_0/i_{\lim}$, α and $E^{0'}$ in the model. The Solver tool is the used to adjust $i_0/i_{\lim}$, α and $E^{0'}$ so as to minimize the value of chi-square. Values for α were constrained between 1 and 0 and values for $E^{0'}$ were constrained between -0.1 and 0.2 volts. None of the fittings reached these limits with their final values. Various initial guesses were used for each fitting so as to avoid local minimums. It is noted that the model is for kinetics limited to single electron transfer. The first electron transfer for oxygen is likely rate determining in quiescent solution. As sonic intensity increases, other events may limit the response and the model may be poorly applicable.

Once all the curves were fit, plots of k^0 as a function of $V\Delta P$ and α as a function of $V\Delta P$ were generated. See Figures 50 and 51. A summary of the voltammetric data, E_{pred}, E_{pox} and ΔE_p for various sonication intensities are given in Table 8. Figures 52, 53, and 54 and Table 9 show additional studies of 0.28 mM O_2 saturated in 0.100 M nitric acid. At atmospheric pressure and 25 °C, the saturated oxygen concentration is known to be 0.28 mM [48]. Values differ slightly between experiments but the general cyclic voltammetric behavior and extracted k^0 are the same with increased kinetics at higher sonic intensity.

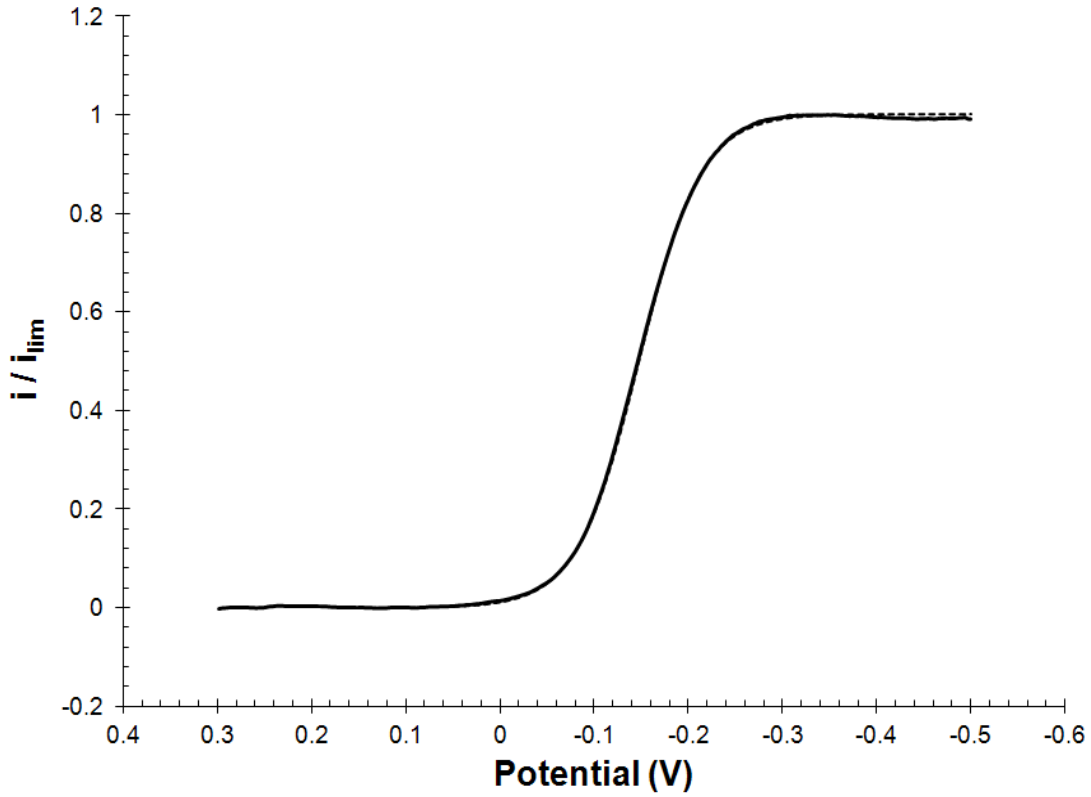

Figure 49. Example of fitted sonicated, saturated O_2 cyclic voltammetric data to current overpotential model. Sweep recorded at 90 % sonic intensity. $\chi^2 = 0.11$. Data (solid); Model (Dashed)

Table 8. Tabulation of cyclic voltammetric data set 1 for 0.28 mM O_2 in 0.100 M nitric acid taken at various levels of sonication.

Sonication Intensity (%)	k_0 (cm/s)	α	$E^{0'}$ (mV)	$V\Delta P$ (J/mol)
100	5.4 ($\pm$ 0.1) $\times 10^{-4}$	0.68 ($\pm$ 0.04)	10 ($\pm$ 1)	0.23
90	9.4 ($\pm$ 0.6) $\times 10^{-5}$	0.77 ($\pm$ 0.01)	40 ($\pm$ 5)	0.22
80	2.2 ($\pm$ 1) $\times 10^{-5}$	0.75 ($\pm$ 0.01)	90 ($\pm$ 20)	0.20
70	2.6 ($\pm$ 0.9) $\times 10^{-5}$	0.72 ($\pm$ 0.02)	90 ($\pm$ 20)	0.19
60	2.4 ($\pm$ 0.9) $\times 10^{-5}$	0.68 ($\pm$ 0.01)	90 ($\pm$ 10)	0.17
50	1.8 ($\pm$ 0.1) $\times 10^{-5}$	0.66 ($\pm$ 0.01)	107 ($\pm$ 6)	0.16
40	2.6 ($\pm$ 0.5) $\times 10^{-5}$	0.63 ($\pm$ 0.01)	102 ($\pm$ 2)	0.14
Unsonicated (post)	8.2 ($\pm$ 0.4) $\times 10^{-6}$	0.46 ($\pm$ 0.01)	223 ($\pm$ 6)	0

Note: Potentials recored versus a silver | silver oxide reference. Data include the apparent standard heterogeneous electron transfer rate, α, $E^{0'}$, and VΔP. Each point is the average of three replicates.

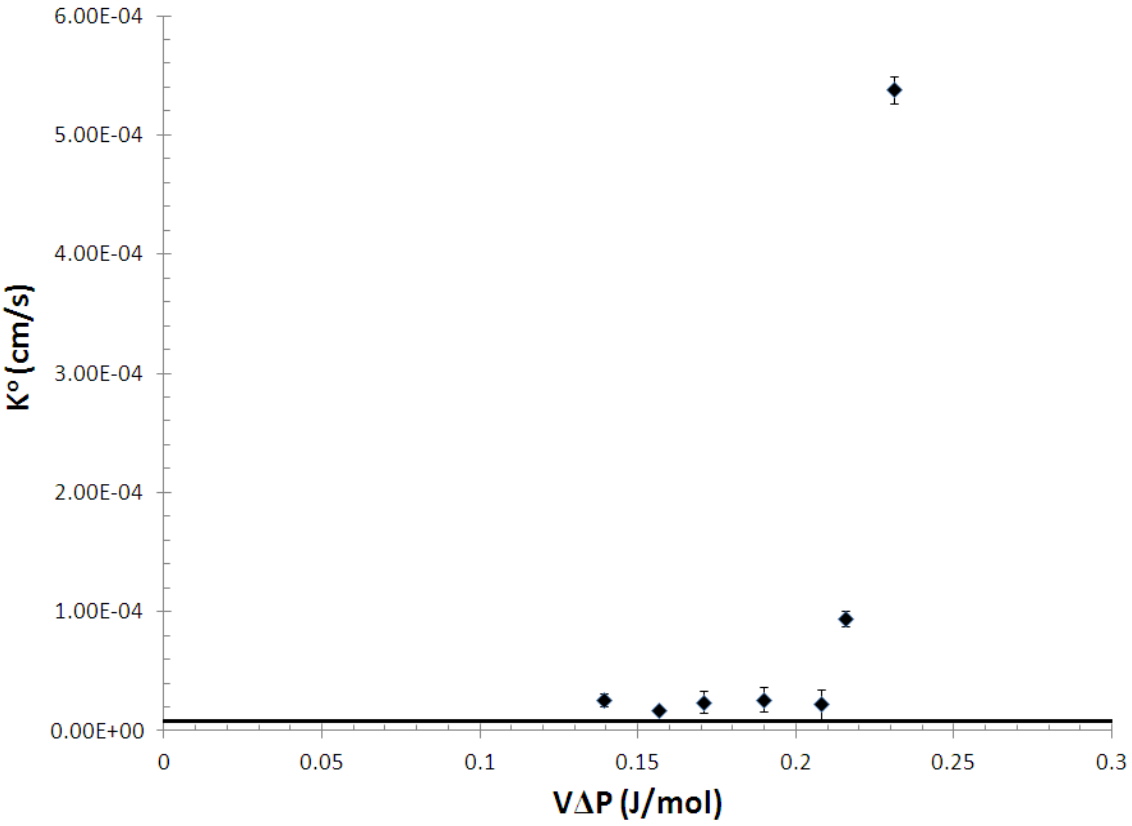

Figure 50. Plot of the apparent standard heterogeneous electron transfer rate constant, k^0, as a function of $V\Delta P$ for sonicated O_2 cyclic voltammetric data set 1. Error bars represent standard deviation. Each point is an average of three scans. Solid line represents the apparent standard heterogeneous electron transfer rate constant, k^0, of post-sonicated unsonicated scans.

Table 9. Tabulation of cyclic voltammetric data set 2 for 0.28 mM O_2 in 0.100 M nitric acid taken at various levels of sonication.

Sonication Intensity (%)	k_0 (cm/s)	α	$E^{0'}$ (mV)	$V\Delta P$ (J/mol)
100	2.4 ($\pm$ 0.1) $\times 10^{-4}$	0.51 ($\pm$ 0.01)	18 ($\pm$ 1)	0.23
90	1.4 ($\pm$ 0.4) $\times 10^{-4}$	0.63 ($\pm$ 0.06)	53 ($\pm$ 5)	0.22
80	3.7 ($\pm$ 0.2) $\times 10^{-5}$	0.61 ($\pm$ 0.02)	100 ($\pm$ 20)	0.20
70	3.7 ($\pm$ 0.3) $\times 10^{-5}$	0.57 ($\pm$ 0.05)	90 ($\pm$ 20)	0.19
60	3.1 ($\pm$ 0.1) $\times 10^{-5}$	0.56 ($\pm$ 0.01)	90 ($\pm$ 10)	0.17
50	2.8 ($\pm$ 0.7) $\times 10^{-5}$	0.53 ($\pm$ 0.02)	98 ($\pm$ 3)	0.16
40	2.9 ($\pm$ 1) $\times 10^{-5}$	0.49 ($\pm$ 0.03)	95 ($\pm$ 5)	0.14
Unsonicated (post)	7.9 ($\pm$ 0.6) $\times 10^{-6}$	0.38 ($\pm$ 0.01)	150 ($\pm$ 10)	0

Note: Potentials recored versus a silver | silver oxide reference. Data include the apparent standard heterogeneous electron transfer rate, α, $E^{0'}$, and VΔP. Each point is the average of three replicates.

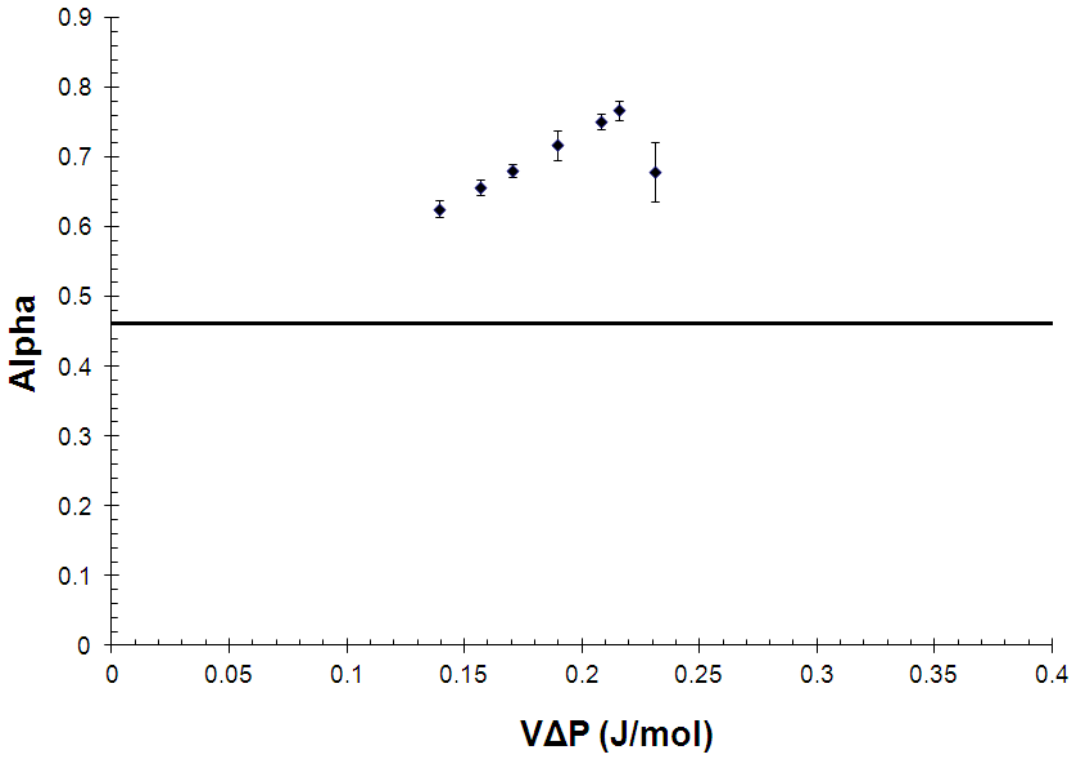

Figure 51. Plot of the transfer coefficient, α, as a function of $V\Delta P$ for sonicated O_2 cyclic voltammetric data set 1. Error bars represent standard deviation. Each point is an average of three scans. The solid line represents the transfer coefficient, α, of unsonicated scans.

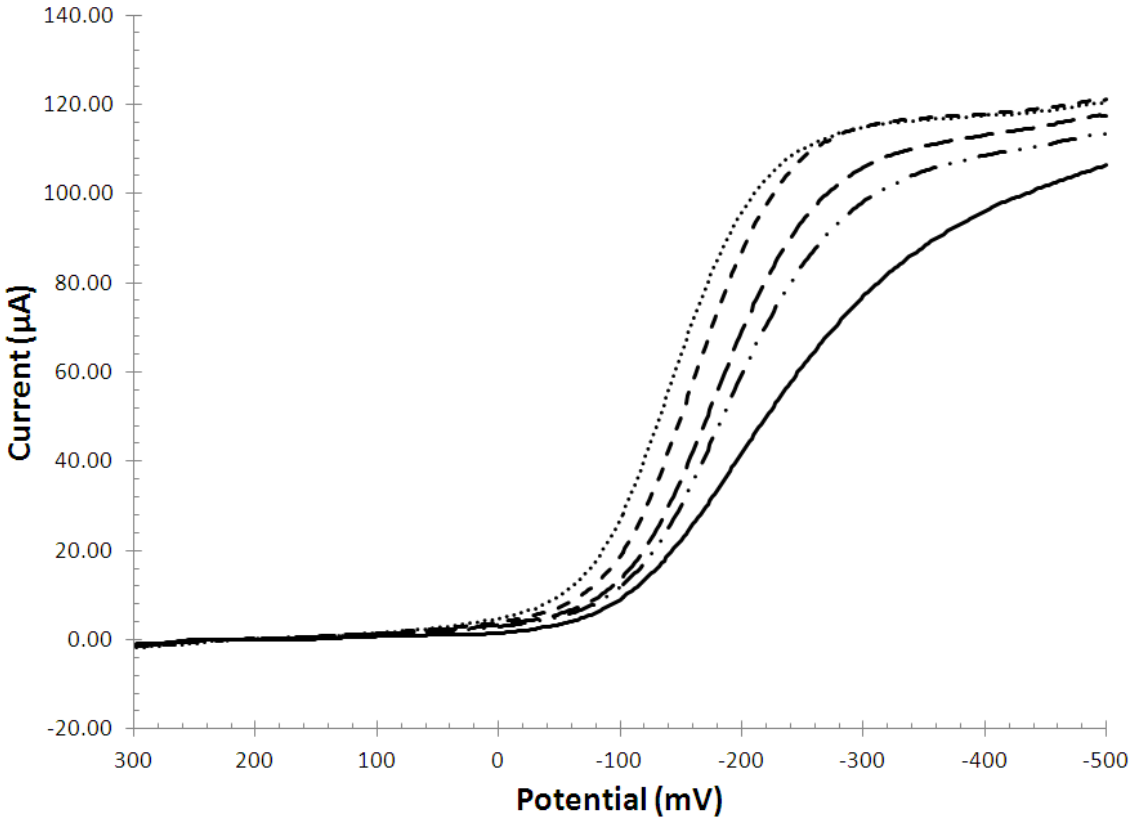

Figure 52. Cyclic voltammograms of 0.28 mM O_2 in 0.100 M nitric acid taken at assorted levels of sonication for data set 2. Sonicated 100 % intensity (dashed); Sonicated 80 % intensity (dash dot); Sonicated 60 % intensity (dash dot dot); Sonicated 40 % intensity (dotted); Unsonicated (post sonication) (solid). Scans were taken in the order listed.

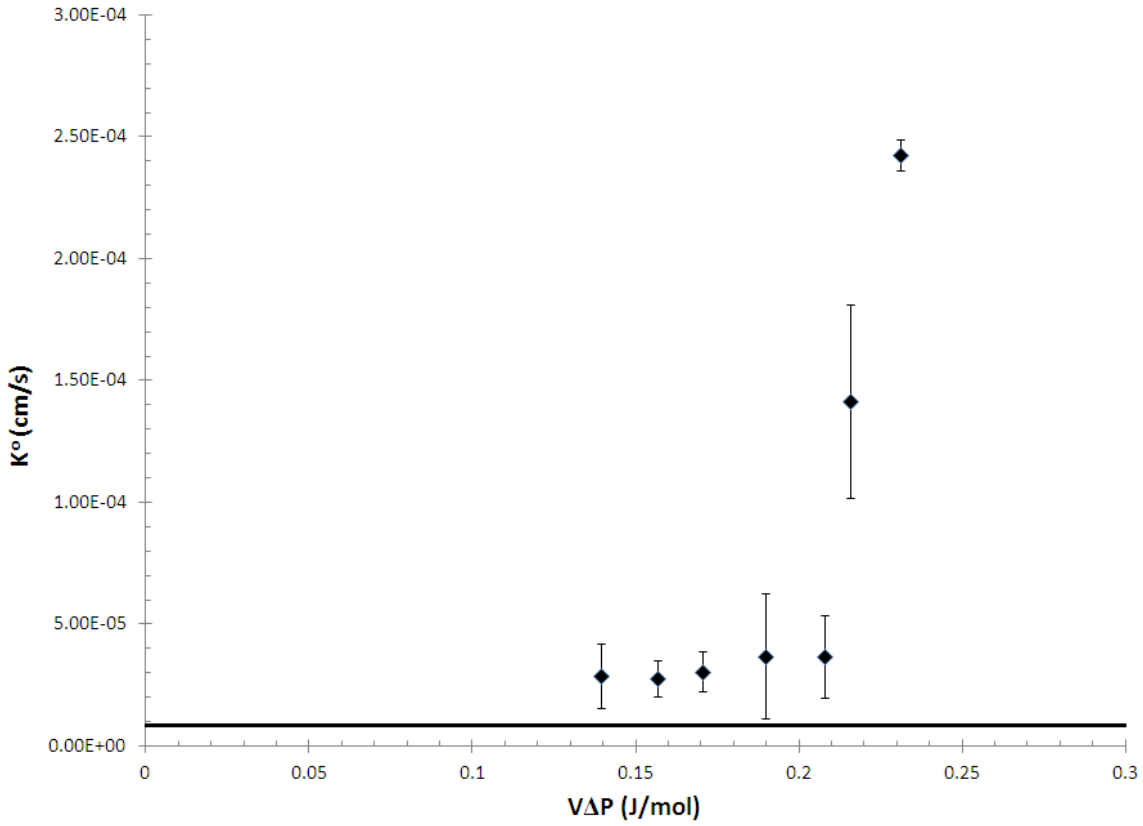

Figure 53. Plot of the apparent standard heterogeneous electron transfer rate constant, k^0, as a function of $V\Delta P$ for sonicated O_2 cyclic voltammetric data set 2. Error bars represent standard deviation. Each point is an average of three scans. Solid line represents the apparent standard heterogeneous electron transfer rate constant, k^0, of post-sonicated unsonicated scans.

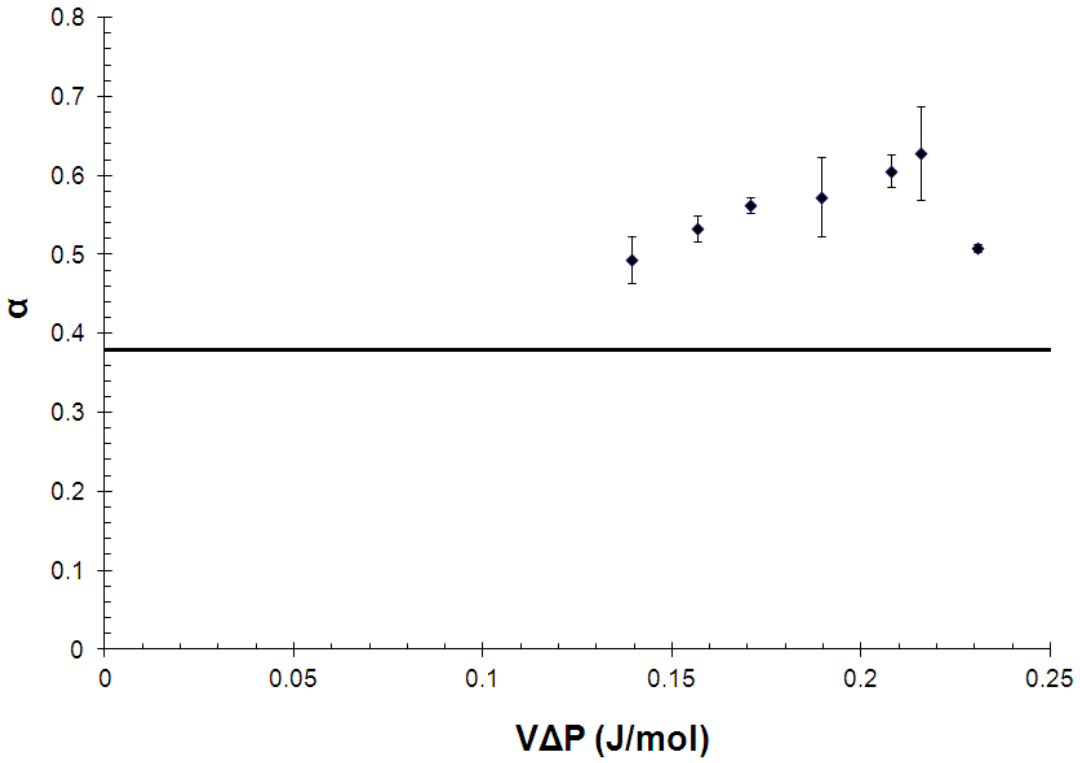

Figure 54. Plot of the transfer coefficient, α, as a function of $V\Delta P$ for sonicated O_2 cyclic voltammetric data set 2. Error bars represent standard deviation. Each point is an average of three scans. The solid line represents the transfer coefficient, α, of unsonicated scans.

5.3.2 Oxygen and Fe^{3+} with and without Sonication

A second cyclic voltammetric experiment was run in the thin layer sonoelectrochemical cell with an oxygenated solution of 5.00 mM Fe^{3+} and 100 mM nitric acid. An initial set of three scans were run prior to sonication, followed by 7 sets of three scans each. A final set of three scans were taken without sonication afterward. Figure 55 is a plot of scans representative of each intensity. The scan sets were spaced out in approximately 10% increments and performed in random order. Data are not fit to the model because a limiting current is needed for each species.

5.4 Discussion

Application of acoustic forces directly impacts the rate of oxygen reduction as shown in Figures 48 and 52 and Tables 8 and 9. The data analysis of oxygen reduction is the same as that used in the ferric reduction. In Figures 50 and 53, k^0 is plotted against $V\Delta P$ and evaluated in Tables 8 and 9. The standard heterogenous rate constant, k^0 behaves much like ferric ion. In both data sets, the first five sonicated points do not show any improvement in the reaction rate; however at 90 % intensity the rate begins to increase. The highest applied sonic intensities, k^0, of 5.4 $(\pm 0.1) \times 10^{-4}$ and 2.4 $(\pm 0.1) \times 10^{-4}$ cm/s are approximately 66 fold higher than the unsonicated solution in the first data set and approximately 30 fold in the second data set.

In Figures 51 and 54, α is shown as a function of $V\Delta P$. The transfer coefficient, α, which gradually increases with $P\Delta V$ is 0.46 and 0.38 (data sets 1 and 2,

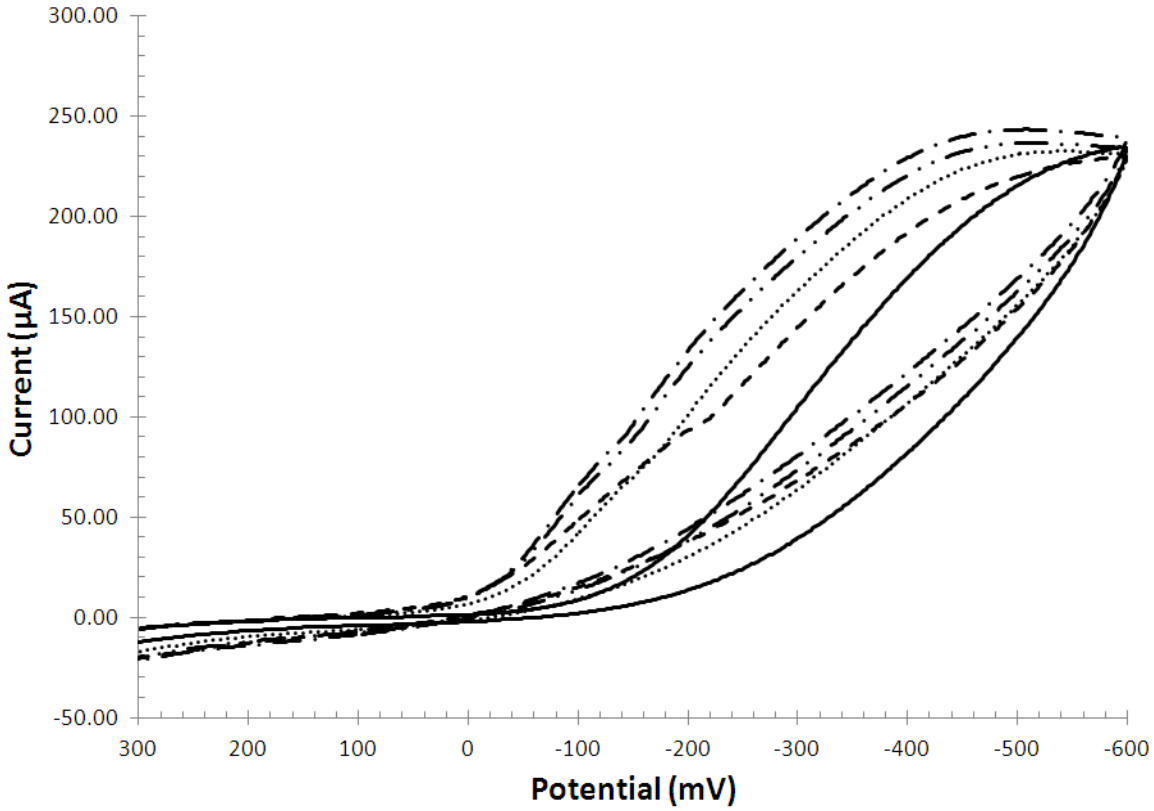

Figure 55. Comparative cyclic voltammograms of 0.28 mM O_2 and 5.00 mM Fe^{3+} in 0.100 M nitric acid taken at assorted levels of sonication. Sonicated 100 % intensity (dashed); Sonicated 80 % intensity (dash dot); Sonicated 60 % intensity (dash dot dot); Sonicated 40 % intensity (dotted); Unsonicated (solid).

respectively) for the unsonicated system and ranges from 0.51 to 0.77 for the sonicated system in both data sets. While the transfer coefficient, α, increases with increased sonic intensity in both sets, while this only occurs in one of the ferric reduction data sets. Like the one comparable ferric ion data set, the last point shows a sharp decrease in the transfer coefficient at the highest intensity.

Visual inspection of the cyclic voltammogram identifies the waves as apparently reversible rapid electron transfer. The analysis of k^0, although illustrating an increased rate, maybe misleading because the four proton, four electron oxygen reduction process is more complex than the single heterogenous electron transfer in the model. Energy dispersed over multiple steps in the process may not be well accounted for in the model. But the cyclic voltammetric morphology is consistent with dramatic increases in overall oxygen reduction reaction.

The electron transfer rate of the oxygen reaction is increasing, as apparent in the cyclic voltammograms in Figures 48 and 52 and the values of k^0 are comparable to those for ferric ion. The rate limiting step is considered to the the first electron transfer, once that is sped up, another step becomes rate limiting. Other potential rate limiting steps include any of the other three electron transfers, any of the proton transfers as well as the adsorption / desorption at the hydrogen peroxide step. The new rate limiting step may or may not be subject to the same aspects of acoustic manipulation. At this point there is not enough information to determine how the acoustic energy is dispersed throughout the reaction.

The reduction of oxygen in the presence of Fe^{3+} results in data consisting of compound curves. The initial rise of the curve, from zero to approximately

1.5×10^{-4} amps constitute one curve, somewhat comparable to the iron data. The remaining portion of the curve, which demonstrates a shallower slope, has an increase in current approximately 80% of the limiting current in the oxygen reduction. It is apparent that as the acoustic energy increases the second curve becomes more apparent. From the additive ferric and oxygen sweeps, it is a reasonable hypothesis that the catalytic influence of the acoustic energy is impacting two different electron transfer steps with varying efficiency. The ability to impact multiple reactions offers the potential to increase the efficiency of multiple steps in complex systems.

CHAPTER 6

APPLICATION OF MARCUS THEORY TO SONOELECTROCHEMISTY

6.1 Results in Light of Marcus Theory

Here Marcus theory is first reviewed for systems without sonication and then modified to allow incorporation of the acoustic energy.

6.1.1 Marcus Theory without Sonication

The current state of theory for electron transfer events is embedded in Marcus theory and its extrapolations. In its original incarnation (∼1956), Rudolph Marcus proposed that the activation barrier originally specified in activated complex and transition state theories was formed by the imposition of two parabolas, one each for the reactant and the product where their minima are placed at two separate positions along the reaction coordinate. [49–51] The parabolas were defined according to Hooke's law for a spring. That is, the potential energy is proportional to the spring constant and the square of the displacement from the initial proposition, x_0.

$$Potential\ Energy = \frac{1}{2}k\left(x - x_0\right)^2 \tag{100}$$

The reaction coordinate diagram is a plot of potential energy for each the reactants and products. In heterogeneous electrochemical reactions, the reactants are typically $O + e$ and the products are R, as shown in Figure 56.

In Figure 56, the reaction coordinate from reactant to product is shown along the

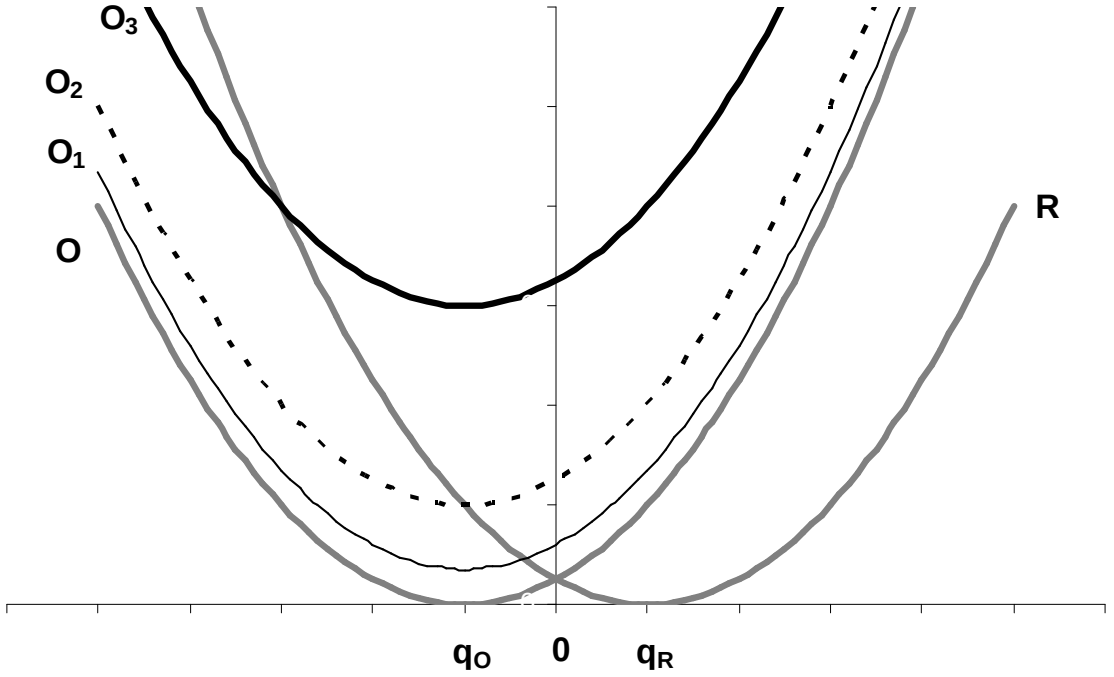

Figure 56. Potential energy curves are shown in light of Marcus theory for applied electrode potential, E. When $E = E^{0'}$, the energy surfaces are represented by the thick gray lines marked as O and R. When $E = E^{0'}$, the energy of the reactants and products at q_O and q_R, respectively, are equal, as represented by the common energy at the bottom of the two parabolas, O and R. As the electrode is polarized toward negative potentials, $E < E^{0'}$, the energy for the reactant O increases relative to the product R. The curve marked O_1 illustrates a perturbation of a few hundred millivolts such that the energy of the reactant is raised relative to that of the product. This is the most typical condition under quiescent voltammetric conditions. The curve marked O_2 is the case where the applied potential is sufficient to eliminate the barrier to electron transfer. In the extreme case, marked O_3, sufficient energy is applied to the electrode surface to move the conditions for electron transfer into the inverted region. That is, as more energy is applied to the system, a domain is reached where despite additional energy input, the rate slows because when the energy of the reactant at the bottom of the well is compared to the energy at the intersection point, there is an activation barrier to move the electron from the reactant to product potential energy curve and a shift along the reaction coordinate further away from the product R. This disfavors the electron transfer reaction.

x axis and the energy of the reactant and product along the reaction coordinate are shown by the parabolas on the y coordinate. For the electron transfer reaction with formal potential, $E^{0'}$,

$$O + e \underset{k_b(E)}{\overset{k_f(E)}{\rightleftarrows}} R \qquad E^{0'} \tag{101}$$

the forward ($k_f(E)$) and backward ($k_b(E)$) rate of electron transfer are potential dependent. When the applied potential $E = E^{0'}$, the potential energy curves are shown as the wide, solid gray lines with isoergic minima; the energy of the O and R curves are equal at the reaction coordinates q_O and q_R, where the species O and R are in their equilibrium atomic configurations. The parabolas for the free energy curves, $G_O^0(q)$ and $G_R^0(q)$, are defined as a function of the reaction coordinate q as[2]

$$G_O^0(q) = \frac{k}{2}(q - q_O)^2 \tag{102}$$

$$G_R^0(q) = \frac{k}{2}(q - q_R)^2 \tag{103}$$

The free energy of activation in the forward direction, $\Delta G_f^{\ddagger}$, is measured on the energy axis from the bottom of the O parabola to the point of intersection of the O and R curves. At the potential $E = E^{0'}$, the free energies of activation in the forward and reverse directions are equal and the rates of electron transfer forward and back are equal.

When a potential is applied to the electrode, the relative position of the parabolas shifts with the applied potential as $\Delta G^0 = F\left(E - E^{0'}\right)$. As drawn in Figure 56, the electrode polarization E is negative of $E^{0'}$ and the parabola for O is shifted upward relative to the parabola for R or equivalently, R is shifted down relative to O. So, for example, under voltammetric perturbation, $G_R^0(q)$ is defined as above and $G_O^0(q)$

becomes

$$G_O^0(q) = \frac{k}{2}(q - q_O)^2 - \Delta G^0 \tag{104}$$

In the Figure, a small perturbation, typically on the order of a few hundred millivolts, is applied to the electrode, the O curve shifts as shown in Figure 56 by the thin solid black line. The point of intersection that defines $\Delta G_f^{\ddagger}$ remains the height from the bottom of the O parabola at the applied potential $\left(E - E^{0'}\right)$ to the point of intersection of the O and R curves. The point of intersection is defined as $q^{\ddagger}$, where the configuration of O and R are the same consistent with the instant of electron transfer. For the applied potential, $\Delta G_f^{\ddagger}$ is less than that when $E = E^{0'}$ and the forward rate $O + e \longrightarrow R$ is faster. Typically, the energy surface under voltammetric perturbation such as cyclic voltammetry lies in this domain where the right ascending branch of the reactant O intersects the left ascending branch for the product R.

Consider the point of intersection, $q^{\ddagger}$ and associated free energy expressions.

$$G_O^0\left(q^{\ddagger}\right) = \frac{k}{2}\left(q^{\ddagger} - q_O\right)^2 - \Delta G^0 \tag{105}$$

$$G_R^0\left(q^{\ddagger}\right) = \frac{k}{2}\left(q^{\ddagger} - q_R\right)^2 \tag{106}$$

At $q^{\ddagger}$, the intersection yields $G_O^0\left(q^{\ddagger}\right) = G_R^0\left(q^{\ddagger}\right)$. Thus,

$$\frac{k}{2}\left(q^{\ddagger} - q_O\right)^2 - \Delta G^0 = \frac{k}{2}\left(q^{\ddagger} - q_R\right)^2 \tag{107}$$

$$\left(q^{\ddagger} - q_O\right)^2 - \left(q^{\ddagger} - q_R\right)^2 = \frac{2}{k}\Delta G^0 \tag{108}$$

$$-2q^{\ddagger}q_O + q_O^2 + 2q^{\ddagger}q_R - q_R^2 = \frac{2}{k}\Delta G^0 \tag{109}$$

$$\left(q_O - q_R\right)\left(q_O + q_R\right) - 2q^{\ddagger}\left(q_O - q_R\right) = \frac{2}{k}\Delta G^0 \tag{110}$$

then,

$$q^{\ddagger} = \frac{(q_O + q_R)}{2} - \frac{\Delta G^0}{k\,(q_O - q_R)} \tag{111}$$

$$q^{\ddagger} = \frac{q_O + q_R}{2} + \frac{\Delta G^0}{k\,(q_R - q_O)} \tag{112}$$

$\Delta G_f^{\ddagger}$ is measured from $G_O^0\,(q_0)$, the minimum on the curve for O under the applied potential to the point of intersection at $q^{\ddagger}$. In the figure, where the solid thin black line of O intersects the thick gray line of R. From Equation 104

$$\Delta G_f^{\ddagger} = G_O^0\left(q^{\ddagger}\right) - G_O^0\,(q_O) \tag{113}$$

$$= G_O^0\left(q^{\ddagger}\right) - \left(\frac{k}{2}\,(q_O - q_O)^2 - \Delta G^0\right) \tag{114}$$

$$= G_O^0\left(q^{\ddagger}\right) + \Delta G^0 \tag{115}$$

From the definition of $q^{\ddagger}$ in Equation 112

$$\Delta G_f^{\ddagger} = G_O^0\,(q) + \Delta G^0 \tag{116}$$

$$= \frac{k}{2}\left(\frac{q_O + q_R}{2} + \frac{\Delta G^0}{k\,(q_R - q_O)} - q_O\right)^2 - \Delta G^0 + \Delta G^0 \tag{117}$$

$$= \frac{k}{2}\left(\frac{q_R - q_O}{2} + \frac{\Delta G^0}{k\,(q_R - q_O)}\right)^2 \tag{118}$$

$$\Delta G_f^{\ddagger} = \frac{k\,(q_R - q_O)^2}{8}\left(1 + \frac{2\Delta G^0}{k\,(q_R - q_O)^2}\right)^2 \tag{119}$$

Define the reorganization energy λ in terms of the spring constant and the coordinates in the minimum energy states state q_O and q_R.

$$\lambda = \frac{k\,(q_R - q_O)^2}{2} \tag{120}$$

Then,

$$\Delta G_f^{\ddagger} = \frac{\lambda}{4}\left(1+\frac{\Delta G^0}{\lambda}\right)^2 \quad (121)$$

$$= \frac{\lambda}{4}\left(1+\frac{F\left(E-E^{0'}\right)}{\lambda}\right)^2 \quad (122)$$

Electrostatic work terms are not included but would be included as added to ΔG^0.

The forward rate constant $k\left(E\right)$ is defined in terms of $\Delta G_f^{\ddagger}$ as

$$k_f\left(E\right) = A\exp\left[-\frac{\Delta G_f^{\ddagger}}{RT}\right] \quad (123)$$

$$= A\exp\left[-\frac{\lambda}{4RT}\left(1+\frac{F\left(E-E^{0'}\right)}{\lambda}\right)^2\right] \quad (124)$$

where A is the pre-exponential factor. When $E = E^{0'}$, the standard rate constant is set by the pre-exponential term, A, temperature, and reorganization energy λ.

$$k^0 = A\exp\left[-\frac{\lambda}{4RT}\right] \quad (125)$$

The reorganization energy is the energy necessary to rearrange the reactants and solvent to the same nuclear configuration as the products at the instant of electron transfer, the intersection of the energy curves at $q^{\ddagger}$. Reorganization energy is usually partitioned into the inner (λ_i) and outer (λ_o) reorganization energies where λ_i is the energy needed to rearrange the nuclear configuration of the reactant species O and λ_o is the energy to reorganize the solvent. For conditions where the normal vibrational modes of the reactants remain harmonic over the range of distortion, λ_i is calculated by summing over the normal vibrational modes.

$$\lambda_i = \sum_j \frac{1}{2}k_j\left(q_{O,j}-q_{R,j}\right)^2 \quad (126)$$

For the solvent components, λ_o is based on a spherical reactant of radius a_O and a dielectric continuum for heterogeneous electron transfer.

$$\lambda_o = \frac{e^2}{8\pi\varepsilon_0}\left[\frac{1}{a_O} - \frac{1}{R}\right]\left[\frac{1}{\varepsilon_{op}} - \frac{1}{\varepsilon_s}\right] \tag{127}$$

where e is the elementary charge (1.602×10^{-19} C) and ε_0 is the permittivity of free space (8.8542×10^{-12} C^2/Nm^2). $R = 2a_O$. The optical and static dielectric constants of the solvent are ε_{op} and ε_s respectivly.

Note that the barrier height for the forward reaction under potential perturbation is defined by Equation 122.

$$\Delta G_f^{\ddagger} = \frac{\lambda}{4}\left(1 + \frac{F\left(E - E^{0'}\right)}{\lambda}\right)^2 \tag{128}$$

There is a potential where the forward reaction becomes a barrierless transition, $-\lambda = F\left(E - E^{0'}\right)$. From Equation 124, $k\left(E\right) = A$. This is shown in Figure 56 by the broken black line. Because the reaction is without a barrier, the rate of electron transfer is high.

The solid black line in Figure 56 corresponds to a more extreme applied potential. That is, where energy beyond the barrierless transition is applied and the rate of the reaction is slowed despite the addition of more energy. This is the inverted region. The additional energy has shifted the O curve sufficiently higher relative to the R curve, that $q^{\ddagger}$ is set by the intersection of left branches of both the O and R curves, a point that is to the left of q_O or further from q_R on the reaction coordinate than when $E = E^{0'}$. There is again an energy barrier to the electron transfer and the reaction coordinate $q^{\ddagger}$ is displaced to the left of q_O; both slow the reaction rate.

In 1984, experimental demonstration of the inverted region was made at electrodes modified with alkane monolayers of varying numbers of methylene units where there was an electroactive moiety bound to the outer edge of the monolayer [52]. As the number of alkane units increased, the heterogeneous electron transfer rate fell as $\exp[-\beta x]$ where x is the distance from the electrode and for alkanes, β is $\sim 1\ \mathring{A}^{-1}$. These experiments were accomplished approximately thirty years after Marcus first proposed the parabolic representation of the energy surfaces and demonstrated the inverted region. Marcus received the Nobel Prize in chemistry in 1992. For energy input solely under voltammetric perturbation, it is difficult to achieve the inverted region.

Consider the definition of the transfer coefficient, α within this model.

$$\alpha = \frac{1}{F}\frac{\partial G_f^{\ddagger}}{\partial E} \tag{129}$$

From the definition of $\Delta G_f^{\ddagger}$ given in Equation 122,

$$\alpha = \frac{1}{2}\left(1 + \frac{F\left(E - E^{0'}\right)}{\lambda}\right) \tag{130}$$

FE has units of CV or J. For $F\left(E - E^{0'}\right) << \lambda$, the typically encountered $\alpha \sim 0.5$ is found. As the potential perturbation becomes more extreme and $F\left(E - E^{0'}\right)$ approaches λ, α approaches 1.

6.1.2 Marcus Theory with Sonication

Multiple attempts have been made to derive a model of the sonicatied data in conjunction with Marcus theory. Because there is no consistent trend for the

transfer coefficient between data sets, any model would be of limited perdictive value. Despite this limitation, set 1 of the ferric ion data was used as a basis for modeling. In Figure 32, k^0 is plotted against $V\Delta P$. The curve includes the unsonicated value for k^0 as the horizontal line at $k^0 = 1.3 \times 10^{-4}$ cm/s. The lowest intensity sonication is higher than the unsonicated value. The k^0 increases exponentially with increasing values of $V\Delta P$. This increase in rate with $V\Delta P$ is consistent with acoustic energy as an effective means for introducing additional energy to the system. In Figure 57, the natural log of the standard rate constant, $ln(k^0)$, is plotted against $V\Delta P$. This linearizes the data from Figure 32 and allows a linear regression where $ln(k^0) = 28 \pm 3 \times V\Delta P - 11.4 \pm 0.6$ with $R^2 = 0.94$. Figure 40 shows the commonality of $ln(k^0)$ between the other two ferric ion data sets.

6.1.2.1 Work Terms

When additional energies, whether inputs or taxes (e.g., electrostatic terms), are considered under Marcus theory, the energies are included along with ΔG^0. These terms are often described as work terms and can be represented as w_O and w_R for the partition of the energy between the energy curves for O and R. The work terms are in addition to that of the applied potential $F\left(E - E^{0'}\right)$. This yields an expression for $\Delta G_f^{\ddagger}$ such as

$$\Delta G_f^{\ddagger} = \frac{\lambda}{4}\left(1 + \frac{\Delta G^0 - w_O + w_R}{\lambda}\right) \tag{131}$$

Similar terms were used here to aportion the acoustic energy. Let ΔG_A^0 be the

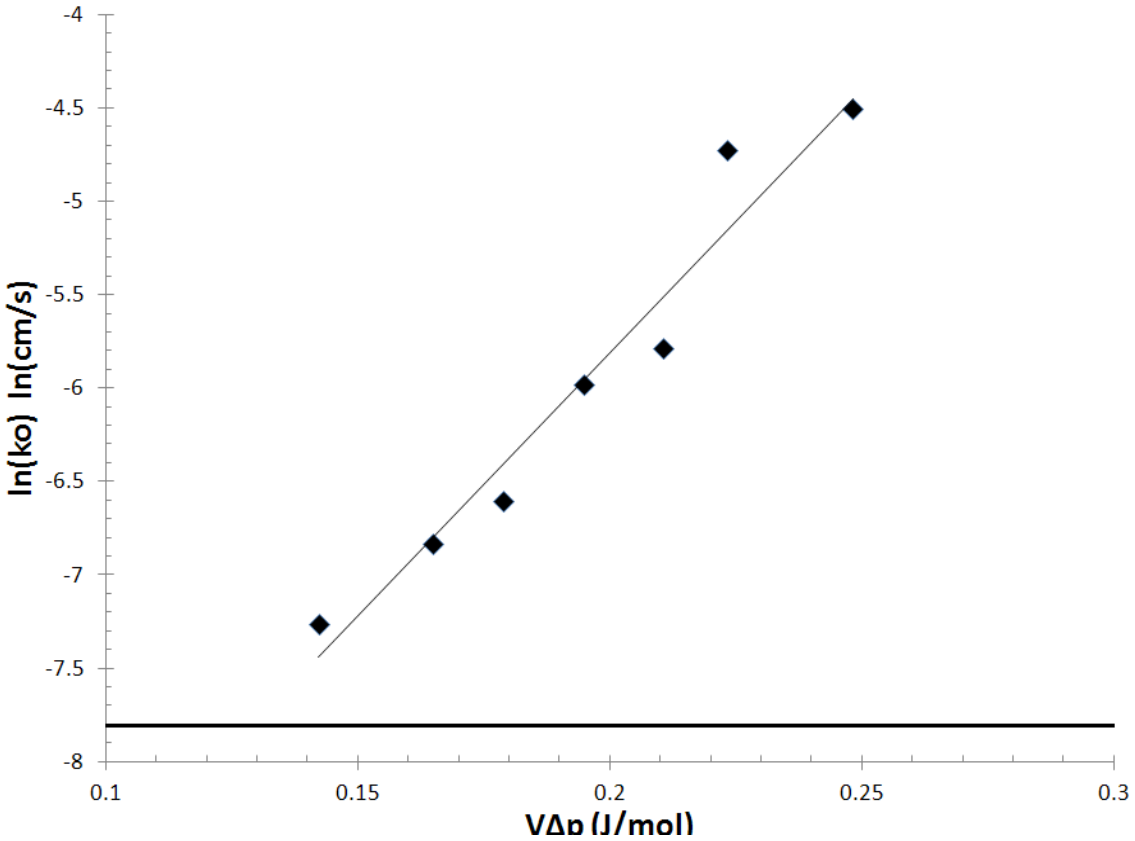

Figure 57. The natural log of standard rate constant. $ln(k^0)$ as a function of $V\Delta P$ for the reduction of Fe^{3+}. The heavy solid line indicates $ln(k^0)$ when the system is unsonicated. The light solid line is a linear regression: $ln(k^0) = 28 \pm 3 \times V\Delta P - 11.4 \pm 0.6$ with $R^2 = 0.94$.

acoustic energy. Allow that the acoustic energy is provided to the O curve as a function that defines a fraction between 0 and 1 as $g\left(\Delta G_A^0\right) = f\ \left(\Delta PV\right)$ where the functions could be independent of acoustic energy; the fraction of the acoustic energy to curve R is $1 - g\left(\Delta G_A^0\right) = 1 - g\left(\Delta PV\right)$. The free energy of activation for the forward reaction is then

$$\Delta G_f^{\ddagger} = \frac{\lambda}{4}\left(1 + \frac{\Delta G^0 - g\left(\Delta G_A^0\right)\Delta G_A^0 + \left(1 - g\left(\Delta G_A^0\right)\right)\Delta G_A^0}{\lambda}\right)^2 \tag{132}$$

$$= \frac{\lambda}{4}\left(1 + \frac{F\left(E - E^{0'}\right) - \left(2g\left(\Delta G_A^0\right) - 1\right)\Delta G_A^0}{\lambda}\right)^2 \tag{133}$$

$$= \frac{\lambda}{4}\left(1 + \frac{F\left(E - E^{0'}\right) + \left(1 - 2g\left(\Delta G_A^0\right)\right)\Delta G_A^0}{\lambda}\right)^2 \tag{134}$$

The forward rate constant is

$$k_f\left(E\right) = A\exp\left[-\frac{\lambda}{4RT}\left(1 + \frac{F\left(E - E^{0'}\right) + \left(1 - 2g\left(\Delta G_A^0\right)\right)\Delta G_A^0}{\lambda}\right)^2\right] \tag{135}$$

When $E = E^{0'}$, the standard rate constant is

$$k^0 = A\exp\left[-\frac{\lambda}{4RT}\left(1 + \frac{\left(1 - 2g\left(\Delta G_A^0\right)\right)\Delta G_A^0}{\lambda}\right)^2\right] \tag{136}$$

Equation 136 states that the $\ln(k^0)$ would be a second order polynomial function of $\left(1 - 2g\left(\Delta G_A^0\right)\right)\Delta G_A^0$. If values of $P\Delta V$ allow $\left(\left(1 - 2g\left(\Delta G_A^0\right)\right)\Delta G_A^0\right)^2$ to be negligible, Equation 136 could appear linear when plotted.

6.1.2.2 Reorganization Energy

Consider the results for $Fe^{3+} + e^- \longrightarrow Fe^{2+}$ as shown in Figures 32 and 57 for k^0 increasing with $V\Delta P$. The k^0 increases exponentially with increasing values of $V\Delta P$. In contrast, consider the results for $Ru\left(bpy\right)_3^{3+} + e \longrightarrow Ru\left(bpy\right)_3^{2+}$. For the

$Ru\,(bpy)_3^{2+}$ data, there is little impact on the voltammetry with sonication. All wave forms are consistent with rapid, outer sphere electron transfer. This difference in the response to acoustic energy for Fe^{3+} and $Ru\,(bpy)_3^{2+}$ may arise from the slight difference in inner and outer sphere properties. $Ru\,(bpy)_3^{2+}$ is an strictly outer sphere electron transfer process and it is rapid relative to voltammetric perturbations. The reorganization energy for $Ru\,(bpy)_3^{2+}$ is strictly in the solution, so $\lambda = \lambda_o$, where lambda naught is the outer sphere reorganization energy. From the definition of λ_o, little effect on the solvent reorganization energy is anticipated. See equation 127 where none of the variables are expected to be dependent on ΔG_A^0. For Fe^{3+}, there is a small inner sphere component. From equation 126, there is a possibility of the acoustic energy coupling into the harmonics of the species reaction coordinate. This in turn leads to dependencies on the acoustic energy as shown. The coupling of the acoustic energy to the inner sphere modes is pictorially presented in Figure 58.

This difference in the distribution of the reorganization energy provided another basis for derivation of a Marcus theory based model. Reorganization energy is usually partitioned into the inner (λ_i) and outer (λ_o) reorganization energies where λ_i is the energy needed to rearrange the nuclear configuration of the reactant species O and λ_o is the energy to reorganize the solvent. In this model, additional energies are attributed to changes in the inner sphere reorganization energy where

$$\lambda = \lambda_i f(P\Delta V) + \lambda_o \tag{137}$$

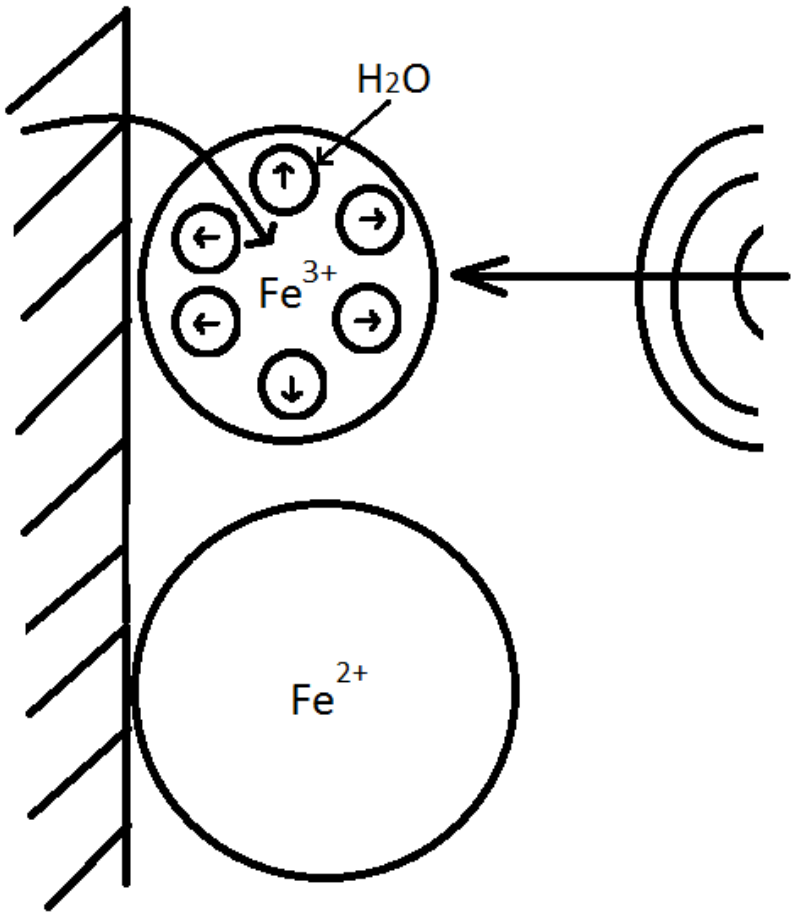

Figure 58. Illustration of the inner sphere component of Fe^{3+} heterogeneous electron transfer at the electrode surface. The coupling of the acoustic energy to the inner sphere modes allows the transferred electron access to Fe^{3+}.

This yields an expression for $\Delta G_f^{\ddagger}$ such as

$$\Delta G_f^{\ddagger} = \frac{\lambda}{4}\left(1+\frac{\Delta G^0}{\lambda}\right) \tag{138}$$

$$\Delta G_f^{\ddagger} = \frac{\lambda_i f(P\Delta V)+\lambda_o}{4}\left(1+\frac{\Delta G^0}{\lambda_i f(P\Delta V)+\lambda_o}\right) \tag{139}$$

The same rational as used for the work term model shows the forward rate constant is

$$k_f\left(E\right) = A\exp\left[-\frac{\lambda_i f(P\Delta V)+\lambda_o}{4RT}\left(1+\frac{F\left(E-E^{0'}\right)}{\lambda_i f(P\Delta V)+\lambda_o}\right)^2\right] \tag{140}$$

When $E = E^{0'}$, the standard rate constant is

$$k^0 = A\exp\left[-\frac{\lambda_i f(P\Delta V)+\lambda_o}{4RT}\right] \tag{141}$$

Equation 141 is similar to the Arrhenius based Equation 94 in that both indicate that $ln(k^0)$ as a function of $V\Delta P$ should be linear. This is consistent with Figures 32 and 40 that show linear plots of natural log of standard heterogeneous electron transfer constant. $ln(k^0)$ as a function of $P\Delta V$ and the fraction of available acoustic pressure, F_p, respectively.

6.2 Conclusion

Impacts on the rates of heterogeneous electron transfer are evaluated by consideration of two redox couples. One couple, iron trication, exhibits a slow rate of heterogeneous electron transfer whereas the other couple, ruthenium tris-bipyridal, exhibits reversible or rapid rate of heterogeneous electron transfer. Evaluation of the two probes by cyclic voltammetry showed that the rate of heterogeneous electron transfer for the slow species, iron ion, is dramatically increased but the

already rapid electron transfer species, ruthenium tris-bipyridal, shows no impact of sonication. These effects are consistent with effective transfer of acoustic energy into the electrode surface as a means to accelerate the rate of heterogeneous electron transfer when the rate without sonication is slow and there is at least some component of inner sphere reorganization energy. There was no evidence of substantial impacts on mass transport rates as the voltammograms did not exhibit markedly enhanced overall currents. This is consistent with the selective input of energy at the solution electrode interface where the energy is effective for the inner sphere reorganization. Equations to attempt to characterize the behavior with ΔG_A^0 are presented. Incorporation of the acoustic energy as a work term provides a relationship consistent with the data only if the values are sufficiently small with respect to one, as in equation 136. A model that assumes the acoustic energy impact the reorganization energy demonstrates a relationship that is consistent with data plots of $ln(k^0)$ as a function of $P\Delta V$, Figures 32 and 40. Until a trend in the behavior of the transfer coefficient with sonication is established, a predictive model of the sonoelectrochemical behavior can not be fuly established. The two variations of Marcus theory presented here are consistent with the observed behavior in k^0.

CHAPTER 7

IMPACT OF LOW INTENSITY SONICATION IN A THIN LAYER ON METHANOL KINETICS

7.1 Introduction

Throughout these studies, there is evidence that sonication impacts reaction kinetics at electrode surfaces. For the simple but slow heterogeneous electron transfer processes of iron, the rates are improved. For the more complex multielectron transfer to oxygen, there is an observed increase in the apparent standard heterogeneous rate constant and transfer coefficient. For the oxygen electron transfer process, the first step is the slow step but there is subsequently three additional electron transfer processes. Once the first step is made rapid, the limitations in the transfer coefficient may be associated with the subsequent and following steps.

In their current embodiment, fuel cells work well on hydrogen as a fuel and oxygen or air as the oxidant in a hydrogen | oxygen fuel cell. The rate determining kinetics are at the oxygen electrode. In operational hydrogen oxygen fuel cell, 30% of the theoretical power and energy is lost to poor oxygen kinetics. The data presented here for the increase in oxygen reduction rate are attractive as a means to improve hydrogen oxygen fuel cell performance at low temperatures. A second difficulty with extant fuel cell technology is that hydrogen is difficult to store and costly to harvest. If hydrogen is generated by electrolysis, there is the same tax of the poor oxygen reduction kinetics. Again, the oxygen results indicate that sonoelectrochemistry may

be a means to improve the efficiency of both electrolysis and hydrogen oxygen fuel cells.

The most readily commercialized fuel cells will use a liquid fuel, such as alcohols and hydrocarbons. Liquid fuels provide high energy density, ease of transport, safety, and low cost. In the current technology for liquid fed, direct reformation fuel cells, catalyst loadings are 10 times higher than in hydrogen oxygen fuel cells and the power output is 1/10 that of hydrogen oxygen fuel cells. This means that currently, direct reformation fuel cells are only 1% as efficient as hydrogen oxygen fuel cells. Complexities for fuel cells run on organic fuels include carbon monoxide poisoning of the noble metal catalysts as well as deposition of partial oxidation products across the electrode surface; both passivated the electrode.

The thermodynamic potential for methanol oxidation to CO_2 lies close to the equilibrium potential of hydrogen: [53]

$$CH_3OH + H_2O \rightarrow CO_2 + 6H^+ + 6e^- \qquad E^0 = 0.02\ V \tag{142}$$

The total oxidation process consists of parallel reactions that can be summarized as [54]:

$$CH_3OH \rightarrow (Absorbed\ Intermediate) \begin{array}{ll} \nearrow & CO_{ad} \rightarrow CO_2 \\ \searrow & HCHO, HCOOH \rightarrow CO_2 \end{array} \tag{143}$$

Both pathways require a catalyst to dissociate the C-H bond and complete the reaction of the residue with an oxygen containing species. The final products of the chemisorption process that are thought to result in passivation and poisoning of the noble metal electrode are COH and singly or multiply bonded CO_{ads} [46]. These

steps in the oxidation of methanol are the largest impediment to the realization of a direct methanol fuel cell (DMFC).

The thin layer sonoelectrochemistry system may provide a means to better direct reformation systems. Sonication can remove deposited byproducts. Thin layer sonoelectrochemistry has been shown to improve oxygen reduction kinetics. As an initial evaluation of whether a direct reformation fuel cell under sonication would be effective, sonoelectrochemistry of methanol was undertaken. Here, the outcome of that initial screening is presented. Sonoelectrochemistry allows more effective oxidation of methanol. The outcome suggests that a direct reformation fuel cell system that uses a liquid fuel may be viable under sonication.

7.2 Experimental

Electrochemical Cell A second generation sonoelectrochemical cell as described in Chapter 2 is cleaned with concentrated nitric acid (Fisher Scientific) and deionized water (Millipore Model Milli Q plus 18.2 MΩ) .

Working, Counter and Reference Electrodes The working and counter electrodes consisted of 0.5 mm platinum wire (Sigma-Aldrich) inserted 8 mm into the solution. Prior to use the electrode is immersed in concentrated nitric acid (Fisher Scientific) for four minutes and rinsed in deionized water (Millipore Model Milli Q plus 18.2 MΩ).

Electrolyte A solution of 0.100 M nitric acid (Fisher Scientific) in deionized water (Millipore Model Milli Q plus 18.2 MΩ) is used as the electrolyte.

Materials Unless otherwise noted, all chemicals used were obtained by

Sigma-Aldrich Chemical Co. and were used as received. A 50 % (v/v) solution of methanol 0.100 M nitric acid electrolyte is used. 1 mL of solution was placed in the sonoelectochemical cell well with a disposable pipet.

Sonication Sound waves are generated in the sonoelectrochemical cell at a frequency of 41 kHz. Intensity was varied from 100 % (maximum) down to approximately 40 % in roughly 10 % increments. Unsonicated scans were run before and after the sonication sets. Peak voltage (V_p) was monitored with an oscilloscope.

Voltammetry A BAS 100B Electrochemical Analyzer is used to collect all voltammetry measurements. Voltammograms are recorded at scan rates of 0.1 V/s.

7.3 Results and Discussion

The 50 % (v/v) methanol solution is approximately correct for appropriate stoichiometry of Equation 142. The methanol concentration used in these studies is high. Most direct reformation systems are run on 1 to 2 molar methanol in water. However, the efficacy of sonication at these high concentrations is apparent.

Cyclic voltammetry for a platinum electrode without sonication is shown in Figure 59. There is a reduction current at about -400 mV and a shoulder oxidation at +800 mV, but the electrolysis efficiency for methanol is poor.

In Figure 60, cyclic voltammetry is shown for a sonicated platinum electrode where the intensity of the sonication is half maximum intensity. There was prior, more intense sonication of the electrode before this voltammogram was recorded. It is apparent from this voltammogram that sonication allows an increase in the effective methanol electrolysis because an oxidation wave is observed near 200 mV.

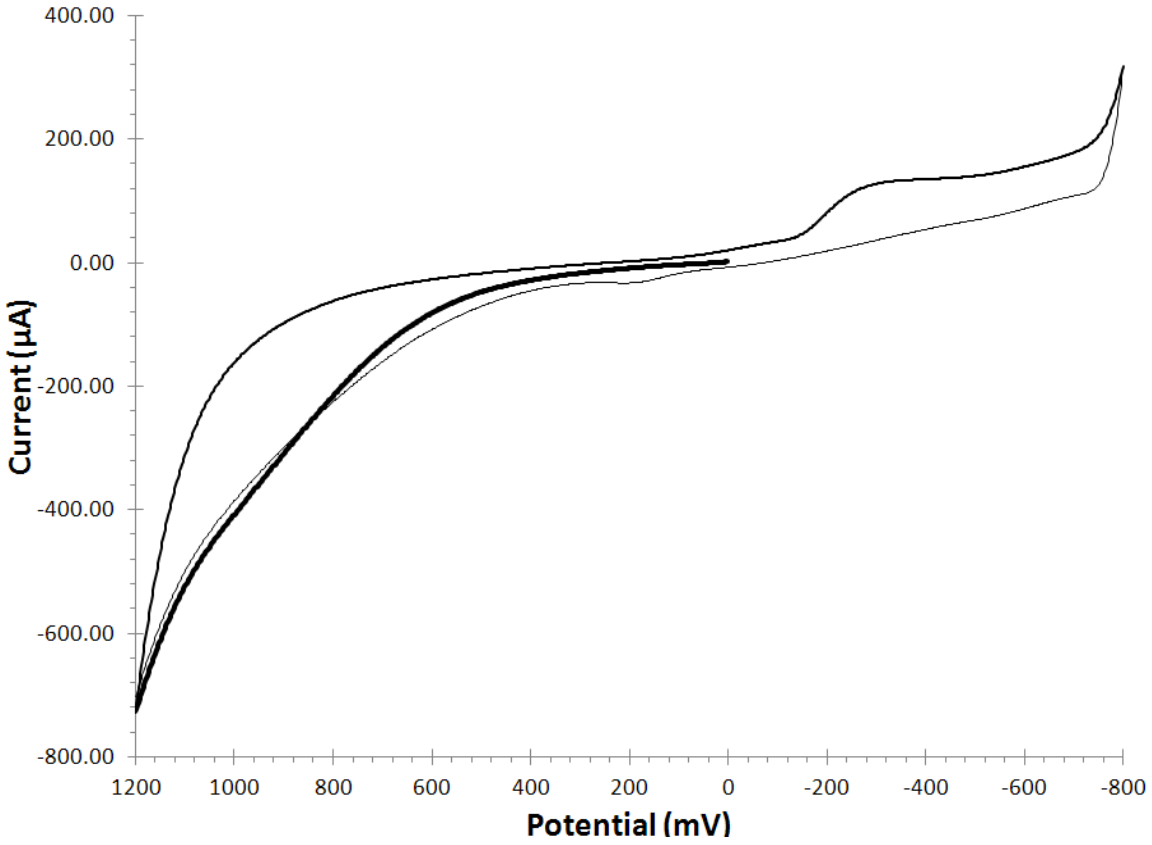

Figure 59. Cyclic voltammetric scans of 50 % (v/v) methanol / water mixture, unsonicated. Three sweeps are run sequentially without pause in the following order: 0 to 1200 mV (heavy solid); 1200 to -800 mV (medium solid): -800 to 1200 mV (light solid).

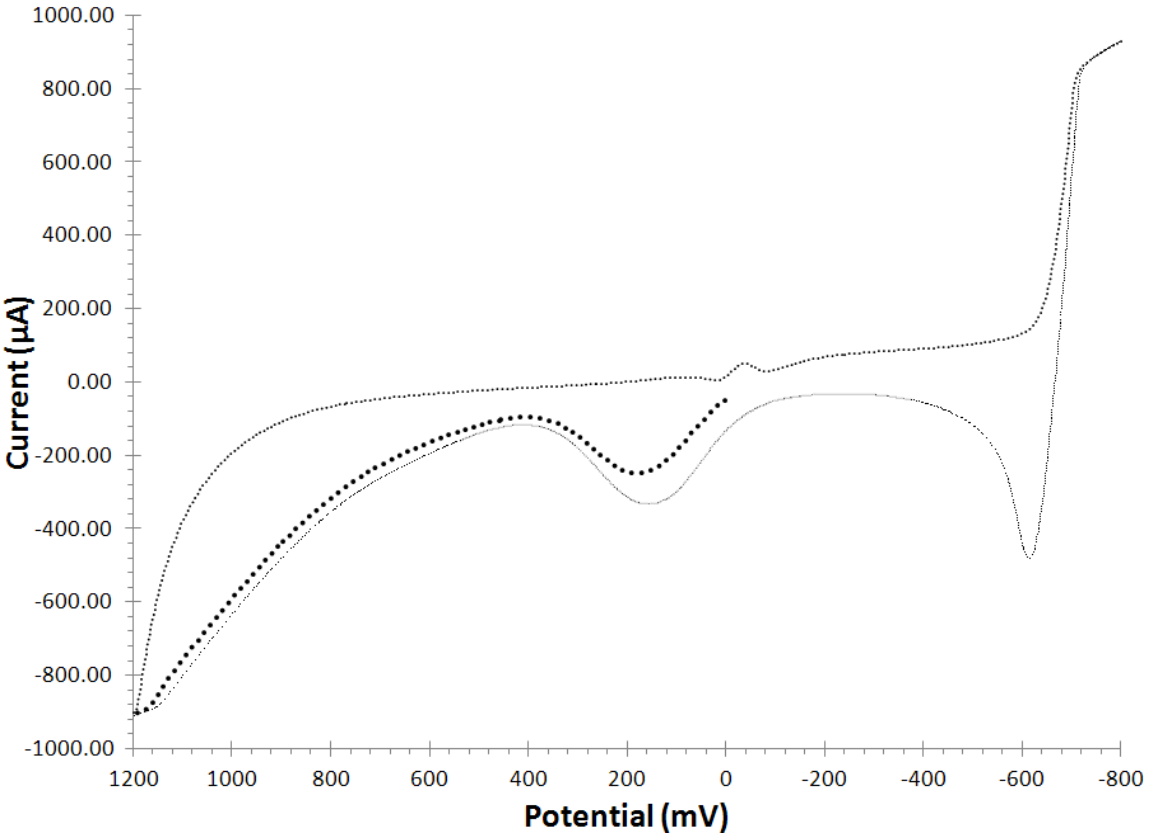

Figure 60. Cyclic voltammetric scans of 50 % (v/v) methanol / water mixture, sonicated at 50 % intensity. Three sweeps are run sequentially without pause in the following order: 0 to 1200 mV (heavy dotted); 1200 to -800 mV (medium dotted): -800 to 1200 mV (light dotted).

Table 10. Tabulation of cyclic voltammetric data for 50 percent (v/v) methanol in 0.100 M nitric acid taken at various levels of sonication.

Sonication Intensity (%)	Peak Current (μA)	$V\Delta P$ (J/mol)
quiescent, 1st sweep	9.02	0
pre-unsonicated	79 (± 7)	0
100	720 (± 70)	0.33
90	610 (±60)	0.30
80	420 (± 20)	0.27
70	323 (± 9)	0.24
60	236 (± 1)	0.21
50	176 (± 9)	0.16
post-unsonicated	165 (± 5)	0

Note: Data include peak oxidation current and VΔP. Each point is the average of three replicates.

In Figure 61, a cyclic voltammogram is shown for a platinum electrode sonicated at maximum intensity (dashed). This is shown in contrast to the unsonicated methanol cyclic voltammogram (solid). Comparison of the two voltammograms shows a significant increase in the effective methanol electrolysis observed near 200 mV. The full sonic intensity scan starts at 0 V and the potential is increased (left) with no peak at 200 mV, but a symmetric wave at 400 mV. The symmetric wave is likely a stripping wave for the removal of absorbates such as COH and CO. The return scan shows an oxidative peak at 200 mV, which is doubled on the final pass.

Figure 62 shows the peak oxidative currents on the positive sweep of methanol increases with sonic intensity. The data are tabulated in Table 10. The increasing current with increasing $P\Delta V$ indicates that the apparent reaction is more efficient. The improvement in the poor kinetics of methanol may be the result of an actual improvement in the electron transfer rate or the result of the removal of partial oxidant products form the electrode surface. There is an 80 fold change between the unsonicated peak and the peak a maximum intensity.

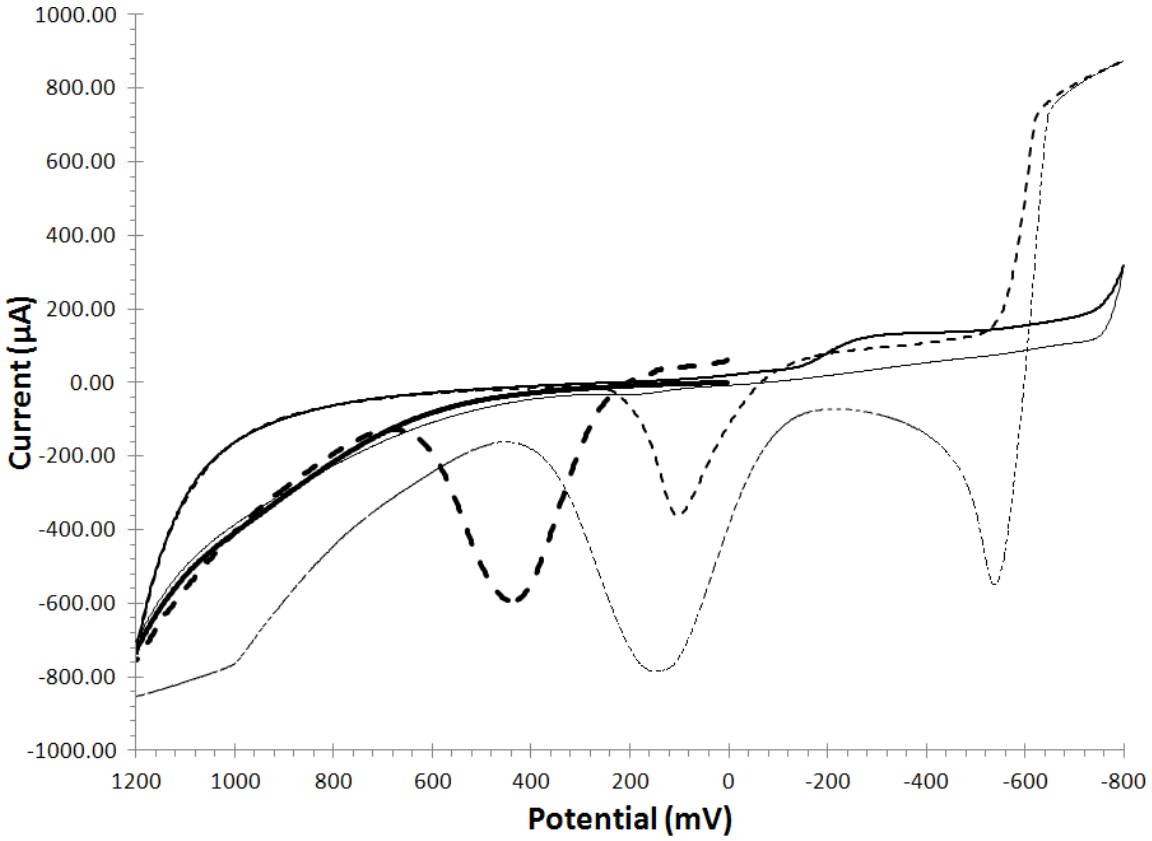

Figure 61. Cyclic voltammetry scans of 50 % (v/v) methanol / water mixture. Each scan consisted of three sweeps run sequentially without pause in the following order: Unsonicated scan: 0 to 1200 mV (heavy solid); 1200 to -800 mV (medium solid): -800 to 1200 mV (light solid); Sonicated scan (maximum intensity): 0 to 1200 mV (heavy dotted); 1200 to -800 mV (medium dotted): -800 to 1200 mV (light dotted).

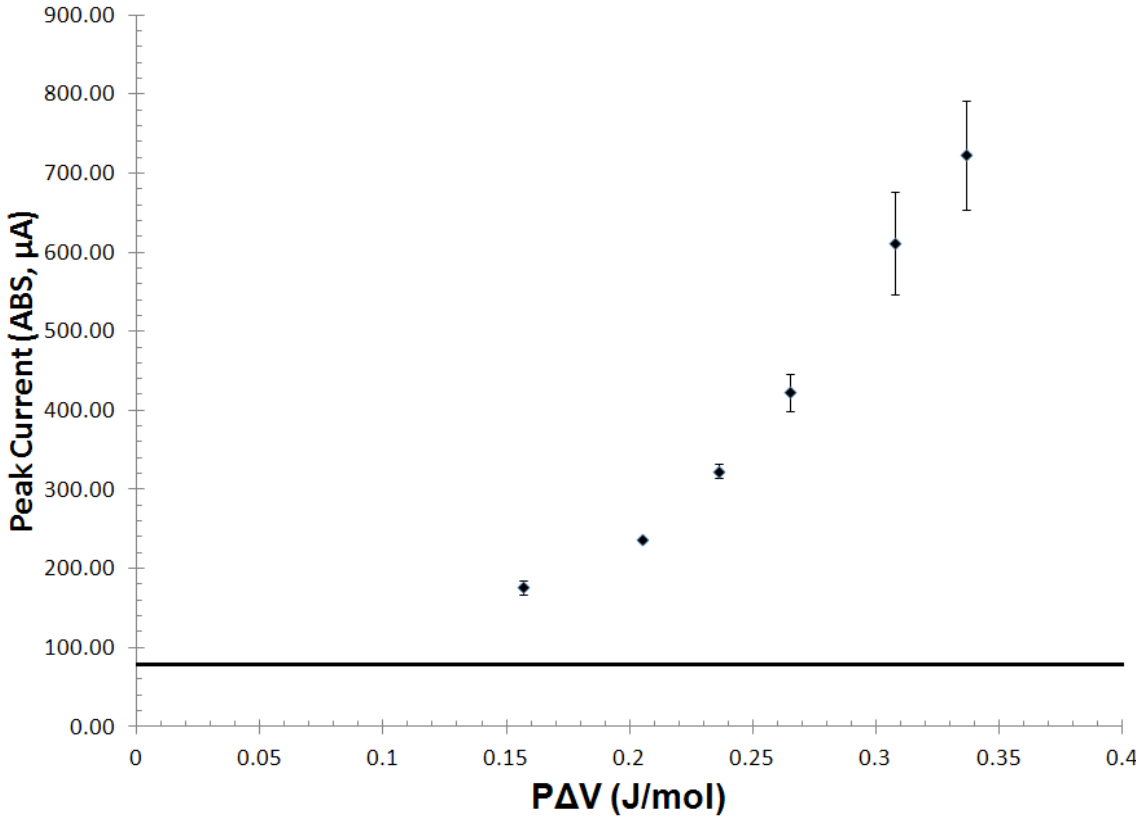

Figure 62. Plot of the peak oxidative current of the third sweep of each scan of methanol as a function of $V\Delta P$ for sonicated 50 % methanol cyclic voltammetric data. Error bars represent standard deviation. Each point is an average of three scans. Solid line represents the peak current of unsonicated scans.

7.4 Conclusion

Initial inspection of methanol electrolysis with and without sonication yields strong evidence that sonication substantially increases the efficiency of methanol electrolysis. Comparison of peak currents at maximum sonication intensity and quiescent shows current at 200 mV is enhanced approximately 80 fold. This suggests that because methanol oxidation is the efficiency limiting process in direct methanol fuel cells (DMFCs), sonication will improve the efficiency of DMFCs substantially. The improvement of oxygen kinetics may also contribute to improved direct reformation fuel cells. A 25 fold enhancement to DMFC efficiency would be about 20% efficiency, an efficiency comparable to most automobiles on the road. The observed 80 fold increase, well above 25 fold, implies the use of sonication allows efficient methanol oxidation which may translate to liquid fuel cells. Further evaluation of methanol electrolysis under sonication is justified.

CHAPTER 8

EXAMINATION OF ALTERNATIVE ELECTRODES

8.1 Introduction

In the development of the thin layer sonoelectrochemical system, various electrode materials were tested to identify other electrode materials that are stable under experimental conditions. Platinum remained the best choice as different materials were examined. The electrodes must satisfy conditions of good mechanical stability and electrochemical effectiveness as an electrode surface. Brittle material and materials solubilized on sonication fail as electrodes. The electrodes must have sufficient mechanical integrity as not to lose integrity upon sonication.

For the platinum electrode, there is some evidence that sonication removes the oxide layer on platinum. The oxide layer on platinum complicates many voltammetric processes in water. Sonication that removes the oxide layer would produce a more effective electrode, both as an electrode and electrocatalytic surface.

A brief synopsis is presented here of the variety of electrode materials that were tested in the development of the sonoelectrochemical system. Most of the electrodes were working electrodes but there are also examples of reference electrodes.

Some electrodes are thermodynamically effective but are not commonly used as electrodes at room temperature because an oxide layer that forms on the electrode surface passivates the electrode [55]. Electrode materials are investigated under sonoelectrochemical conditions to determine whether or not the oxide layer can be

removed so as to render these electrodes effective. Materials such as aluminum and tungsten are less costly than noble metal electrodes, and thermodynamically as active as platinum. In an attempt to remove the thin, native oxide layer on these passivating electrode materials, sonication is used.

8.2 Experimental

The experimental studies for these systems are analogous to those undertaken above and the various electrodes evaluated. An acid electrolyte was used for the various electrodes evaluated.

Electrochemical Cell Unless otherwise indicated, a second generation sonoelectrochemical cell as descibed in Chapter 2 is cleaned with concentarted nitric acid (Fisher Scientific) and deionized water (Millipore Model Milli Q Plus, 18.2 MΩ).

Working, Counter and Reference Electrodes Unless otherwise indicated, the working, counter and reference electrodes consisted of 0.5 mm platinum wire (Sigma-Aldrich) inserted 8 mm into the solution. Prior to use, the electode is immersed in concentrated nitric acid (Fisher Scientific) for four minutes and rinsed in deionized water (Millipore Model Milli Q Plus, 18.2 MΩ).

Electrolyte A solution of 0.100 M nitric acid (Fisher Scientific) in deionized water (Millipore Model Milli Q Plus, 18.2 MΩ) is used as the electrolyte.

Materials Unless otherwise noted, all chemicals used were obtained by Sigma-Alderich Chemical Co. and were used as received. Iron (III) nitrate nonahydrate (Fe^{3+}) is a commerically available redox probe. A 1.00 mM solution of Fe^{3+} in the aforementioned 0.500 M nitric acid electrolyte is used as a redox probe

where mentioned.

Sonication Sound waves are generated in the sonoelectrochemical cell at a frequency of 41 kHz. Unless otherwise notes, intensity was varied from 100 % (maximum) down to approximately 30 % in roughly 10 % incriments. Unsonicated scans were run before and after the sonication sets. Peak voltage (V_p) was monitored with an oscilloscope. Where noted, sonication intensity was set in random order to eliminate bias.

Voltammerty A BAS 100B Electrochemical Analyzer is used to collect all voltammerty measurements. Voltammograms are recorded at scan rates of 0.1 V/s.

8.3 Results and Discussion

Here, a report on the various electrode materials is made.

8.3.1 Ag|AgCl

Initially, with the use of the first generation sonoelectrochemical cell, a silver | silver chloride reference electrode is used in the studies. Occasionally there is a noticeable shifting of subsequent voltammograms over the course of sonication not related to the change in kinetics. The result is consistent with sonication that dislodges silver chloride from the reference electrode and subsequent dissolution of the underlying silver metal. The silver metal is then adsorbed or reduced on the platinum working electrode such that when the voltammetric oxidation sweep is undertaken the adsorbs silver on the platinum is strip from the electrode surface and to yield silver ions in solution. The reference electrode is visibly diminished over

the course of several experiments. Silver | silver oxide reference electrodes exhibit similar dissolution, but are more resistant to this effect.

8.3.2 Carbon

Working electrodes have been made of wires in these studies. A carbon electrode is an effective electrode, especially in water. To evaluate carbon electrodes in the sonoelectrochemical system, commercial pencil leads and graphite rods are used as the working electrode. The pencil leads are 0.5 millimeters in diameter and the graphite rods are approximatly 2 millimeters in diameter. The experiments are not successful because after a brief sonication both the pencil lead and the graphite rods disintegrate and are no longer useful. Similar results with carbon electrodes were observed by Coury and coworkers under more aggressive sonoelectrochemical conditions [23].

8.3.3 Aluminum

Aluminum is evaluated electrode material because, dynamically it is a very reactive and conductive material. Thermodynamically, is a very active metal, but aluminum is not commonly used as an electrode because it forms a very thin, passivated oxide layer. In the platinum data, there is evidence that sonication removes the oxide layer on platinum to activate the platinum surface. Analogously, aluminum was evaluated as a working electrode at room temperature under sonication.

Aluminum wire was substituted for the platinum wire working electrode and

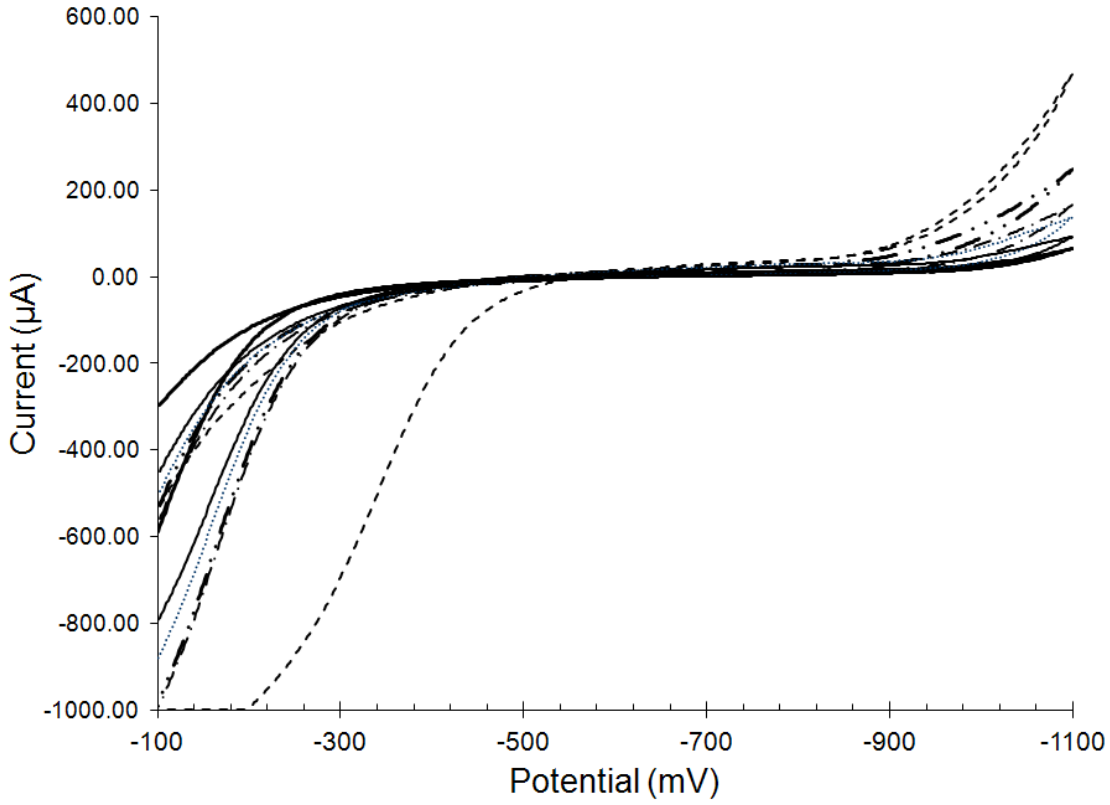

Figure 63. Comparative cyclic voltammograms of 1.00 mM Fe^{3+} in 0.500 M nitric acid taken at assorted levels of sonication with an aluminum working electrode. The Fe^{3+} reduction wave is not observed near 0 V. The available window decreases with sonication. Initial unsonicated (heavy solid); Sonicated 100 % (dashed); Sonicated 90 % intensity (dash-dot); Sonicated 80 % intensity (dash-dot-dot); Sonicated 50 % intensity (dotted); Final unsonicated (light solid).

cyclic voltammetric studies under sonication were undertaken. A voltammogram is shown in Figure 63 for 0.100 M nitric acid solution that contains 5.00 mM of Fe^{3+}.

Cyclic voltammetric data are consistent with an apparent narrowing of the ideally polarized domain on sonication. The similarity between the initial and final unsonicated scans implies that any removed passivating oxide layer is quickly regenerated once sonication ceases.

8.3.4 Tungsten

Similarly to aluminum, tungsten develops a passivated thin oxide layer. Lightly sanded tungsten wire is substituted for the platinum wire working electrode and cyclic voltammetric studies are undertaken with 0.100 M nitric acid solution that contains 5.00 mM of Fe^{3+}. Figure 64 is a plot of representative scans. From the figure, the highest current is for the freshly sanded tungsten. As the experiment progresses and sonication intensity decreases. current decreases. The final unsonicated scan exhibits the lowest current. This may arise because the oxide layer has been rebuilt over the course of the experiment.

Sonication is not effective at removal of the passive in layer. In Figure 64, the initial and final unsonicated scans (thick and thin solid lines respectively) indicate no improvement in the electrode surface. This is in contrast to observations at the platinum electrodes. This may be due to the differences in bond strength between Pt-O ($391.6 \pm 41.8\ kJ/mol$) and W-O ($672.0 \pm 41.8\ kJ/mol$). Furthermore, the limiting current decreases over the course of the experiment indicating that whatever tungsten was exposed by the initial sanding is passivated. Application of a more intense or lengthier sonication may render tungsten an effective electrode material.

8.4 Conclusion

Initial studies into electrode materials unintentionally began with the destruction of the silver | silver chloride reference electrodes. Ag-Cl bonds are slightly weaker than Pt-O bonds, 314.2 and $391.6 \pm 41.8\ kJ/mol$ respectively. From this standpoint,

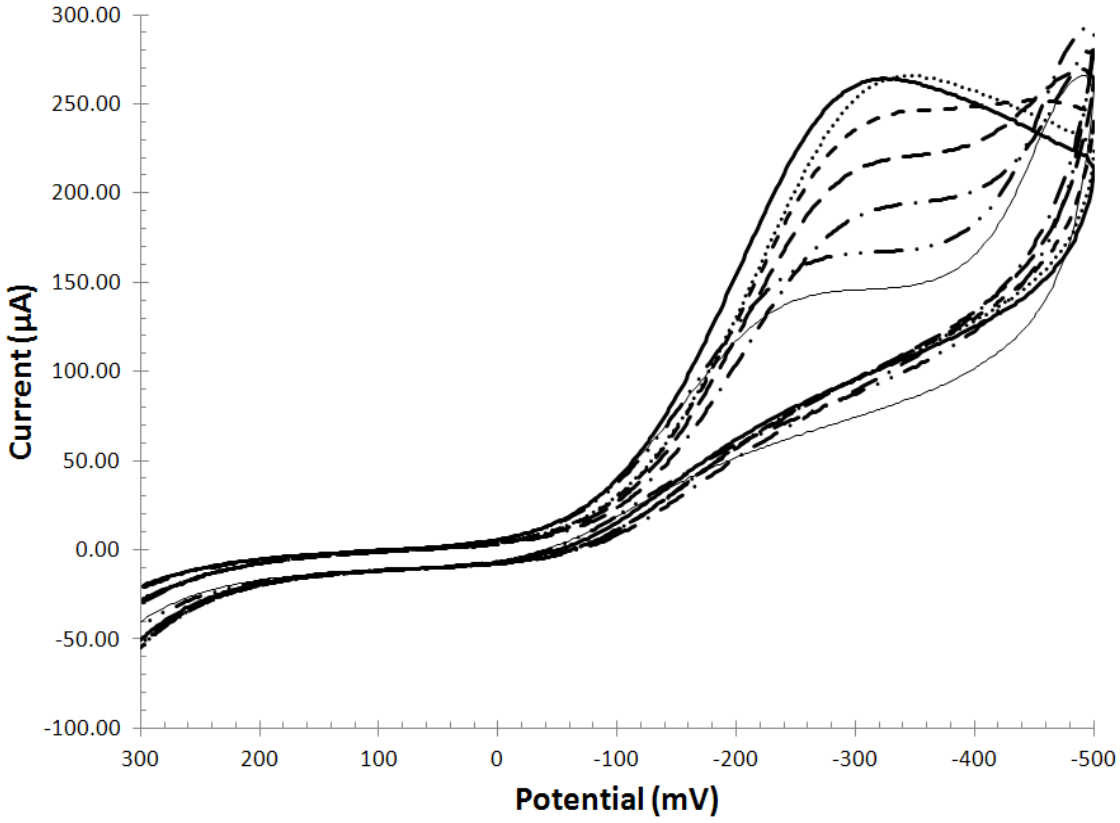

Figure 64. Comparative cyclic voltammograms of 1.00 mM Fe^{3+} in 0.500 M nitric acid taken at assorted levels of sonication with a tungsten working electrode. Initial Unsonicated (heavy solid); Sonicated 100 % (dotted); Sonicated 80 % intensity (short dash); Sonicated 60 % intensity (long dashed); Sonicated 40 % intensity (dash-dot); Sonicated 20 % intensity (dash-dot-dot); Final unsonicated (light solid). Scans were taken in the order listed.

the loss of the sliver chloride from the reference electrode surface is not surprising. Paradoxically, Ag-O has a bond energy of $220.1 \pm 20.9\ kJ/mol$, although it seems to perform better as a reference. This may be due to the oxygen already present in the system being able to replenish the lost oxide; whereas a portion of the chloride generated from such a loss would diffuse away from the electrode. Further, the oxide layer may be denser than the chloride precipitate.

The attempt to use carbon as a working electrode stems mainly from its common use as an electrode. Because C-C bonds have a relatively high bond energy, $610 \pm 2.0\ kJ/mol$, is it unlikely that C-C bonds are being broken during sonication. However, both pencil lead and graphite rod contain the same form of carbon, graphite. Graphite has weak intermolecular forces between its sheets, which is most likely what is disrupted by sonication.

For the platinum data, there is evidence that sonication is sufficient to remove the oxide layer on platinum. The removal of the passivated oxide layer on aluminum surfaces is attempted. The apparent cyclic voltammetric window for aluminum is -400 to -900 mV which was decreased under sonication to -600 to -800 mV. The bond strength of Al-O, $511 \pm 3\ kJ/mol$, is higher is platinum but lower than tungsten. It is unclear how removal of an oxide layer would narrow the potential window.

For tungsten, the regrowth of the oxide layer likely decreases the reductive wave in Figure 64. Higher levels of sonic intensity may overcome this issue.

CHAPTER 9

CONCLUSION AND FUTURE WORK

The addition of acoustic energy to a thin layer electrochemical system has a positive impact on the kinetics of the electrochemical reactions studied. This increase is understood to come from a combination of the acoustic energy directly affecting the redox probes as well as changes in the electrode surface, although it is unknown to what extent either phenomena contributes to the observed effect. A number of issues must be further addressed before the effects of thin layer sonication can be fully understood and optimized.

9.1 Summary of Sonoelectochemical Experiments

The initial objective of this project was to construct a device that would harvest acoustic energy in the form of heat and pressure to catalyze electrochemical reactions. The use of acoustic energy in a thin layer configuration as an electrochemical catalyst proved effective at increasing electron transfer rates.

The initial pilot studies were directed at demonstrating the impact of acoustic energy on heterogenous electron transfer. Redox couples with different electron transfer rates were evaluated. $Ru[bpy]_3^{2+}$, which has fast (reversible) electron transfer kinetics, showed no little discernible improvement. Ferric ion, Fe^{3+}, by contrast has slower electron transfer kinetics that are in the quaisireversible region. In this case, the application of acoustic forces enhanced the reaction rate. Alterations within Marcus theory were considered in light of variation in k^0 and α with respect to

acoustic intensity. There may be a optimum intensity for reactions with an inner sphere component; but this was not explored.

The reduction of oxygen, known for slow kinetics attributed to the initial step in a complex four proton, four electron process, is of particular technological importance in that the slow kinetics of the reduction of oxygen is the one of the primary causes for loss of efficiency in electrochemical power sources. The study found an increase in the electron transfer rate with the applied acoustic energy. The rate parameter for oxygen increased but not as significantly as those for iron. The model used to analyze the data was simple compared to the four proton, four electron reaction of oxygen. On addition of iron to the oxygen system the current measured was the sum of the current for Fe^{3+} and O_2.

The ability to increase oxygen electron transfer rate in a controlled manner offers the opportunity to improve the efficiency of electrochemical systems that rely on oxygen reduction. Given the high level of demand for compact power sources, the additional benefit of a thin layer configuration is apparent.

Preliminary studies in the oxidation of methanol demonstrated a sonocatalyic effect with increased oxidation currents. This is of particular interest for the development of liquid based fuel cells. The cleaning power inherent in sonication moderates the levels of residue that tend to passivate during alcohol electrolysis. The increased reaction rate starts to overcome the kinetic losses that plague alcohol based fuel cells.

9.2 Expansion of Sonoelectochemical Studies

The future directions for this project can be split into aspects for further fundamental research and development of practical application. Aspects worthy of immediate interest for fundamental development include expansion of the number of redox probes in which an effect is observed and development of trends to map out the relationship between acoustic energy, electron transfer rate and potential energy surface. A comparison of probes with differing amounts of inner and outer sphere dependence may offer further insight into the mechanisms involved in sonication of the system. Expansion into the viability of organic couples is also of interest.

This system also offers the potential to enter the inverted region. This offers a means to optimize reaction rates where further development of the model would aid in prediction. This can potentially be achieved with the use of amplifiers and possibly other transducers.

Another area of interest for fundamental research is the optimization of the acoustics, specifically the optimum frequency and intensity. Because transducers are constructed of crystals and ceramics that are cut to produce a specific frequency, this would require an array of transducers. Unfortunately commercial demand limits most ultrasonic transducer components to 20 and 40 kHz. In that same vein, constructive and destructive interference deserves attention by the manipulation of layer thickness, menicus manipulation and modification of well configuration to generate focusing.

Areas that lead more toward the development for practical application include

expanding into other liquid fuels such as ethanol and other longer chain hydrocarbons. Development of fuel cell configurations that optimize the exploitation of increased sonoelectocatalysis is also of particular interest. The cleaning power inherent in sonication along with the noted effect of sonication on the electrode surface offers the potential to create direct reformation fuel cells. To this point, the oxidation of alcohols has resulted in products and intermediates that poison or otherwise contaminate the catalytic surface. The expansion into longer chain hydrocarbons provides an opportunities to explore the limits of this effect. The experiments utilizing alternate electrode material imply that noble metals may not be required.

The application of sonoelectocatalysis in existing industrial and technological application such as ammonia production, the creation of fluorinated compounds and power storage (such as flow batteries) also offer areas where efficiency may be improved.

Sonication removing the passivated thin oxide layers from active metal presents the opportunity to use nonnoble metals as catalysts. With the current system, oxides with lower bond energies bond energies (e.g., Pt-O) were removed from the electrode surface. The further testing of other metals and alloys to find cheaper catalytic materials is warranted. Alloys such as bronze, brass and aluminum brass may be worthwhile for the low bond energy of the Cu-O bond, coupled with the durability the alloy provides.

Sonication affecting the electrode surface as well as the reaction rate implied there may be improvements in the field of electroplating and the application of coatings to metal surfaces. Cleaner surfaces typically result in coatings that last longer and

bulk sonication is already used to harden coatings.

The implications of sonic addition of energy to the electrode surface that is well in excess of the energy that is imparted by potential perturbation has manifestations in electroanalysis. Potentially, the addition of sonic energy can be sufficient to move electron transfer systems into the reversible (rapid) electron transfer domain. If this is possible across a wide range of redox couples, the complexities of electroanalysis are reduced. For example, analyses that account for slow electron transfer kinetics comparable to the rate of voltammetric perturbation are removed. All reactions would become reversible. This means all responses can be described by the Nernst equation, given the $E^{0'}$ for the analyte. Second, it may be possible to design a sonovoltammetric perturbation scheme that allows the response to be simplified to sigmoids or spikes that enhances the selectivity of voltammetric analysis.

Sonication is also used as a means of separation in microfluidics where the sound waves are propagated perpendicular to overlying laminar flows. Particles are then separated by being pushed into different layers of laminar flow [56]. The same sonication could also be used to enhance the sensitivity (and perhaps selectivity) of a nanoscale electrode array.

APPENDIX

CIRCUIT SCHEMATICS FOR ALTERNATIVE MODIFICATIONS

A.1 Amplifier

An average frequency generator is typically limited to a peak amplitude of ±10.0 V. The transducer selected for this project has a maximum driving peak voltage of 21 V. For this reason, an amplifier was constructed to be able to run the transducer at full capacity. The downside of this is that the increased acoustic energy tended to increase the amount of noise in the measurements. Its use was suspended; however its application to other transducers (optimized for other frequencies) is still relevant for future studies.

The op-amp based amplifier was built round a OPA551PA (Digi-key OPA551PA-ND) IC High current /power op-amp 8-dip integrated circuit powered with a ±20 V Proteck dual DC Power Supply 3015B. The gain was set at a multiple of 2.3 allowing a maximum 23 V peak voltage. (See Figure A.1)

A.2 Alternate Driving Circuit

Because one of the long range objectives of this project is to be able to catalyze electrochemical reactions with a parasitic draw from the power generated in a device, an independent driving circuit was constructed. It was built around a pair of LF353 op-amps which generate a 9 V peak sinusoidal driving potential from a 9 V battery. (See Figure A.2)

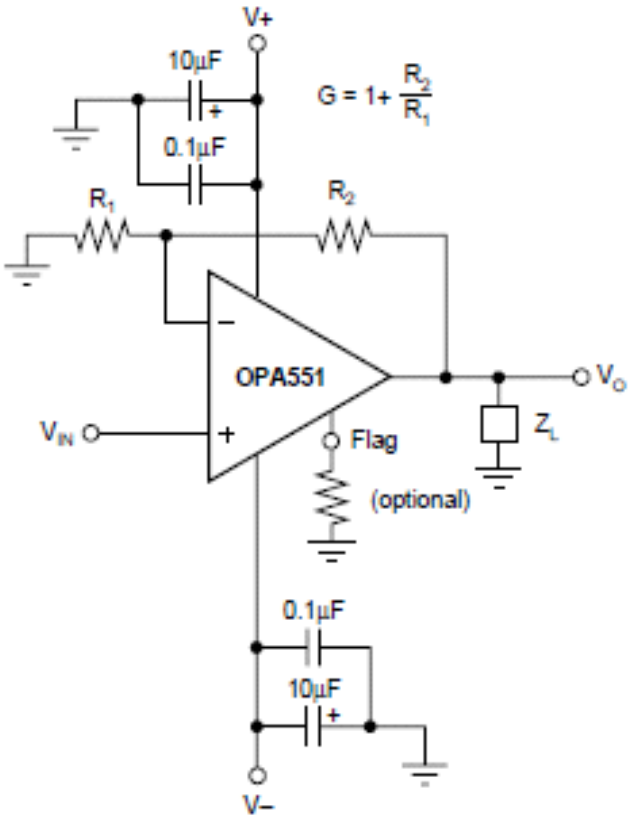

Figure A1. Circuit diagram of amplifier designed to increase driving potential supplied to the transducer.

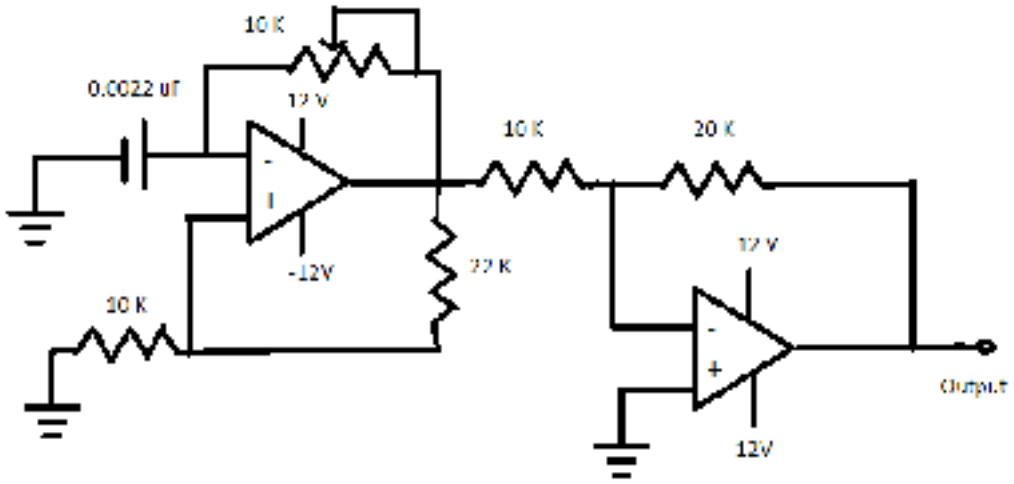

Figure A2. Circuit diagram of freestanding driver to supply driving potential the transducer.

REFERENCES

[1] Corporation, P. E. "Air Ultrasonic Ceramic Transducers 400ET/R180 Specification Sheet", .

[2] Bard, A.; Faulkner, L. *Electrochemical Methods;* John Wiley & Sons, Inc.: New York, Second ed.; 2001.

[3] Mason, T. J. *Sonochemistry: The Uses of Ultrasound in Chemistry;* The Royal Society of Chemistry: Cambridge, 1990.

[4] Suslick, K. S. *Britannica* **2006,** *http://www.scs.uiuc.edu/suslick/britannica,* html.

[5] Suslick, K. S. *The Chemistry and Physical Effects of Ultrasound* **2006,** *www.scs.uiuc.edu/suslick/britannica,* html.

[6] Doktycz, S. J.; Suslick, K. S. *Science* **1990,** *247,* 1067-1068.

[7] Suslick, K. S.; Didenko, Y.; Fang, M. M.; Hyeon, T.; Kolbeck, K. J.; III, W. B. M.; Mdleleni, M. M.; Wong, M. *Phil. Trans. Roy. Soc. A* **1999,** .

[8] Suslick, K. S.; john J. Gawlenowski,; Schubert, P. F.; Wang, H. H. *J. Phys. Chem.* **1983,** *87,* 2299-2301.

[9] Suslick, K. S.; Hemmerton, D. A. *IEEE Transactions on Ultrasonics, Ferroelectrics, and Frequency Control* **1986,** *UFFC-33,* 143-147.

[10] Suslick, K. S.; Hammerton, D. A.; Cline, J. R. E. *J. Am. Chem. Soc.* **1986,** *108,* 5641-5642.

[11] Mason, T. J.; Lorimer, J. P. *Sonochemistry: Theory, Applications and Uses of Ultrasound in Chemistry;* John Wiley &Sons: New York, 1988.

[12] Mason, T. J. *Phil. Trans. R. Soc. Lond. A* **1999,** *357,* 355-369.

[13] Mason, T. J. *Ultrasonics Sonochemistry* **2003,** *10,* 176-179.

[14] Lorimer, J. P.; Mason, T. J. *Chem. Soc. Rev.* **1987,** *16,* 239-274.

[15] Lindley, J.; Mason, T. J. *Chem. Soc. Rev.* **1987,** *16,* 275-311.

[16] Goh, N. K.; Teoh, A. C. C.; Chia, L. S.; Teo, K. C. *Ultrasonics Sonochemistry* **1996,** *3,* S209-S214.

[17] Boldyrev, V. V. *Ultrasonics Sonochemistry* **1995,** *2,* S143-S145.

[18] Riesz, P.; Berdahl, D.; Christman, C. L. *Environmental Health Perspectives* **1985,** *64,* 233-252.

[19] Riesse, J.; Caulier, T.; Deckerheer, C.; Fabre, O.; Vandercammen, J.; Delplancke, J. L.; Winand, R. *Ultrasonics Sonochemistry* **1996,** *3,* S147-S151.

[20] Hoffman, M. R.; Hua, I.; Hochemer, R. *Ultrasonics Sonochemistry* **1996,** *3,* S163-S172.

[21] Margulis, M. A. *High Energy Chemistry* **2004,** *38,* 135-142.

[22] Thompson, L. H.; Doraiswamy, L. K. *Ind. Eng. Chem. Res.* **1999,** *38,* 1215-1249.

[23] Zhang, H.; Coury, J. L. A. *Analytical Chemistry* **1993,** *65,* 1552-1558.

[24] Hagan, C. R. S.; Coury, J. L. A. *Analytical Chemistry* **1994,** *66,* 399-405.

[25] Madigan, N. A.; Hagan, C. R. S.; Zhang, H.; Coury, J. L. A. *Ultrasonics Sonochemistry* **1996,** *3,* S239-S247.

[26] Madigan, N. A.; Jr., L. A. C. *Anal. Chem.* **1997,** *69,* 5-15.

[27] Cooper, E. L.; Jr., L. A. C. *Journal of the Electrochemical Society* **1998,** *145,* 1994-1999.

[28] Wadhawan, J. D.; Marken, F.; Compton, R. G. *Pure Appl. Chem.* **2001,** *73,* 1947-1955.

[29] Banks, C. E.; Compton, R. G. *Chem. Phys. Chem.* **2003,** *4,* 169-178.

[30] Banks, C. E.; Compton, R. G. *Electroanalysis* **2003,** *16,* 329-346.

[31] Walton, D. J.; Phull, S. S.; Chyla, A.; Lorimer, J. P.; Mason, T. J.; Burke, L. D.; Murphy, M.; Compton, R. G.; Eklund, J. C.; Page, S. D. *Journal of Applied Electrochemistry* **1995,** *25,* 1083-1090.

[32] Marken, F.; Eklund, J. C.; Compton, R. G. *Journal of Electroanalytical Chemistry* **1995,** *395,* 335-339.

[33] Cartwright, K. V. *Technology Interface* **2007,** *8,* 20.

[34] Bies, D. A.; Hansen, C. H. *Engineering Noise Control: Theory and Practice;* Taylor Francis: New York, 4th ed.; 2009.

[35] Blauert, J. *Acoustics for Engineers;* Troy Lectures Springer-Verlag: Berlin, 2009.

[36] Fahy, F. J. *Sound Intensity;* Elsevier Science Publishers, Ltd.: New York, 1989.

[37] University of New South Wales; School of Physics, *Acoustic impedance, intensity and power* **2011,** *http://www.animations.physics.unsw.edu.au/jw/sound-impedance-intensity,* htm.

[38] Bloemhof, H. *Applied Acoustics* **1986,** *19,* 159-166.

[39] Davis, J. D.; Patronis, E. *Sound System Engineering;* Elsevier Focal Press: Boston, 3rd ed.; 2006.

[40] Chadderton, D. V. "Building Services Engineering", 2007.

[41] Stokes, G. G. *Trans. Camb. Phil. Soc.* **1849,** *8,* 287.

[42] Kirchhoff, G. *Ann. Phys. Chem.* **1868,** *134,* 177.

[43] Bard, A. J.; Faulkner, L. R. *Electrochemical Methods;* John Wiley & Sons, Inc.: New York, 1980.

[44] Hush, N. *Transactions of the Faraday Society* **1961,** *57,* 557-580.

[45] Lide, D. R. *CRC Handbook of Chemistry and Physics;* CRC Press: New York, 2001.

[46] Wieckowski, A. *Interfacial Electrochemistry;* Marcel-Dekker, Inc.: New York, 1999.

[47] Conway, B. E.; Jerkiewicz, G. *Journal of Electroanalytical Chemistry* **1992,** *339,* 123-146.

[48] Truesdale, G. A.; Downing, A. L. *Nature* **1954,** *173,* 1236.

[49] Marcus, R. A. *Journal of Physical Chemistry* **1963,** *67,* 853-857.

[50] Marcus, R. A. *Journal of Chemical Physics* **1965,** *43,* 679-701.

[51] Marcus, R. *Electrochim. Acta* **1968,** *13,* 995-1003.

[52] Miller, J.; Calcaterra, L.; Closs, G. *J.Am.Chem.Soc.* **1984,** *106,* 3047.

[53] Iwasita, T. *Electrochimica Acta* **2002,** *47,* 3663-3674.

[54] Breiter, M. *Electrochimica Acta* **1967,** *12,* 1213-1218.

[55] Mott, N. F. *Trans. Faraday Soc.* **1947,** *43,* 429-434.

[56] Petersson, F.; Nilsson, A.; Jonsson, H.; Laurell, T. *Anal. Chem.* **2005,** *77,* 1216-1221.